THE FUNCTIONAL AND REMODELING RESPONSE OF COLLECTING LYMPHATIC VESSELS TO DISRUPTION OF LYMPHATIC DRAINAGE PATHWAYS

A Dissertation
Presented to
The Academic Faculty

by

Tyler S. Nelson

In Partial Fulfillment
Of the Requirements for the Degree
Doctor of Philosophy in Bioengineering in the
George W. Woodruff School of Mechanical Engineering

Georgia Institute of Technology

August 2018

THE FUNCTIONAL AND REMODELING RESPONSE OF COLLECTING LYMPHATIC VESSELS TO DISRUPTION OF LYMPHATIC DRAINAGE PATHWAYS

Approved by:

Dr. J. Brandon Dixon, Advisor
School of Mechanical Engineering
Georgia Institute of Technology

Dr. Babak Mehrara
Plastic and Reconstructive Surgery
Memorial Sloan Kettering Cancer Center

Dr. Krishnendu Roy
School of Biomedical Engineering
Georgia Institute of Technology

Dr. Wei Sun
School of Biomedical Engineering
Georgia Institute of Technology

Dr. Susan Thomas
School of Mechanical Engineering
Georgia Institute of Technology

Date Approved: 5/16/2018

ACKNOWLEDGEMENTS

Firstly, I would like to thank my parents, Scott and Karen Nelson, for the love and support that they have given me throughout my life. They are responsible for instilling in me a strong foundation of values on which all else has been built. From a young age they fostered the curiosity and creativity that has ultimately given me the abilities to accomplish this work. I thank them for encouraging me to pursue my interests and passions without fear of failure. Without them I would not have had the opportunity to engage in my academic pursuits. In addition, I would like to thank my sister, Lauren Nelson, for her love and encouragement. Her creative abilities have and will continue to inspire me to apply artistry in whatever I do. I also wish to thank my grandmother, Marcia Schnitker, and my aunt, Susan Burch, for their lifelong love and support. Their encouragement and humor has helped me to surmount many challenges.

I would like to thank Robyn Bundy for the love that she has shown me while preparing this dissertation. Her many sacrifices have enabled me to devote myself to my scholarly work. Her humor and positivity is infectious and has helped me to achieve many goals that I believed to be unobtainable.

I would like to acknowledge my friends, colleagues, and lab mates, whose comradery was invaluable when faced with many deadlines and sleepless nights. Their friendship has provided an outlet for escaping my studies.

Additionally, I would like to thank my funding sources, the American Heart Association and the TI:GER program at Georgia Tech, for supporting my professional development during my graduate studies.

Finally, I would like to express my sincere gratitude to the individuals who played a direct role in preparing this dissertation. Specifically, my advisor Dr. J. Brandon Dixon for supporting my research. His guidance, knowledge, and patience were essential for training me as a scientist. In the years we have worked together, he has served as a model scientist and I have greatly learned from his creativity, Faith, and love for his family. I would also like to thank my committee members whose input and guidance have helped me broaden my scientific perspectives. Their contributions have elevated this work to a level that I had not imagined.

TABLE OF CONTENTS

LIST OF TABLES

LIST OF FIGURES

Overlaid pressure and intensity plots demonstrate the calculation of the effective pumping pressure (P_{eff}) and the emptying rate (ER). Typical pack flow that is present before the beginning of flow occlusion (bottom left) is recovered after occlusion (bottom right). To quantify the point at which packet flow was restored, the time at which the magnitude of the power spectral density function (PSD) recovered to a specified value was calculated as described in the methods section.

located on the lateral aspects of the tail. 1 week after ligation chow fed control animals exhibit uptake of fluorophore in the intact lymphatic vessel that subsequently transits the wound site. This was delayed in obese animals. However, this difference is attenuated by the 10-week time point.

frequency of fluorescent pulsations within the vessel, exhibited significant differences between control and obese groups. (B) Packet transport, the integral of the packet frequency signal over time, was used to evaluate fluorescence transport driven by intrinsic lymphatic contractions. (C) Effective pumping pressure was used to evaluate the maximal pressure generated by the collecting vessel to overcome occlusion. Error bars represent SEM. (n=8, control) (n=6, obese) (*, denotes significant difference between control and obese; †, denotes significant difference between control value and the baseline pre-surgical control value; ‡, denotes significant difference between obese value and the baseline pre-surgical obese value, $p < 0.05$).

lymphatic ligation. Pre-surgical images show both the cranial and caudal collecting lymphatics intact. Immediately after ligation of the caudal collecting lymphatic, an absence of fluorophore transport confirmed successful ligation and excision of the vessel. (C) The diameter of the cranial vessel on the control and wounded leg was measured distal to the wound site using the MR images before and 42 days after surgery. Values were normalized by the pre-surgical average diameter of the respective vessel. (****, $p < 0.0001$).

between wounded and wounded baseline at 1.5 cmH2O transmural pressure, $p < 0.05$)

column- transverse, right column- axial) exhibited atrophy of the musculature surrounding the vessel compared to control. Additionally, vessel segments from the wounded leg appear to have an increase in matrix surrounding the vessel. (C) Biaxial testing was conducted on isolated vessel segments at various axial stretches and transmural pressures. Wounded vessels exhibited increases in vessel compliance compared to control. The biaxial data was fit to a constitutive model to calculate material parameters that capture pressure-diameter behavior (details in theory).

SUMMARY

The lymphatic system is composed of a network of vessels, nodes, and accessory organs that is present in most soft tissues of the body. The lymphatics play a vital role in maintaining tissue fluid homeostasis, trafficking immune cells from the periphery to the nodes, and transporting dietary lipids from the intestines to the blood stream. Unlike the blood vasculature, the lymphatic system does not have a central pump. Instead, transport is promoted by collecting lymphatic vessels that are composed of a series of contractile segments separated by one-way valves. When the normal function of the lymphatics is compromised a disease called lymphedema may develop, which is characterized by tissue fluid retention, fibrosis, and adipose accumulation. Unfortunately, lymphedema is a relatively common complication of cancer therapies that damage the lymphatic vasculature, such as lymph node dissections and radiation treatment.

Despite being integral driver of lymphatic transport, relatively little is known about how collecting lymphatic function and remodeling may influence the development of lymphedema. This work demonstrates the development of novel near-infrared imaging methods with the ability to quantify and phenotype collecting lymphatic failure during lymphatic disease. These methods provide biological insight into the functional and remodeling response of the collecting lymphatic vessels to surgical disruption of lymphatic drainage pathways. Specifically, we demonstrate that diet-induced obesity adversely impacts collecting lymphatic contractility and pump function during lymphedema in a mouse model. Further, in a clinically relevant sheep model, we demonstrate that the uninjured vessel can compensate in vivo by altering its intrinsic functional response and

structure; however, through this process, the collecting lymphatic muscle experiences increased oxidative stress due to increased contractility. The results of this work demonstrate that functional adaptations of the collecting lymphatic vessels may influence the development of lymphedema in a clinical setting.

CHAPTER 1.   INTRODUCTION AND BACKGROUND

In this chapter I will begin with an introduction to the lymphatic system and discuss the essential roles that it plays in physiology. I will subsequently introduce lymphedema and discuss current research that contributes to our understanding of the disease and its progression. I will then focus on our current understanding of the collecting lymphatic vessel's role in lymphedema and the techniques developed to quantify this contribution. Finally, I will give an overview of the specific aims that have motivated my work.

1.1   Lymphatic Physiology

The lymphatic system is a network of vessels, nodes, and accessory organs that plays essential roles in regulating tissue fluid homeostasis, trafficking immune cells, and transporting dietary lipids (209). The lymphatic vasculature is present in most soft tissues of the body and is responsible for transport of between 4-8 liters of fluid per day back to the blood circulation (178). This fluid, called lymph, originates from the interstitial spaces of the body, where capillary beds continuously extravasate water, small solutes, and ions in accordance with the hydrostatic and oncotic pressure gradients described by Starling's equation (119). While nearly 90% of this extravasated fluid is reabsorbed at the pre-venous end of the capillary beds, a fraction of the remaining 10% is transported by the lymphatics as lymph.

Lymphatic transport begins when lymph is absorbed by lymphatic capillaries, called initial lymphatics, that infiltrate the capillary beds and are tethered by anchoring filaments to the extra-cellular matrix (18). The initial lymphatics are blind-ended structures

typically composed of a single endothelial cell layer that is highly permeable to macromolecules. These initial lymphatics converge and transport fluid to the collecting lymphatic vessels that possess smooth muscle cells, capable of tonic and phasic contraction, in addition to one-way valves to prevent backflow (251). The afferent collecting lymphatics subsequently transport fluid to the lymph nodes, which play an essential role in antigen presentation to residing lymphocytes (243). Efferent collecting vessels exit the nodes and progressively converge to form the collecting lymphatic ducts that drain to the largest lymphatic vessel in the body, called the thoracic duct. The thoracic duct ultimately expels its contents into the blood circulation via the left subclavian vein (148).

The collecting lymphatic vessels are composed of laminar layers in a manner similar to veins and arteries. The internal layer is composed of lymphatic endothelial cells (LECs) adhered to a basement membrane (129). LECs are highly specialized and possess a number of lymphatic specific markers that differentiate them from blood endothelial cells (168, 238). These include VEGF-R3, the receptor for vascular endothelial growth factor type C (VEGF-C) (1, 97, 160); Prox-1, the homeobox gene product involved in the developmental regulation of the lymphatic system (90, 100); LYVE-1, a hyaluronan receptor (181, 200); and podoplanin (PDPN), a glomerular podocyte membrane mucoprotein (33, 240). The outer layers of the lymphatic vessels are composed of elastin, surrounded by lymphatic smooth muscle cells (LMCs), and collagen (129). Unlike the blood vasculature, the lymphatic vasculature does not have the benefit of a centralized pump, like the heart, to propel fluid; because of this, lymph is transported through the collecting lymphatics via a combination of intrinsic and extrinsic factors (162, 172).

2

Intrinsic factors describe the active lymphatic pump, in which discrete pumping segments, known as lymphangions, contract to generate pressure that propels lymph flow (146, 172, 233). Lymphangions are separated by one-way bi-leaflet valves to prevent backflow and their contractile activity is highly sensitive to mechanical and molecular stimuli (110, 251). Extrinsic factors are composed of other mechanisms that assist to propel lymphatic flow in addition to the intrinsic lymphatic contractions. These include lymph formation, pulsations in the circulatory system, respiration, and muscle pumps during musculoskeletal movement (38, 71). A combination of both intrinsic and extrinsic factors are essential to propel lymph against both an adverse pressure gradient from the interstitium and unfavorable hydrostatic pressure gradients caused by gravity (75, 251).

The contractile activity of the collecting lymphatic vessels is enabled by the LMCs embedded within the vessel walls that govern both the tonic and phasic contractions of the vessels. Interestingly, these cells exhibit an array of contractile proteins that parallel the phenotypic characteristics of both vascular smooth muscle cells and cardiac myocytes (146). This enables the collecting lymphatic vessels to alter their tone to change their inherent resistance to flow, thus, becoming better fluid conduits in response to favorable upstream pressure gradients; however, when pressure gradients are unfavorable, the LMCs can rapidly contract the vessels by up 75% of their diameter, ejecting fluid from one lymphangion to the next. This pump-conduit behavior of the lymphatics stems from the ability of the vessels to sense their unique mechanical environments to maintain fluid transport (72, 171, 172). For example, isolated lymphatic vessels have been shown to react to increases in transmural pressure (vessel stretch) and elevated outflow pressure by increasing their contractile activity (60, 217, 252). In addition to regulation of lymphatic

3

contractility via smooth muscle stretch, the lymphatic endothelium serves as a complementary and potent regulator of the lymphatic contractile response to flow (31, 73, 110). Flow imposed on the lymphatic vessel induces contractile inhibition, relaxed vessel tone, and results in passive conduit behavior via endothelial nitric oxide synthase (eNOS) (171, 172, 193).

Because the lymphatics play an essential role in draining immune cells, lipid, proteins, and detritus from tissues, loss of lymphatic function has been implicated and demonstrated in many highly prevalent diseases such as obesity (84, 89, 153, 239), congestive heart failure (242), atherosclerosis (113, 230), diabetes (143), and cancer (127); however, the condition most directly linked to loss of lymphatic function is lymphedema.

1.2 Introduction to Lymphedema

Lymphedema is a debilitating incurable disease that is characterized by excessive regional fluid accumulation, tissue fibrosis, and adipose deposition (173). The disease is separated into primary and secondary forms that are delineated by how the condition is acquired. Primary lymphedema is the congenital or hereditary form of the disease and is rare, affecting roughly 1.15 in 100,000 children and adolescents (184, 202). Secondary lymphedema is the acquired form of the disease and is relatively common, with incidence rates estimated at 1.33 to 1.44 in 1,000 individuals (184, 202); however, lymphedema incidence rates are difficult to quantify due to lymphedema being under and mis-diagnosed (141, 184).

Globally, the most common cause of lymphedema is due to a parasitic nematode infection called lymphatic filariasis. The filarial worms are thought to infect nearly 120

million individuals in 83 countries located primarily in tropical regions (30, 216). The infection is transmitted via a mosquito vector that deposits filarial larva on the skin of the host while seeking a blood meal. The larvae then penetrate the skin at the site of the mosquito bite and migrate to the lymphatic vessels and nodes where they dwell and subsequently reproduce for 5 - 8 years (103, 216). Our knowledge of the mechanism that triggers lymphedema pathogenesis following infection is incomplete (13, 40); however, studies have implicated a chronic inflammatory response mediated by CD4+ T-cells that may impair lymphatic function and subsequently induce lymphatic remodelling (6, 12). Interestingly, similar mechanisms have been linked to the development of non-filarial lymphedema.

In more developed countries, the population most at risk for development of lymphedema is post-procedural cancer patients. This is because common cancer therapies such as radiotherapy and lymph node resection seek to target lymph nodes and lymphatic vessels to prevent metastasis of cancer (173, 232); however, any surgical intervention that inadvertently damages the lymphatic system can result in lymphedema. There is even evidence present that secondary lymphedema can occur without surgical disruption (84). Breast-cancer patients are the most at risk for developing lymphedema with incidence rates estimated 15% to 40% but prostate cancer, melanoma, and endometriosis also have moderately high incidence rates likely greater than 15% percent (7, 52). Cancer-related lymphedema typically localizes to the extremities that are drained by the damaged lymph nodes and vessels. In the case of breast cancer, lymphedema typically affects the arms while pelvic cancers are associated with leg lymphedema. The onset of lymphedema can occur months to years following cancer therapies, with the majority of patients presenting

clinical lymphedema within 1 year of lymph node dissection or biopsy (154). Overall, 80% to 90% of individuals who will develop lymphedema do so within 3 years post-treatment (196); however, the remaining 10% to 20% will develop lymphedema at a rate of roughly 1% per year (155, 164). It is believed that the delayed onset of lymphedema contributes to under and misdiagnosis of the disease due to the decreased likelihood that patients will continue clinical follow-ups to detect lymphedema after oncology follow-up visits have ceased (132).

Treatments for lymphedema have traditionally utilized mechanical methods to remove fluid and prevent fluid build-up in the affected limb (88, 183). Manual lymphatic drainage therapy (MLD), is a specialized massage technique designed to rhythmically move fluid from the distal portions of the limb to the trunk of the body (5). Compression therapy relies on wrapping the limbs with bandages to achieve desired compressive pressures and to subsequently prevent fluid accumulation (14). Typically, a combination of these techniques, coupled with skin care and exercise, represents the standard of care for patients with lymphedema (111). Long-term management of lymphedema is achieved with the use of elastic compression garments (sleeves and stockings) (78, 99, 106). While these treatments can be effective even in progressed lymphedema, early detection is an integral part of preventing the drastic tissue changes associated with the disease (53, 207, 208); however, clinical detection methods often rely on measurements of tissue swelling as opposed to measuring the underlying lymphatic dysfunction that causes the disease. This is due in no small part to the dearth of technologies and techniques available to quantify dysfunction (235). Further, this has historically hindered research that aims to investigate the interplay between lymphatic dysfunction and the pathogenesis of lymphedema.

1.3 Pathogenesis and Pathophysiology of Lymphedema

Lymphedema is a progressive disease that begins with a primary insult to the lymphatic vasculature. In the context of cancer-related lymphedema this insult is typically surgical and/or radiation induced disruption to the lymph nodes and vessels (144, 173, 182). It is important to note that the time between primary insult and the onset of swelling, when the disease is clinically diagnosed, may be many years (7); however, the mechanisms involved in development of lymphatic transport insufficiency following initial insult are largely unknown. Despite this, the resulting stasis of lymph in the interstitium induces profound changes in tissue composition including cutaneous thickening, fibrosis, and adipose deposition that progressively worsens during lymphedema. It is this gross, progressive, tissue remodelling that is the hallmark of lymphedema.

Given that the lymphatic system acts as the nexus between cardiovascular and immune systems it is unsurprising that the progressive tissue remodelling observed in lymphedema has been linked to inflammation; a complex biological response to harmful stimuli such as pathogens, cell damage, or other irritants. Although acute inflammation is a healthy physiological response associated with normal healing processes, chronic inflammation is implicated in a wide range of degenerative health disorders (64, 86, 101, 167). Lymphatic vessels are directly involved in the inflammatory process by draining extravasated fluid and leukocytes from inflamed tissue space to the lymph nodes (231). Studies have shown that inflammatory mediators such as cytokines (3), prostanoids (245), histamine (66), and nitric oxide (NO) (32, 139, 149, 235) modulate lymphatic contractile activity and drainage. Others have demonstrated that the administration of pro-inflammatory factors exacerbates lymphedema phenotypes in mouse models (147, 250).

7

Conversely, administration of non-steroidal anti-inflammatory drugs (NSAIDs) has been shown to ameliorate lymphedema phenotypes in mouse models (147).

The biological mechanisms that govern inflammation's role in lymphedema development have been widely studied in recent years and have produced exciting insights into the processes that drive lymphedema. CD4+ T-cells are an important mediator of the inflammatory response. Antigen presenting cells, such as dendritic cells, present antigen peptide via major histocompatibility complex II (MHC II) to activate naïve CD4+ T-cells; however, CD4+ T-cells can be activated by other cell types expressing MHC II such as adipocytes (61, 246). These cells subsequently differentiate into different T-helper (Th) subtypes, proliferate, and secrete their own cytokines to facilitate an immune response (108, 150, 203). Clinical and animal biopsies collected from lymphedematous tissue have demonstrated positive correlations between tissue fibrosis and the number of infiltrating CD4+ T-cells (11). Mice deficient in CD4+ T-cells have been shown to develop less swelling and tissue fibrosis in lymphedema models (11). Further, preventing T-cell differentiation, via topical treatment with the calcineurin inhibitor tacrolimus (156), has shown promising results in treating lymphedema in mouse models (70).

Previously, decreasing inflammation via the cyclooxygenase (COX) and arachidonate 5-lipoxygenase (5-LO) inhibiting NSAID ketoprofen, has been shown to treat lymphedema in mice (147); however, ketoprofen treatment had undesirable off-target effects including gastrointestinal, cardiac, nervous system, renal, and hepatic toxicities, that limited clinical use for treating the disease. Therefore, a recent study sought to systematically identify the more targeted downstream mechanism of action that ketoprofen utilized to ameliorate lymphedema (219). The study identified that the effects of ketoprofen

8

on treating lymphedema can primarily be attributed to inhibition of leukotriene B4 (LTB-4) synthesis, an inflammatory mediator produced by leukocytes. Further, LTB-4 antagonism via pharmacological treatment with bestatin proved to effectively treat lymphedema. The results demonstrate that LTB-4 levels rise during lymphedema pathogenesis in the mouse tail. By inhibiting LTB-4 with bestatin 3 days after initial induction of lymphedema, the researchers demonstrated significant reductions in tail volume, tissue fibrosis, and increases in lymphatic function. Given that both LTB-4 and CD4+ T-cells seem to play integral roles in regulating lymphedema pathogenesis, it is unclear if the two pathways act independent of each other or if they act in concert. CD4+ T-cells are known to possess the LTB-4 receptor BLT-1, which is involved in chemotaxis, it seems reasonable to believe that the latter hypothesis is more likely (212).

Currently, it is unclear why inflammation goes unresolved during lymphedema; however, impairment of lymphatic transport is hypothesized to play a role. The lymphatic system acts to mediate the inflammatory response by draining macrophages, dendritic cells, T-cells, antigen, and cytokines from the periphery to the lymph nodes and subsequently the blood stream (122, 174). This plays an important role in resolving acute inflammation; however, the prolonged presence of inflammatory cytokines and mediators can increase synthesis of compounds that are known to downregulate lymphatic contractile activity such as NO via iNOS (121, 193, 199, 222). Therefore, it is possible that inflammation goes unresolved during lymphedema due to negative feedback between the leukocytes producing pro-inflammatory factors that subsequently result in decreased lymphatic transport necessary to drain said leukocytes. This is supported by studies that have shown improvements in tissue swelling, fibrosis, and CD4+ T-cell infiltration upon surgical

lympho-venous bypass (223). In effect, this technique breaks the negative feedback cycle, increases lymph drainage from the tissue, and subsequently ameliorates inflammation. In addition to having direct effects on lymphatic function, inflammation has also been shown to induce lymphatic growth and remodeling that may be functionally mal-adaptive (82, 105). Mechanistically, lymphangiogenesis is mediated by inflammation. This process is a result of macrophage production VEGF-C that in turn induces proliferation and growth of new lymphatic vessels (19, 104, 130, 186); however, the majority of the newly formed vessels are immature, leaky, and their ability to properly facilitate lymph drainage from the tissue is unclear (82, 159). Additionally, recent studies have demonstrated hyperplasia of the lymphatic vessels coupled with progressive lymphatic dysfunction associated with increased inflammatory cell types during lymphedema (83).

Multiple comorbidities that exacerbate inflammation are believed to negatively influence lymphedema development (39, 69, 128, 134, 229); however, obesity is the most widely demonstrated (48, 91). Obesity has been shown to cause chronic inflammation due to interactions between adipose tissue and immune cells (85, 93, 151, 247). This is believed to be initiated by T-cell inflammatory reactions that induce macrophage chemotaxis to adipose tissue. These macrophages then phagocytize necrotic adipocytes leading to release of inflammatory cytokines, recruiting other inflammatory cells, and progressive inflammation (151). Recent studies have also demonstrated that adipocytes express MHC II and can independently activate T-cells and thus aggravate inflammation (61, 246). Clinically, post-operative weight gain is recognized as a major risk factor for developing lymphedema (91). In fact, a recent clinical study has shown that obesity alone can cause lymphedema with no surgical intervention (84). Investigations using animal models have

demonstrated that obese mice possess impaired lymphatic function due to T-cell mediated inflammation (27, 192, 222). Specifically, collecting lymphatic contractile function is significantly decreased (27, 152, 192). Interestingly, this decrease in contractile activity does not appear to be a result of lymphatic remodeling because function is restored through weight loss (152). Upon induction of lymphedema via surgical insult obese mice have a more severe tail lymphedema phenotype, with increased adipose deposition, fibrosis, and CD4+ T-cell infiltration (192).

Given that baseline lymphatic function is impaired during obesity, it seems reasonable to believe that this could play a role in the pathogenesis of the disease. For example, although obesity impairs baseline lymphatic function, this is still sufficient to mediate the chronic low-grade inflammation and to maintain tissue fluid homeostasis. Upon surgical insult that impairs lymph transport, inflammation can no longer be mediated by lymphatic drainage, thus increasing the number of leukocytes in the tissue, further impairing lymphatic transport, and further inducing tissue remodeling. It is therefore one of the goals of this thesis to investigate the influence of obesity on collecting lymphatic pump function during lymphedema.

1.4   Collecting Lymphatic Pump Failure in Lymphedema

The recent advancements discussed in the previous section have provided remarkable insights into the biological mechanisms and risk factors that regulate the profound tissue alterations associated with the development of lymphedema. The studies have demonstrated the unique interplay between immune mediated inflammation and the development of lymphedema that have led to emerging therapies that seek to cure the

disease. Unfortunately, there is still very little known about how lymphatic transport, or loss thereof, is altered during and/or influences the development of lymphedema. This is particularly true with regards to the collecting lymphatic vessels that actively regulate their intrinsic function to facilitate the transport of lymph. This section will discuss the observations that have motivated the study of the collecting lymphatic's role in lymphedema progression, the technical challenges associated with this, and explore the current research in the field.

Histological analysis conducted in lymphedema patients have demonstrated correlations between collecting lymphatic failure and lymphedema progression. Mihara et. al. sampled collecting lymphatic vessels from the legs of patients with gynecological cancers with varying stages of lymphedema, ranging from stage 0 (pre-clinical) to stage III (severely progressed) (137). Their findings demonstrate that alterations to the structure of the lymphatic vessels correspond to the severity of lymphedema in the limbs. This occurs in a progressive manner beginning with dilation of the vessels followed by subsequent contraction and vessel thickening ultimately resulting in stenosis of the lumen. They hypothesized that increases in the intralumenal pressure of the collecting vessels, due to the increased fluid load associated with lymphedema, subsequently induced a compensatory remodelling response that ends in an inability for the vessels to pump and transport fluid. This has been supported by more recent work from Ogata et al. demonstrating that the progressive thickening of the vessel walls is driven by the proliferation of smooth muscle cells (158). More specifically, they discovered an increase in smooth muscle cells exhibiting synthetic phenotypes with decreases in the contractile

markers SM1 and SM2. These cell types are associated with increased fibrosis of the vessel wall and decreased contractility.

It has been proposed that individuals who develop lymphedema have a constitutional predisposition to the disease (15, 46, 205, 206). These studies have demonstrated that patients who have higher rates of lymphatic drainage before axial lymph node dissection are at greater risk for developing lymphedema after surgery. Although this seems paradoxical, the authors hypothesize that these patients have higher lymphatic drainage because they have elevated lymph load that could potentially overload the functional capacity of the lymphatic vessels upon injury. This has been supported by recent work that demonstrates elevated pre-surgical lymphatic pumping pressure in women who later develop lymphedema (46). Further, it has been shown that patients with progressed chronic lymphedema have decreased lymphatic pumping pressure (140, 226). Taken together, these studies suggest that elevated lymph load corresponds to an increase in the functional capacity of the collecting lymphatic vessels; however, these vessels are likely operating at maximal capacity. Upon injury, the functional demands on the lymphatic vessels increase further, subsequently leading to overwork, muscle fatigue, and vessel remodelling. Ultimately, this results in hypertrophy of the vessels (137, 158) and an inability to pump (140, 226). This is, in a sense, analogous to cardiovascular hypertension that results in hypertrophy of the heart and subsequent heart failure.

Given that collecting lymphatic pump dysfunction appears to play a role in the development of lymphedema, several studies have been conducted in mouse lymphedema models that seek to quantify this contribution. Gousopoulos et. al. induced lymphedema in the mouse tail by ligating the collecting lymphatic vessels and dermal layer initial

lymphatics (83). They discovered that the collecting lymphatic vessels responded to the induction of lymphedema by slightly lowering their contraction frequency and amplitude. This decreased the average pumping score of the vessels, which is analogous to ejection fraction. This decrease in collecting lymphatic function corresponded with increases in interstitial fluid, tissue swelling, and infiltration of macrophages and CD4+ T-cells. Interestingly, in the early stages of lymphedema, they observed significant hyperplasia of the lymphatic vessels and profound remodeling of the lymphatic vasculature. Given that the increased infiltration of immune cells in the tissue corresponded with the declines in lymphatic function, it seems plausible that the collecting lymphatics play an active role in mediating the development of lymphedema.

Mouse lymphedema models have traditionally relied on ligating all of the lymphatic vessels or nodes draining a distal tissue space (80, 147, 186, 214); however, in a clinical setting, lymphedema can develop even though there are remaining intact and functional collecting vessels (124, 189, 204, 253). Yet, it appears those intact vessels are unable to compensate for the increased fluid load caused by the initial surgical insult (15, 46, 205, 206). Recent work has sought to determine the involvement of these intact collecting lymphatic vessels in the development of lymphedema. This was accomplished using a novel mouse tail lymphedema model that involved cauterization of one of two collecting lymphatics, along with the dermal initial lymphatics, while leaving the remaining collecting vessel intact for longitudinal functional imaging (236). Results from this study indicate that 2-4 days following the single-vessel ligation, the intact collecting lymphatic vessels exhibit relatively normal contractile activity and transport. Declines in the contractile activity of the vessel were delayed and observed 7-14 days after surgery,

resulting in decreased intrinsically driven transport. This result was observed even 3 months after surgery, when tissue swelling had subsided. At the same time point, lymphatic pumping pressure was significantly decreased from baseline. This is in agreement with clinical studies that have demonstrated that patients with chronic lymphedema have lower lymphatic pumping pressure (140, 226). Interestingly, tail swelling was found to have correlated with loss of intrinsically driven transport at the early time points before peak swelling; however, after peaking, tail swelling no longer correlated with intrinsic transport. This indicates a co-dependence between collecting lymphatic contractile function and the degree of tissue swelling observed in the early stages of lymphedema. As a whole, these results are impactful from a clinical standpoint because they demonstrate that injury to the lymphatic vasculature can adversely affect the otherwise normally functioning collecting lymphatic vessel that are spared during surgery. It is possible that this is driven by a combination of mechanical and inflammatory factors, such as those discussed in the previous sections.

1.5   Quantification of Collecting Lymphatic Function In Vivo

A major hurdle to the study of collecting lymphatic pump function in the context of lymphedema is the paucity of non-invasive in vivo imaging methods that are capable of quantifying the effectiveness of intrinsically driven lymphatic transport (176). While numerous techniques have been used to visualize bulk lymphatic drainage including lymphoscintigraphy and MRI they lack the appropriate spatial and temporal resolution to assess lymphatic pump function (20, 136, 138, 197). Lymphoscintigraphy in particular has served as the "gold-standard" method in clinical diagnosis of fluid stasis caused by lymphatic dysfunction (142, 183, 220, 237). Near-infrared (NIR) imaging emerged as one

of the more promising imaging modalities due to its ideal combination of spatial and temporal resolution, allowing for dynamic imaging of initial and collecting lymphatics in real time (197, 225). NIR imaging provides excellent spatial resolution for superficial lymphatics because NIR excitation light resides in wavelength ranges (>750 nm) that are minimally scattered and absorbed by biological tissues (17, 67). When these resolution capabilities are combined with the video frame-rates available with EM-CCDs, the technique is optimal for dynamic imaging of collecting lymphatic function (235). Using these techniques, a concentration of NIR fluorophore (typically bound to large molecular weight polyethylene glycol or albumin) is injected intradermally where it is taken up by the lymphatics (170, 235). It is then excited at NIR wavelengths and imaged using a CCD or EM-CCD camera with appropriate optics and filters (235). By utilizing these modalities, various quantitative metrics have been developed to characterize lymphatic function, including packet velocity, packet frequency, and transport time that correspond to the intrinsic contractile activity of the collecting lymphatic vessels (115, 116, 170, 176, 197, 225–228, 235, 236).

Novel NIR imaging approaches have been used to assess the structural and functional alterations of the collecting lymphatics associated with lymphedema in humans. A study by Unno and colleagues used NIR lymphatic imaging in patients to identify qualitative characteristics associated with lymphedema. These included dermal backflow, fluorophore retention at the injection site, dilated collecting lymphatics, and fluorescence diffusion due to leaky vessels (225). Similar qualitative assessments have confirmed these results (131, 136, 175). More recent work by Liu et. al. has demonstrated that patients with breast cancer related lymphedema have significantly more tortuous lymphatic vessel morphology in the

affected arms; however, these vessels were also found to be functional, highlighting the necessity to quantify lymphatic function (124). Subsequent studies have developed quantitative techniques to non-invasively assess lymphatic contractile function. A method to measure lymphatic pumping pressure was pioneered by Modi and colleagues (140). This technique utilized lymphoscintigraphy to visualize lymph flow, coupled with a pressure cuff to apply an occlusive force. They subsequently utilized this technique to demonstrate, for the first time in-vivo, that patients with arm lymphedema had lower lymphatic pumping pressure. Unno et. al. expanded upon these techniques using NIR imaging methods as opposed to lymphoscintigraphy, to demonstrate that patients with leg lymphedema also had significantly lower lymphatic pumping pressure. The frequency and velocity of fluorescence packets has also been used to demonstrate declines in lymphatic contractile activity during lymphedema and increased functional response of these vessels to MLD therapy (215).

Although NIR lymphatic imaging methods were pioneered in humans, they were quickly adapted for use in common animal research models (115, 197). These methods focused on tracking the frequency and velocity of fluorescent packets caused by the intrinsic contractile function of the lymphatics. Work by our group explored the sensitivity of these metrics to quantify the effects of known modulators of lymphatic function in the rodent tail (235). Subsequent studies developed a framework to characterize collecting vessel function in tissues that have a plurality of draining collecting lymphatics (234). More recent work has demonstrated that the amplitude of fluorescent packets correlates with the contraction amplitude of the vessels (45, 236). This has enabled non-invasive measurement of proxy metrics that quantify lymph transport driven by intrinsic contraction. As discussed

in detail within the previous section, these NIR imaging techniques have provided significant insight into collecting lymphatic function in both health and disease. Unfortunately, these methods have primarily focused on tracking and characterizing fluorescent packets or other singular metrics of collecting lymphatic performance. Thus, their use in determining collecting lymphatic dysfunction is limited. For example, there are numerous other factors that affect the overall lymph flow rate such as of contractile strength, valve performance, and vessel leakiness. Therefore, this thesis will explore the ability to non-invasively phenotype and longitudinally track a multiplicity of lymphatic failure modes in-vivo.

1.6   Specific Aims

Despite being an integral driver of lymphatic transport, relatively little is known about how lymphatic pump function and remodeling is affected following injury that results in a loss of lymphatic drainage pathways. In some cases, this loss ultimately results in chronic lymphedema whereas others do not. It is possible that predisposing factors that impact baseline lymphatic pump function become exacerbated by increased fluid loads due to surgical insult, ultimately manifesting in lymphedema. For example, in the context of obesity, impaired baseline lymphatic pump function could lead to a decline in the drainage and clearance of cells that mediate inflammation following injury. This could instigate a negative feedback loop where inflammatory cells induce adverse functional and remodeling responses from the lymphatic vessels, decreasing lymph clearance and drainage of said cells, ultimately resulting in continued lymph stasis and tissue remodeling. Alternatively, in scenarios where lymphedema does not immediately develop, it is unclear how collecting lymphatic vessels are able to alter their structure and function to compensate

18

for losses in lymphatic drainage pathways. Given that lymphedema often takes years to manifest, it is reasonable to believe that in many cases, despite initial functional compensation following surgery, the lymphatic pump becomes more susceptible to later insult or fatigue that finally induces lymphatic insufficiency. It is my central hypothesis that the collecting lymphatic vessels alter their functional and remodeling response to injury that disrupts lymphatic drainage pathways. Specifically; (1) known risk factors for lymphedema, such as obesity, will result in a greater degree of contractile dysfunction during lymphedema (Figure 1) and; (2) when lymphedema does not develop, the collecting lymphatic vessels will exhibit compensatory functional and remodeling responses (Figure 2).
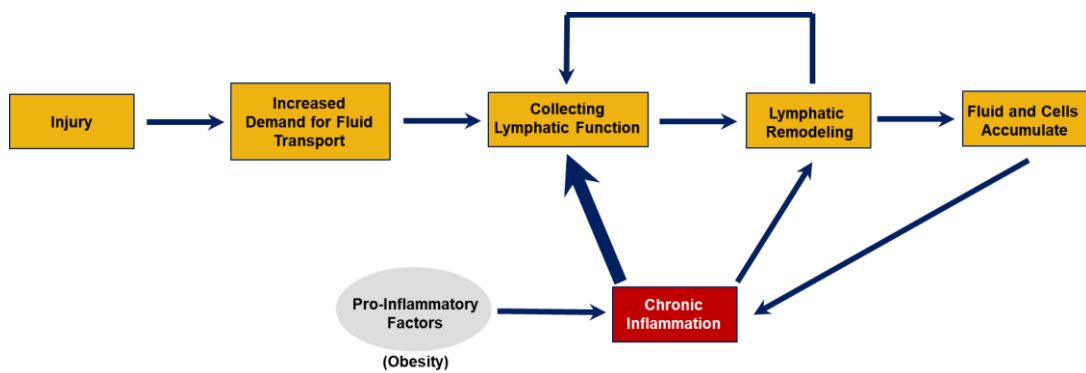
Figure 1: Flow chart summary for our working understanding of the interplay between collecting lymphatic function, inflammation, and lymphedema development
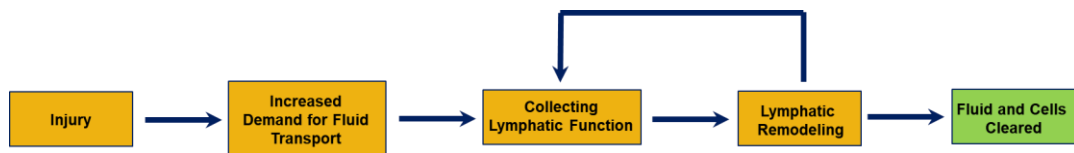
Figure 2: Flow chart summary for our working understanding of compensatory functional and remodeling responses that prevent lymphedema development

It is therefore the goal of this thesis to longitudinally determine the phenotypes of lymphatic pump dysfunction following a loss of lymphatic drainage pathways across research models with varying predispositions to lymphedema. To this end, I have outlined three specific aims of this thesis that, when complete, will; (1) Enable non-invasive phenotyping of lymphatic pump failure modes during disease; (2) Determine the effects of diet-induced obesity on collecting lymphatic pump function during lymphedema; and (3) Determine how collecting lymphatic pump function and remodeling may compensate for loss of lymphatic drainage pathways when lymphedema does not develop.

1.6.1 Specific Aim 1: Develop and validate near-infrared (NIR) imaging methodologies suitable for phenotyping collecting lymphatic pump function during disease

I hypothesize that different lymphatic pathologies will express differential and unique phenotypes of lymphatic failure. By combining NIR lymphatic imaging with a feedback controlled occlusion cuff and image processing algorithms, I will quantify multiple metrics representative of lymphatic function. These methodologies will provide the ability to phenotype a spectrum of collecting lymphatic failure modalities, allowing us to characterize changes occurring during disease pathogenesis and resolution.

1.6.2 Specific Aim 2: Determine how diet-induced obesity differentially impacts collecting lymphatic pump function and remodelling in a mouse lymphedema model

I hypothesize that diet-induced obesity adversely influences the lymphatic pump function and remodeling phenotype during the progression and resolution of lymphedema

in mice. I will investigate this hypothesis by using the methods developed in Specific Aim 1 to assess the changes in the functional phenotype of the intact collecting lymphatic vessel on the tail in response to ligation of the contralateral vessel in a mouse model of diet-induced obesity.

1.6.3 *Specific Aim 3: Determine how collecting lymphatic pump function and remodelling compensates for loss of lymphatic drainage pathways in a sheep model that does not develop lymphedema*

I hypothesize that surgical ligation of a collecting lymphatic vessel will induce a compensatory functional and remodeling response from an undamaged vessel draining the same tissue space when lymphedema does not develop. Unlike mouse lymphedema models, human lymphedema typically does not manifest immediately after surgery. Therefore, I believe that sheep, given their size similarities to humans, may provide a more clinically relevant model for assessing lymphatic pump function and remodeling response to lymphatic injury. I will utilize the techniques described in Aim 1 to non-invasively assess the functional response of the intact collecting lymphatic vessel. I will subsequently utilize ex-vivo isolated vessel techniques to quantify the remodeling response of the vessels.

CHAPTER 2. DEVELOPMENT OF NEAR-INFRARED IMAGING METHODOLOGIES FOR LYMPHATIC DISEASE PHENOTYPING (AIM 1)

2.1 Introduction

As discussed in the previous chapter NIR imaging methodologies have been used to show differences in lymphatic function and architecture in patients and animals with lymphedema, as well as evaluate acute response to manual lymphatic drainage. Despite this, most functional assessments of lymphatic health have focused on measuring the frequency of fluorescence packets, which has been correlated to the frequency of lymphatic contractions (236). Contractile frequency is only one factor that affects overall lymph transport, and thus its use in determining lymphatic dysfunction is limited. For example, there are numerous other factors that affect the overall lymphatic function such as of contractile strength, valve performance, and vessel leakiness. To fill this gap, we set out to develop and validate new methods to quantify other modalities that contribute to lymphatic transport. In doing so, we can utilize a plurality of metrics in tandem to distinguish between different underlying causes of lymphatic pump failure non-invasively. This provides a powerful toolset for diagnosing specific failure modes that may be involved in the development of lymphatic disease.

Considering the wealth of information about cardiovascular health that measurements of blood pressure provide, it is reasonable to assume that a measurement of lymphatic pumping pressure would provide similar levels of insight about the health of the

lymphatic system. While pumping pressure of lymphangions has been measured *in situ* (21, 87), the ability to obtain a minimally invasive measurement of the pumping capacity of the lymphatic network in vivo would be an invaluable tool, especially for longitudinal studies on disease progression. Excitingly, two important developments had been made in this regard. By utilizing a manually operated pressure cuff to occlude lymphatic flow, deflating the cuff, and then measuring the pressure at which flow is restored by visualizing lymphatic transport with either lymphoscintigraphy (140) or NIR imaging (226, 228), researchers were able to approximate lymphatic pumping pressure; however, these techniques were developed in humans and are thus unsuitable for comprehensive study of the pathophysiological progression of lymphedema in a lab-based setting. Moreover, these previous studies had only measured the lymphatic pumping pressure at a single location on the limb without consideration to how pressure may vary along the longitudinal axis due to the intrinsic contraction of lymphangions in series.

This initial portion of this chapter discusses the development of a novel research platform to determine the effective lymphatic pumping pressure (P_{eff}), packet restoration pressure, and emptying rate in rodents with minimal invasiveness by incorporating a closed-loop feedback system to control the occlusion pressure applied to the lymphatic vessel while simultaneously recording lymph transport with NIR imaging. We established the technique with the rat tail model, which was chosen because of the symmetry and anatomical consistency of the two collecting lymphatic vessels that drain along the sides of the tail. Additionally, the rodent tail is one of the most widely used animal models in lymphatic research and has provided remarkable insight into basic lymphatic physiology (22, 118, 210, 235), lymphangiogenesis (29, 49, 80, 248) and lymphedema pathology (11,

186, 211, 250). In fact, the rodent tail is likely one of the more clinically relevant locations to assess collecting lymphatic function. This is because the tail is an anatomic location on the rodent with collecting lymphatics that are composed of relatively long chains of lymphangions in series in a manner similar to those found in human limbs. We hypothesized that these lymphangion chains have the physiologic function of increasing lymph outflow pressure to overcome the hydrostatic pressure gradients found in the body. Therefore, we measured P_{eff} at multiple locations along the rodent tail to establish if a greater number of lymphangions in series produced greater values of P_{eff} in the proximal portions of the vessels.

To determine the role that a known collecting lymphatic contractile mediator plays in modulating pressure generating ability, we applied a dermal nitric oxide (NO) donor ointment to the rat tails. NO has been shown to be a regulator of lymphatic function in several pathophysiologic or inflammatory conditions (2, 98, 117, 123, 180). Additionally, NO has been implicated in the inhibition of the intrinsic contractile capabilities of isolated lymphatic vessels (73, 139) and the slowing of lymph transport and reduction of lymphatic contractile frequency in vivo (190, 235). Based on these studies we hypothesized that the application of dermal NO donor ointment would reduce the observed P_{eff} values obtained using our system and thus, demonstrate that our method is sufficiently sensitive to detect alterations of lymphatic function in vivo in a minimally invasive fashion.

After developing and validating these methods, we utilized the entirety of our NIR imaging "suite" to phenotype the unique lymphatic failure modes involved in varying lymphatic pathologies. To accomplish this, we utilized two models that were known to possess lymphatic abnormalities, but with unknown failure modes, and thus unknown

24

levels of the severity of dysfunction. These include a mouse knockout model lacking lymphatic endothelial epsins (LEC-DKO) and a mouse model of diet-induced obesity.

Post developmental lymphangiogenesis is critical for the maintenance, remodeling, and regeneration of the initial and collecting lymphatic vessels. The VEGF-C/VEGFR3 signaling axis is a crucial regulator of this process; however, whether alterations in this signaling axis significantly contribute to impaired collecting lymphatic function are not clearly understood. Recent studies have uncovered an important regulatory role for the ubiquitin-binding clathrin-mediated endocytic adaptor family of epsins in the downregulation of VEGF-C/VEGFR3 signaling (125). Loss of lymphatic endothelial epsins has been shown to result in aberrant lymphangiogenesis and delayed pre-natal and early post-natal collecting lymphatic valve development. Despite these early defects, LEC-DKO mice matured into phenotypically normal adults. Although seemingly normal, LEC-DKO mice exhibit more tail swelling and delayed resolution of swelling upon induction of lymphedema (unpublished data). Therefore, we hypothesized that LEC-DKO mice have impaired baseline collecting lymphatic function and subsequently sought to prove or disprove the validity of this hypothesis using our NIR lymphatic imaging techniques to phenotype collecting lymphatic pump function in adult LEC-DKO mice.

As discussed in the previous chapter, obesity is strongly associated with lymphatic dysfunction and the subsequent development of lymphedema. The prevailing hypothesis for this association is that obesity impairs baseline function due to T-cell mediated inflammation, thus positively influencing the development of lymphedema upon injury to the lymphatic vasculature (27, 192, 222). Previous studies supported this hypothesis by demonstrating that obese mice had decreased collecting lymphatic contraction frequency

compared to normal body weight controls (27); however, no studies had characterized other metrics of lymphatic pump performance. Because of this, it was unclear if obesity negatively influenced collecting lymphatic function outside of its effects on contraction frequency. To this end, we utilized our NIR lymphatic functional imaging techniques to phenotype collecting lymphatic function in obese mice.

2.2 Materials and Methods

2.2.1 *Pressure cuff controller*

A closed-loop pressure cuff system was designed utilizing a commercially available pressure cuff (Kent Scientific, Torrington, CT) (Figure 3). The pressure cuff was attached to a 5 mL BD luer-lock syringe via plastic tubing (1/16" ID, 1/8" OD) and to a pre-calibrated pressure transducer (Honeywell Sensing and Control, Morristown, NJ) via a plastic barbed T-fitting and additional plastic tubing (1/8" ID, 1/4" OD). The pressure transducer was connected to a data acquisition (DAQ) device (National Instruments (NI), Austin, TX) and pressure values were read in LabView. The pressure transducer was factory calibrated, but calibration was confirmed via a water column. A customized LabView virtual instrument (VI) (NI, LabView 2012 32-bit) was used to control the serial command output to the syringe pump (Harvard Apparatus PHD 2000 Infusion/Withdraw 70-2001). Pressure transducer readings were sampled at 10 Hz and passed through a 5 point simple moving average filter. The difference between the desired pressure and the sampled pressure was used to control the flow rates on the syringe pump to subsequently inflate or deflate the pressure cuff. This was accomplished using simple on-off control. If the absolute pressure difference between the desired and sampled pressures was greater than 7

mmHg then a "high" infuse or refill flow rate of 1.00 mL/min was sent to the syringe pump. If the absolute pressure difference was less than 7 mmHg then a "low" infuse or refill flow rate of 0.25 mL/min was sent to the syringe pump. This allowed for a quicker response when the difference between the desired and measured pressure was large and a slower, finer response when it was small which minimized overshoot. These prescribed flow rates were used to modulate displacement of the syringe, thereby altering the volume and pressure of air inside the closed-tube system, and thus the pressure applied through the occlusion cuff to the tail or forelimb.
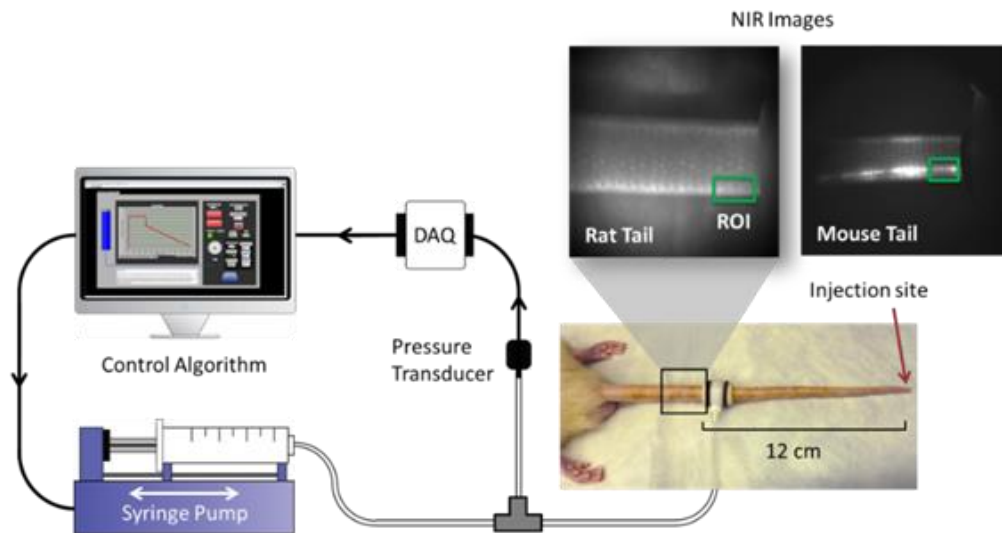
Figure 3: An automated, integrated, feedback-controlled, lymphatic pumping pressure and imaging system with user interfaces serves as a powerful toolset for assessing lymphatic physiology. A schematic of the pressure cuff system including labeled depictions of its various components is shown. (Top right) A sample near-infrared image of a rat and mouse tail with an example ROI identified. The pressure cuff can be seen at the right of the image. While two lymphatic vessels are visualized along the sides of the tail, the excitation source was focused on the lower vessel, which was used for quantification. (Bottom right) Bright field image of the pressure cuff placed on the rat tail as well as the ICG injection site.

Aided by the real-time feedback of the pressure transducer, the closed-loop system allowed for steady-state tracking of the desired pressure with an overall root mean squared (RMS) steady state error of 0.48 mmHg excluding the initial ramp-up to 80mmHg (Figure 4). Fluctuations at steady state were mostly due to noise in the pressure transducer measurements. The rise and fall times were fast enough for accomplishing the purposes of this experiment while avoiding significant undesirable overshoot. Overdamping of the system was acceptable since the slight increase in time to reach a desired pressure value would not significantly affect the total duration of the experiment.
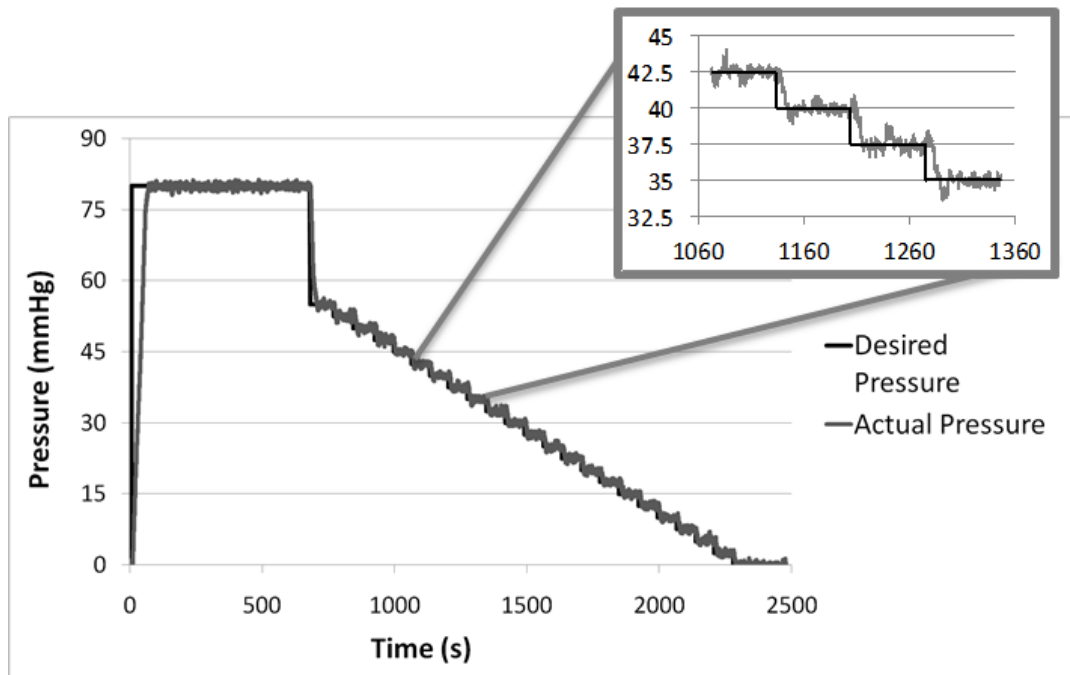
Figure 4: Feedback-controlled pressure curves are applied to the tail with sufficient precision and speed. The pressure curve used to apply pressure during each experiment is shown. The exploded image shows the close tracking of the filtered actual pressure to the desired pressure. Root mean squared error (RMSE) for the entire pressure curve (disregarding the initial ramp up to 80 mmHg) for this curve is 1.821 mmHg. Steady RMSE during the 10 minutes at 80 mmHg is 0.477 mmHg. The actual pressure data was filtered throughout the experiment using a 5 rank mean filter. The reported mean squared errors are based on this filtered data.

2.2.2 Near-infrared imaging system

The NIR imaging system was set-up as described previously (235). A diode driver and temperature control box powered a 1 W 808 nm laser diode (Thorlabs, Newton, NJ), which provided excitation light. To disperse the laser over a larger area of approximately 75 cm^2 with less than 1.9 mW/cm^2, a 20 degree beam diffuser (Thorlabs, Newton, NJ) was fixed in front of the diode. An Infinity K2/SC video 2.15x magnification microscope lens (Edmund Optics, Barrington, NJ) and a bandpass filter (CW: 840 nm, FWHM: 15 nm, Omega Optical, Brattleboro, VT) were attached to a PIXIS 1024B back-illuminated CCD camera (Princeton Instruments, Trenton, NJ) to capture fluorescence emission centered at 840 nm. These wavelengths were chosen based on previous work that showed that ICG undergoes a spectral shift when it binds to albumin (235). The camera was connected to the same computer as used for the pressure cuff system, where the images were acquired by an additional custom LabView VI.

2.2.3 Measurement of effective lymphatic pumping pressure in-vivo

A standardized procedure was carried out on 9 week old male Sprague Dawley (Charles River, Wilmington, MA) rats. In order to minimize light scattering, a depilatory lotion was used to remove hair in the region of interest on the tail or forelimb one day prior to experimentation. Rats were anesthetized with an intramuscular injection of diazepam (2.5 mg/kg) followed by a cocktail of fentanyl (0.12 mg/kg) and droperidol (6 mg/kg). After waiting for approximately 10 minutes for the anesthetics to take effect, the rat was positioned under the camera. To determine the effects of NO on lymphatic pumping pressure, some animals received a topical application of 500 mg glyceryl trinitrate ointment

(GTNO, 0.2% wt⁄wt, Rectogesic, Care Pharmaceuticals) applied to the entirety of the tail..
To confirm that GTNO ointment was not drastically altering lymph formation and dye
uptake at the injection site on the tail, an additional group of treatment animals had GTNO
ointment applied only to areas of the tail 3 cm downstream of the injection site. Control
animals received no GTNO ointment.

The pressure cuff was calibrated by removing and then reattaching the tubing
connected to the syringe to ensure that the steady state pressure was zero. The proximal
edge pressure cuff (0.7 cm ID) was placed 4 cm, 8 cm, and 12 cm from the tip of the tail at
which point the inner diameter of the cuff was uniformly touching the tail without applying
any pressure, as verified by transducer readings. For a subset of rats a larger pressure cuff
(1 cm ID) was fitted on the outstretched forelimb, past the elbow joint, with the proximal
edge of the cuff 4 cm from the phalanges. Also, the cuff was positioned on the tail or
forelimb in the same rotational orientation for each rat to compensate for any non-
uniformity in pressure application by the elastic bladder during inflation. The rat was
positioned so that the field of view was proximal to the cuff, including only the edge of the
cuff. A mixture of 30 µL of ICG/albumin solution (150 µg/mL ICG (Acros Organics, Geel,
Belgium) and 60 g/mL bovine serum albumin (MP Biomedicals, Auckland, New Zealand)
dissolved in deionized water was injected intradermally at the tip of the tail, as described
previously (235), or in the footpad of the forelimb.

Image acquisition began just prior to intradermal injection of the dye. Once steady
state fluorescence was established, more than 3 minutes after injection, a predetermined
sequence of pressure cuff applications was administered to the tail. Specifically, the
pressure was increased to 80 mmHg over a period of approximately 65 seconds and held

at this value for 10 minutes to allow for the proximal vessel to complete empty its contents. This pressure was chosen for lymph flow occlusion because 80 mmHg is close to the diastolic blood pressure of a rat and well below the mean arterial pressure, so blood supply was not occluded during the experiment (34). After 10 minutes at 80 mmHg, the pressure was decreased to 55 mmHg over a period of approximately 25 seconds. The pressure was then decreased in decrements of 2.5 mmHg and held at each pressure step for 60 seconds until the pressure value was zero, where it remained for 3 minutes before the program was terminated. The pressure cuff controller took less than 15 seconds to reach each new pressure decrement. This standardized pressure curve was used for all experiments (Figure 4).

Images of the tail or forelimb were captured by the NIR imaging system throughout the experiment at a frame rate of 1 fps with a camera exposure time of 50 ms. This frame rate has been shown to provide sufficient temporal resolutions for dynamic imaging of lymphatics (235). After the first frame was captured, the system paused to allow the user to select a region of interest (ROI) which was positioned just proximal to the pressure cuff, over the fluorescent vessel. The ROI selected for use in the data analysis was always positioned over the left vessel of the tail (Figure 5) or a lymphatic vessel residing on the front of the left forelimb. This was done both for the sake of consistency and to optimize the optics for achieving the best signal on a single vessel. The intensity plots obtained were consistent in form between all experiments. While flow was occluded at 80 mmHg, a gradual emptying of florescence within the proximal vessel was observed. Florescence was not restored until the pressure applied to the cuff was lowered and was no longer sufficient to occlude flow within the vessel (Figure 5).
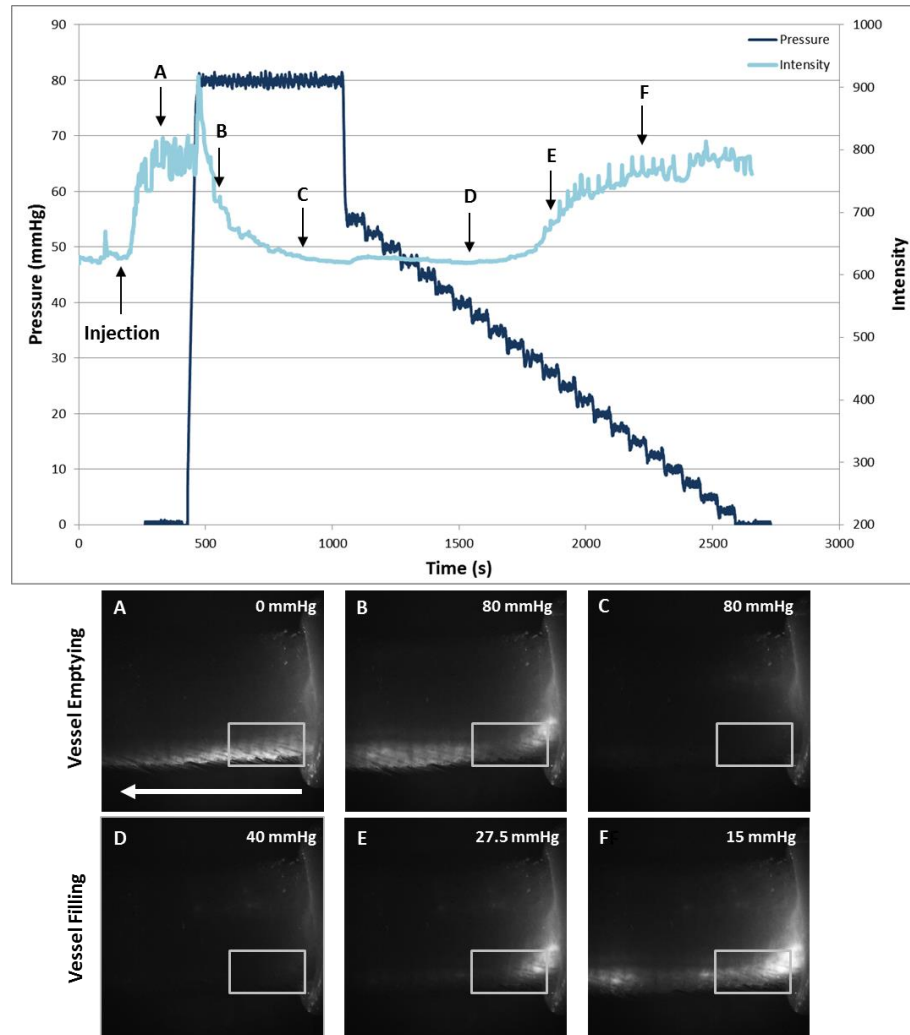
Figure 5: (Top) A representative intensity plot. The intensity spike at around 500 seconds is caused by the inflation of the pressure cuff to 80 mmHg pushing ICG dye into the region of interest (ROI). While the pressure is held at 80 mmHg the intensity within the ROI drops as the vessel is cleared of dye. As the pressure cuff is deflated using the control algorithm, the intensity within the ROI rises, indicating the beginning of flow restoration. Eventually, flow is completely restored within the vessel and intensity plots exhibit typical packet flow. (Bottom) Time lapse images at various time points (A-F) in an experiment showing dye emptying from the vessel during flow occlusion and dye filling the vessel as flow is restored. The pressure cuff can be seen on the right side of the time lapse images. The arrow in image A indicates the direction of lymph flow from the distal to proximal portions of the tail (upstream to downstream).

In order to confirm that GTNO did not have significant effects on the arterial blood pressure (ABP) we measured ABP in four animals pre and 20 minutes post GTNO application. ABP was measured using a Non-Invasive Blood Pressure Monitor NIBP-8 (Columbus Instruments, Columbus, OH). All animal procedures were performed in accordance with the Georgia Institute of Technology Internal Animal Care and Use Committee and complied with National Institutes of Health Guide for Care and Use of Laboratory Animals.

2.2.4 *Image processing*

Three primary measurements were taken from each intensity plot and pressure curve combination using customized data analysis algorithms written in MATLAB. The first was P_{eff}, which was calculated using two points: the minimum intensity value before flow restoration and the maximum intensity value after flow restoration. The average of these two values was the intensity threshold for flow restoration. The pressure at the time where the intensity rose to equal the intensity threshold was P_{eff} (Figure 6). The second parameter determined was the "packet restoration pressure". NIR imaging of lymphatic uptake produces discrete packets of fluorescence that travel through the vessel as a result of the intrinsic contractility of the lymphatic vessels working in coordination with lymphatic valves. The frequency of these packets has previously been reported as a measurement of lymphatic function (235). To determine the pressure at which packet flow was restored in the lymphatic vessel, a fast Fourier transform (FFT) was used to calculate the power spectral density (PSD) of the intensity signal in the frequency range of 0.06 – 2 Hz prior to flow occlusion (before 80 mmHg) and after complete flow restoration (at 0 mmHg). Since packet frequency can be somewhat variable even in non-occluded vessels, the PSD was

used to calculate the magnitude of the spectral content within this frequency range to provide a measure of contractile activity. The point at which this value recovered to 50% of its non-occluded value was indicative of the restoration of packet flow. The packet restoration metric was used to identify the pressure when packets were evident that rivaled those seen during uninhibited flow (Figure 6). The third parameter was the average "emptying rate" of the vessel during flow occlusion, the average rate of fluorescence intensity decrease as the proximal vessel emptied during the period when the pressure was raised and held at 80 mmHg (*ER*, Figure 6). To calculate the average emptying rate of the vessel two time points were used: the time of maximal fluorescence at the beginning of flow occlusion and the time at which the intensity fell within 5% of the minimal steady state value during flow occlusion. The average emptying rate was then calculated as the difference in intensity over the difference in time between the two points. The values for Peff, packet restoration pressure and emptying rate were averaged for the treatment and control groups and checked for statistical significance using a two-tailed unpaired t-test.
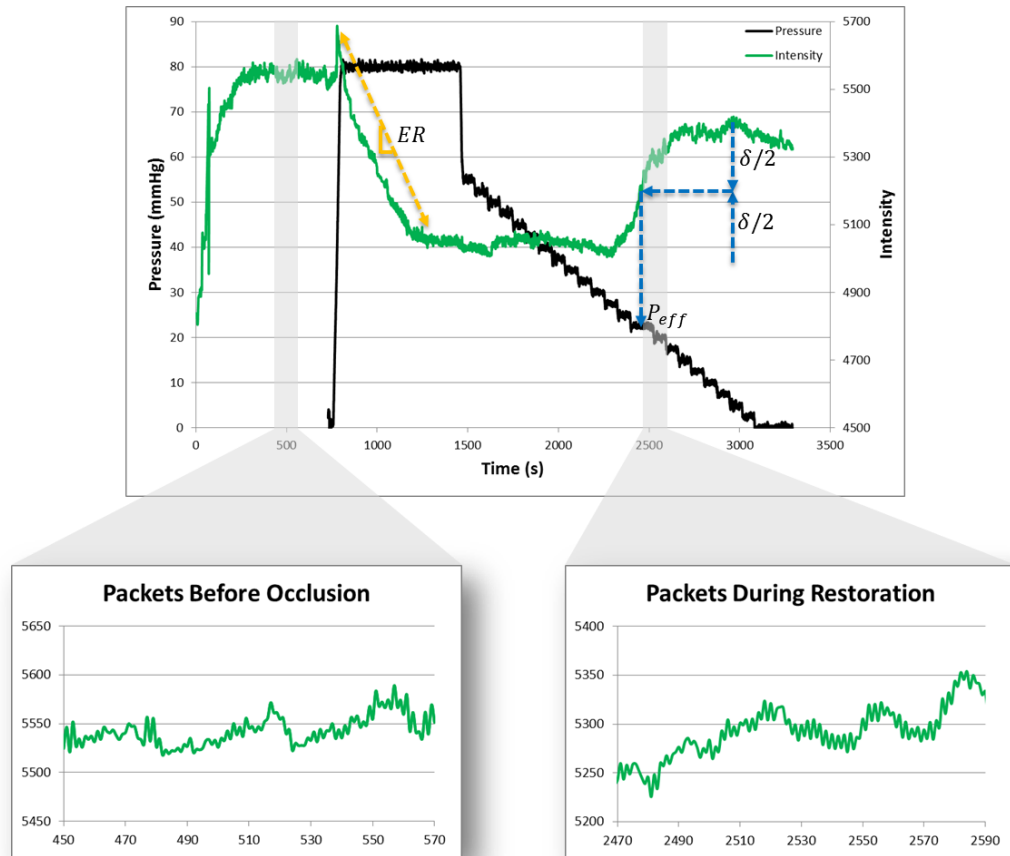
Figure 6: (Top) Overlaid pressure and intensity plots demonstrate the calculation of the effective pumping pressure (P_{eff}) and the emptying rate (ER). Typical pack flow that is present before the beginning of flow occlusion (bottom left) is recovered after occlusion (bottom right). To quantify the point at which packet flow was restored, the time at which the magnitude of the power spectral density function (PSD) recovered to a specified value was calculated as described in the methods section.

2.2.5 Assessment of lymphatic function in disease models

2.2.5.1 <u>Lymphatic endothelial cell epsin knockout</u>

Lyve-1 EGFP-hCre mice were purchased from Jackson Laboratory (Bar Harbor, ME) (166). Epsin1fl/fl; epsin 2-/- ; Lyve-1-Cre (LEC-DKO) were generated by crossing epsin 1fl/fl; epsin 2-/- mice with Lyve-1-Cre mice as previously described (125). 8-10 week old LEC-DKO or WT animals underwent NIR functional imaging procedures as previously described (149, 234, 235). However, an additional functional metric, fluorescence area, was developed to quantify the relative amount of initial lymphatic recruitment in fluid transport. Fluorescence area was calculated by converting the 16-bit greyscale images that were captured during the 10 min imaging segment following fluorophore injection to binary images. The binary threshold was determined by cluster based thresholding using Otsu's method over the entire imaging segment. The total area of pixels above this threshold was calculated and then normalized by the total area of the tail. This yielded the percentage of the tail positive for fluorescence as a function of time. The raw data was then passed through a set of smoothing filters to exclude frames captured during tail movement to limit motion artifact noise. Specifically, the percent fluorescence area signal was discretized into 100 bins of 6 frames. The highest 2 values within these bins was averaged to generate an upper envelope of the percent fluorescence area signal. This upper envelope of the time dependent signal was then fit with a 4-point locally weighted linear least squares regression. The resulting smoothed percent fluorescence area curve was used for expression of percent fluorescence area as a function of time. All experiments using the LEC-DKO model were conducted at the Oklahoma Medical Research Foundation (OMRF) and approved by the OMRF Institutional Animal Care and Use Committee (IACUC).

2.2.5.2 <u>Diet-induced obesity</u>

Six week old male C57BL/6J (Jackson Laboratories, Bar Harbor, Maine) mice were fed either a high fat diet (60% kcal from fat; W.F Fisher & Son, Inc., NJ) or a normal chow diet ad libitum for 12 weeks (191). To facilitate easy access to food, the diet was placed in a dish within the cage as opposed to overhead. At the end of this period chow fed and diet-induced obese animals underwent the NIR functional imaging procedures as previously described (149, 191, 234, 235). These procedures were approved by the Georgia Institute of Technology Institutional Animal Care and Use Committee (IACUC).

2.3 Results

2.3.1 *Nitric oxide reduces lymphatic pumping pressure and emptying rate*

Nitric oxide, via application of the GTNO ointment, significantly reduced P_{eff} of the lymphatics in vivo from 34.8 mmHg to 18.5 mmHg as determined by the functional NIR imaging system ($p<0.05$) (Figure 7). Additionally, GTNO significantly reduced the average packet restoration pressure from 40.3 mmHg to 18.4 mmHg ($p<0.005$). There was no statistical difference between the two different metrics of lymphatic pumping pressure (Peff and packet restoration pressure) for either control or GTNO-treated animals. GTNO application also caused a significant decrease in the emptying rate of fluorescence from the proximal vessel of the cuff after occlusion: from 6.15 IU/s to 2.19 IU/s ($p<0.05$) (Figure 8). To determine the extent that the decreases in lymphatic pump function might have been caused by changes in lymph formation due to the effects of GTNO on blood pressure and/or capillary permeability, rather than due to the direct action of NO on lymphatics, GTNO application was restricted to areas 3 cm downstream of the injection site in a subset of rats.

No differences were observed in Peff, packet restoration pressure, or emptying rate between rats with GTNO applied to the whole tail and those with the altered application protocol (Figure 9). Since no statistical difference was observed between these two treatment groups, they were grouped together in the comparison between GTNO and control (Figure 7) and (Figure 8). In order to determine if dermal NO application may have altered arterial blood pressure in the tail, blood pressure in a subset of rats (n = 4) was measured before and 20 minutes after GTNO application. Mean tail blood pressure was found to be $80/48 \pm 18/14$ mmHg for the control group vs $97/56 \pm 12/8$ mmHg for the GTNO treated group. No statistical differences were observed in either systolic or diastolic arterial blood pressure in the tail as a result of GTNO application.
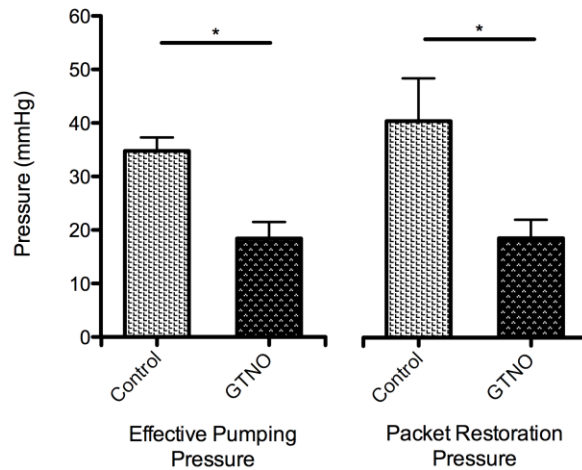
Figure 7: Dermally applied nitric oxide significantly reduced both the Peff and packet restoration pressure of the lymphatics (p<0.05) and (p<0.005). The treatment group received 500 mg GTNO ointment applied to the tail (n=12). The control group received no GTNO ointment (n=5). Error bars represent SEM.
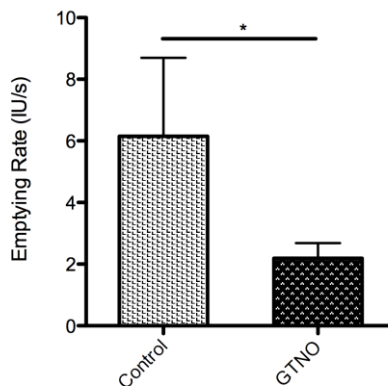
Figure 8: Dermally applied nitric oxide significantly decreased the average rate of emptying of the lymphatic vessel (p<0.05). The treatment group received 500 mg GTNO ointment applied to the tail (n=12). The control group received no GTNO ointment (n=5). Error bars represent SEM.
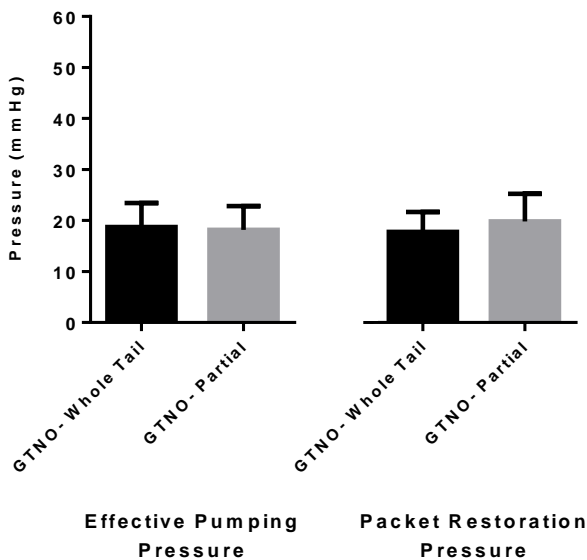
Figure 9: The location of GTNO ointment application did not significantly impact effective lymphatic pumping pressure or packet restoration pressure. 500 mg GTNO ointment was applied to the entire tail (GTNO- Whole Tail) (n= 12) or was restricted to a portion of the tail 3 cm distal to the injection site of fluorophore (GTNO- Partial) (n= 4). Error bars represent SEM.

2.3.2   Effective lymphatic pumping pressure is dependent on measurement location

To demonstrate the feasibility of our method to be used on other anatomical locations more relevant to human pathologies we measured Peff, packet restoration pressure, and emptying rate on the forelimb of rats. Interestingly, when the cuff was placed on the left forelimb 4 cm from the phalanges the measured Peff and packet restoration pressure values of 14.9 mmHg and 14.7 mmHg were not significantly different from the values obtained from measurements taken 4 cm from the tip of the tail but were 2-3x less than the values collected at 12 cm on the tail ($p<0.01$) and ($p<0.05$) (Figure 10). The average emptying rate of vessels on the forelimb was found to be 2.08 IU/s.

Because the average P_{eff} on the forelimb was discovered to be significantly lower than the tail, we sought to determine the extent to which the location of the pressure measurement affected our metric. To investigate this, we positioned the proximal edge of the cuff and the imaging frame 4 cm from the tip of the tail. When functional measurements were taken at 4 cm, the Peff decreased to 15.2 mmHg from 34.8 mmHg ($p<0.01$) in the control animals which were measured at 12 cm from the tip of the tail (Figure 10). A similar trend was observed in the packet restoration pressure which decreased to 11.6 mmHg from 40.3 mmHg ($p<0.05$) (Figure 10). The average emptying rate obtained 4 cm from the tip of the tail was 6.60 IU/s which was not statistically different from values obtained at 12 cm.
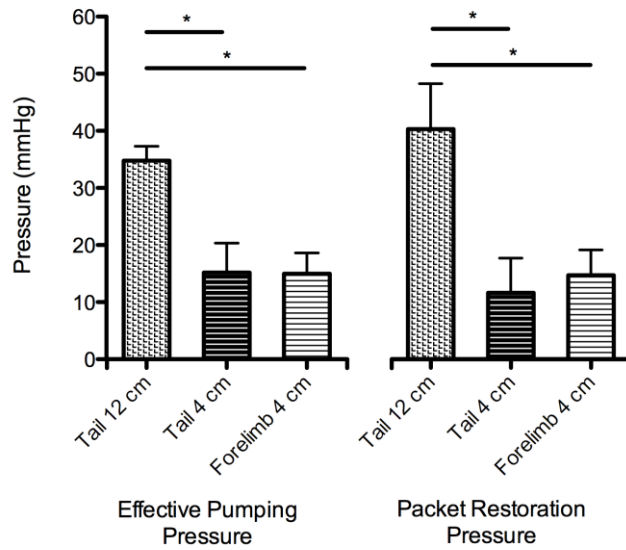
Figure 10: When measurements were taken at 4 cm (n=3) from the tip of the tail versus 12 cm (n=5) a significant decline in the P_{eff} and packet restoration pressure was observed (p<0.01) and (p<0.05). P_{eff} and packet restoration pressure values obtained on the forelimb (n=5), 4 cm from the phalanges, were not significantly different from those obtained 4 cm from the tip of the tail. Values of P_{eff} and packet restoration pressure on the forelimb were significantly different from those obtained at 12 cm from the tip of the tail (p<0.005) and (p<0.05). Forelimb measurements exhibit very little difference in variability from measurements taken on the tail. Error bars represent SEM.

2.3.3 *Effective lymphatic pumping pressure is dependent on lymphangion chain length*

We hypothesized that the length of the collecting lymphatic vessel influenced the pressure measurement due to a relative increase in the number of lymphangions contracting in series. We subsequently investigated this by taking measurements of P_{eff} at 4, 8, and 12 cm from the distal tip of the tail. We discovered that P_{eff} in the rat tail progressively increases along the length of the tail as one moves from the tip of the tail towards the base (Figure 11). Specifically, the average pumping pressure for each group of rats was 15.2 ±

41

5.17 mmHg (n=3), 21.3 ± 5.06 mmHg (n=4), and 34.8 ± 2.52 mmHg (n=5) at distances of 4 cm, 8 cm, and 12 cm from the tip of the tail respectively (Figure 11).

When GTNO was applied to the tails, the average pumping pressure for each group of rats was found to be 10.3 ± 4.02 mmHg (n=4), 12.43 ± 5.80 mmHg (n=3), 18.54 ± 3.4 mmHg (n=12), and distances of 4cm, 8cm, and 12 cm from the tip of the tail, respectively. Comparing to control and GTNO data sets using the extra sum of squares F-test on the quadratic best-fit regressions of the data revealed that the two groups are statistically different ($p < 0.05$) (Figure 11). Interestingly, the effect of GTNO treatment was much more pronounced when the measurement was taken at 12 cm, which is likely due to the increased contribution of the intrinsic lymphatic pump to generate pressure in the more proximal portions of the lymphatic vessel.
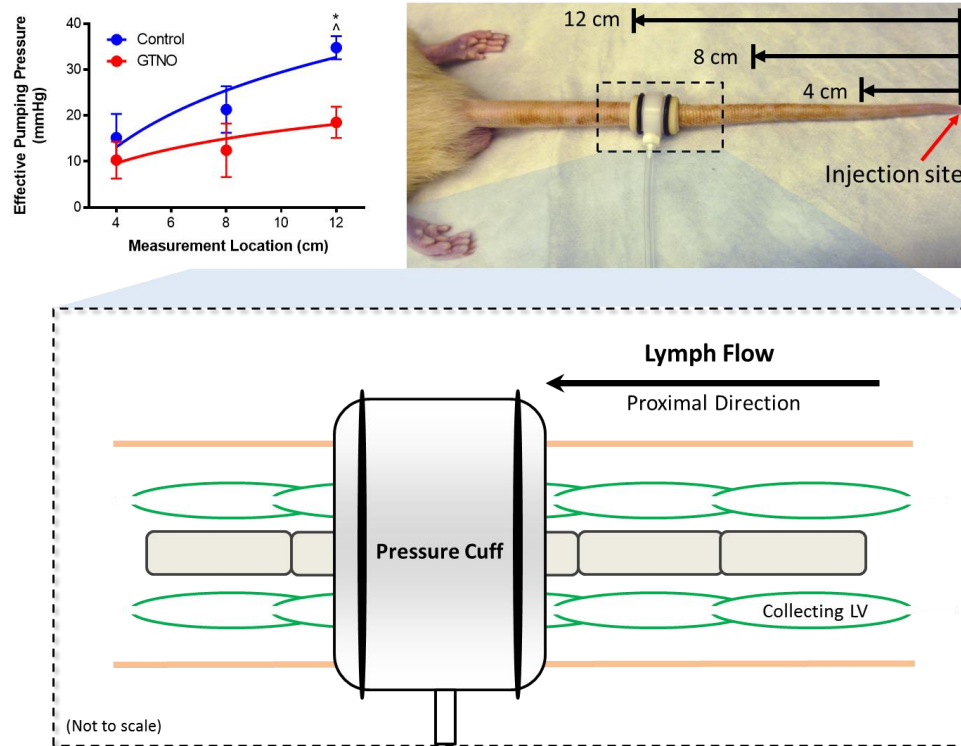
Figure 11: (Top Left) The effective lymphatic pumping pressure increases moving proximally along the tail. GTNO application attenuates this pressure increase (*- denotes significant difference between control and GTNO, p<0.05) (^- denotes significant difference between control at 4 cm and 12 cm, p<0.05). (Top Right and Bottom) Experimental set-up for measuring lymphatic pumping pressure. The pressure cuff is positioned at various locations measured from the tip of the tail. Flow restoration is imaged by capturing the return of fluorescence into the collecting vessel in a region proximal to cuff

2.3.4 *Lymphatic diseases produce unique functional phenotypes*

By combining the pressure cuff techniques described in the prior sections with previously developed methods designed to measure lymphatic contractile function, we enable a more comprehensive assessment of collecting lymphatic health and disease. The combination of these performance metrics is used to generate a unique phenotype of collecting lymphatic function in-vivo (Table 1). This is important for providing novel

insight into how lymphatic diseases differ across etiologies and at different stages of disease progression. The results of the LEC-DKO and diet-induced obesity studies highlight how these phenotyping techniques provide novel insight into the previously uncharacterized spectrum of lymphatic disease.

Table 1 – Summary of the NIR imaging suite used for phenotyping collecting lymphatic dysfunction in the LEC-DKO and diet-induced obesity studies

NIR Functional Metric	Relation to Lymphatic Physiology	Measurement Method
Packet frequency	Intrinsic collecting lymphatic contractile frequency	Number of distinct fluorescent "packets" observed passing through a ROI per minute
Fluorescence area	Relative degree of reliance on the collecting lymphatic vessels vs the initial lymphatics to drain a fluid bolus (higher values indicate a greater reliance on the initial lymphatics to compensate for a lack of collecting lymphatic transport)	Percentage of the tissue positive for fluorescence relative to the total area of the tissue
Effective pumping pressure	Maximal outflow pressure of the lymphatic vessel generated by a combination of intrinsic contraction and extrinsic factors	Pressure at which lymphatic flow is restored upon deflation of the pressure cuff after flow was occluded at 80 mmHg
Emptying rate	Relative rate of fluid ejection when upstream factors that drive flow are negated	Rate of florescence removal from the lymphatic vessel while upstream flow is occluded by the pressure cuff at 80 mmHg

2.3.4.1 <u>Loss of lymphatic endothelial epsins adversely affects collecting lymphatic</u>

        <u>function</u>

Collecting lymphatics in LEC-DKO mice exhibited no discernable anatomical differences in vessel morphology, as assessed by whole mount immunofluorescence staining (125), but appeared to present significant functional deficiencies when assessed using our NIR functional phenotyping techniques. The qualitative differences in fluorescence transport, between control and LEC-DKO mice, were striking. On the tail of control mice, ICG was quickly transported post-injection by the collecting lymphatic vessels, reaching steady state fluorescence within 5 min (Figure 12). On the tails of LEC-DKO mice faint uptake of ICG was observed in collecting lymphatic vessels within 5 min, however at 10 min significant recruitment of the initial lymphatic network, not seen in control mice, was observed (Figure 12). More quantitatively, in control mice a spike in percent fluorescence area, corresponding to collecting vessel uptake of ICG, occurred 30 s post-injection, reaching steady state at 100 s. Uptake by the initial lymphatic network in control mice was not observed, and thus the average percent fluorescence area of the tail for the 10 minute period was 9.5%. In LEC-DKO mice a rise in percent fluorescence area, corresponding to collecting vessel uptake, did not occur until about 90 sec post-injection. Interestingly, a steady rise in percent fluorescence area, corresponding to transport of ICG by the initial lymphatics, was observed throughout the 10 minute period. Because the initial lymphatic network exhibits significant amounts of fluorescence, over large portions of the tail, the average percent fluorescence area of the tail for the 10 minute period was 20.6%. After 10 minutes mean percent fluorescence area of the tail for control and LEC-DKO was 8.1% and 36.4% respectively.

Loss of epsins adversely affected collecting lymphatic vessel function in the mouse tails as assessed by NIR functional lymphatic imaging. Fluorescence packet frequency of collecting lymphatics in the tails of control and LEC-DKO mice was 1.1 min^{-1} vs 0.0 min^{-1} (p< 0.05) respectively (Figure 12). Upon lymphatic flow occlusion, with the pressure cuff at 80 mmHg, significant differences, between control and LEC-DKO mice, in vessel emptying rate were observed. The emptying rate of the collecting lymphatic vessels on the tail for control and LEC-DKO mice was found to be 1.02 IU/s vs -0.32 IU/s (p< 0.001) (Figure 12). Because the lymphatic vessels of LEC-DKO mice did not clear their contents during upstream occlusion, as assessed by the emptying rate metric, effective pumping pressure was unable to be measured. In control mice the effective pumping pressure of the lymphatics was found to be 16.8 mmHg on average (Figure 12).
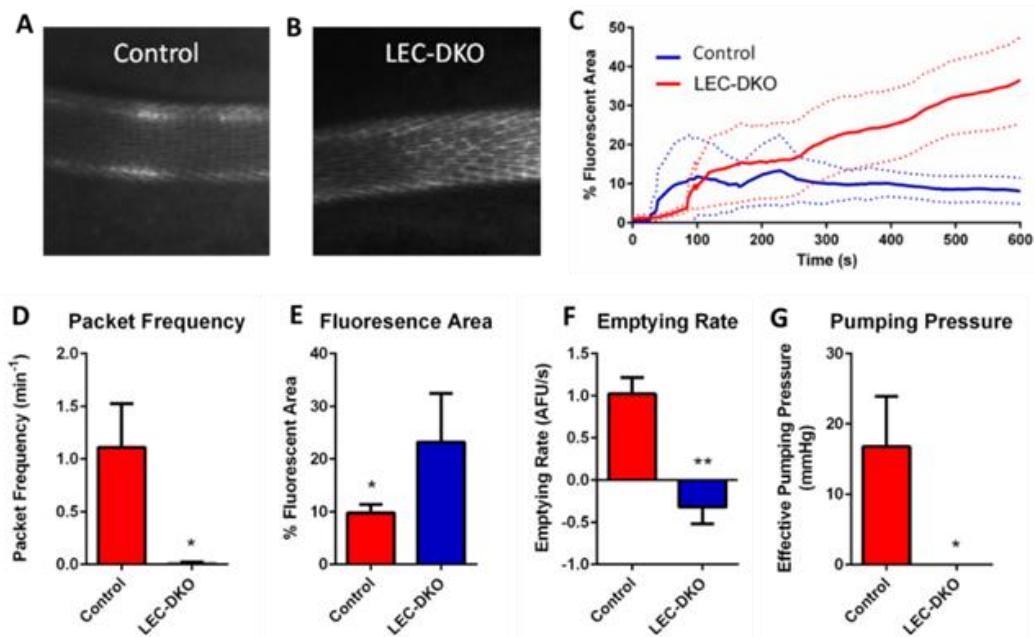
Figure 12: LEC-DKO mice exhibit significantly impaired lymphatic function. (A-B) LEC-DKO mice exhibit abnormal recruitment of the initial lymphatic network to transport fluid to compensate for deficiencies in collecting lymphatic function. This result is quantified in (E) (p<0.05). (D) LEC-DKO mice exhibit significantly lowered

packet frequency (p<0.05). (F) Due to the valve malformations in the lymphatics of LEC-DKO mice, the lymphatics are unable to prevent backflow, and thus results in a negative emptying rate (p<0.01). (G) LEC-DKO mice exhibit no detectable pumping pressure, indicating that the lymphatic contractile strength is impaired (p<0.05). Error bars represent SEM

2.3.4.2   Obesity causes significant decreases in lymphatic contractile frequency

C57BL6J mice placed high fat diet (60% kcal from fat) for 12 weeks exhibited significant increase in body weight compared to chow fed controls with values of 55 ± 1 g and 30 ± 2 g respectively (Figure 13). Functional NIR lymphatic imaging revealed functional alterations caused by obesity. Packet frequency was significantly decreased in obese animals compared to control with values of 2.6 ± 1.6 min^{-1} and 4.0 ± 1.7 min^{-1} respectively (p<0.05) (Figure 13). However, fluorescence area, emptying rate, and pumping pressure did not significantly differ between obese and chow fed control animals.
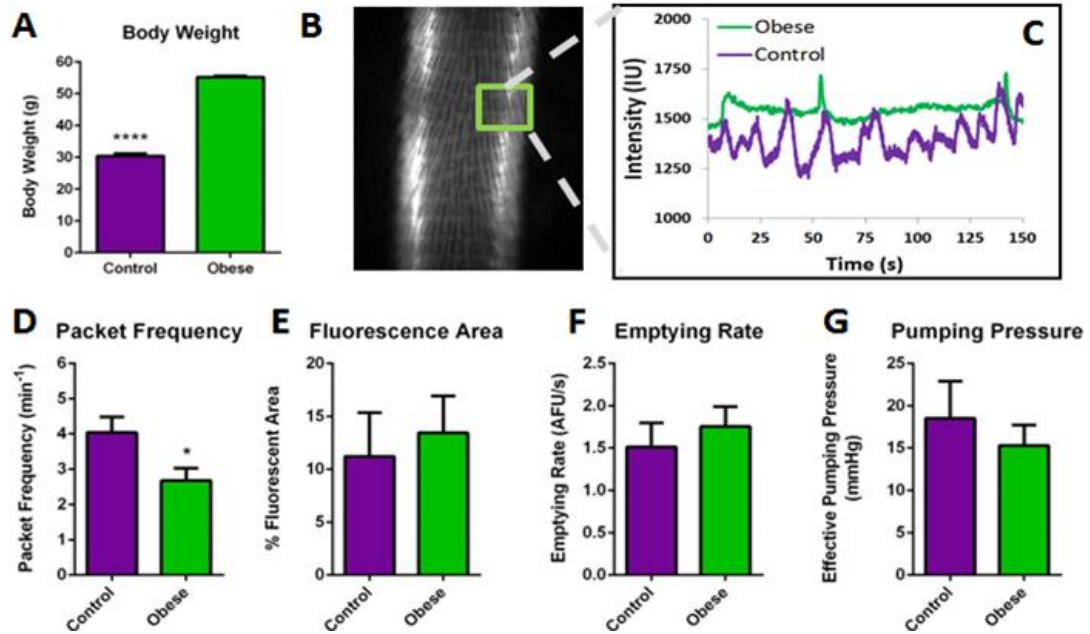
Figure 13: NIR imaging was used to evaluate lymphatic function of obese mice. (A) C57BL/6 mice exhibit significant weight gain on a 60% fat diet compared to chow fed controls (p<0.0001). (B) Representative NIR images of a mouse tail showing the two parallel collecting lymphatic vessels. (C) Representative intensity tracking showing differences in the frequency of fluorescence pulsations between lean and obese mice. (D) Obesity causes significantly lower packet frequency (p<0.05). (E-G) No statistically significant differences were observed in fluorescence area, emptying rate, or pumping pressure. Error bars represent SEM.

2.4   Discussion and Conclusions

2.4.1   *Lymphatic pumping pressure is a novel metric that enables greater insight into collecting lymphatic physiology and pathophysiology*

The ability to monitor pressure and hemodynamics in the blood circulation has been crucial for both assessing vascular health in a clinical setting and for probing the molecular mechanisms that regulate vascular biology in a laboratory setting. Development of technologies that enable similar measurements in the lymphatic vasculature in a non-

48

invasive or minimally invasive fashion, such as those reported here, have the potential to make a substantial impact on the future of lymphatic research and patient care. While the general approach of using an occlusion cuff to stop lymphatic flow as a means of determining the pumping pressure was pioneered previously in humans (140, 226, 228), there are some substantial differences in the presented approach that improve the accuracy of the technique as a laboratory research tool. First, by utilizing an automated, computer-controlled, closed-loop feedback system to generate the desired pressure curves, greater precision and sensitivity were achieved than with previous manually controlled, open-loop feed-forward systems (140, 226, 228). Additionally, by combining this system with our previously optimized experimental functional lymphatic imaging platform (235), improved spatial and temporal resolutions were achieved over lymphoscintigraphy (20, 136, 140, 197).

Applying these techniques to the study of rodent lymphatic vessels has opened the door for *in vivo*, non-invasive, studies on the regulation of lymphatic pumping and pump regeneration. The simple geometry and anatomy of the lymphatic vessels in the rodent tail make this is an ideal location to measure P_{eff}. Also, the rodent tail is one of the most developed animal models of lymphedema (11, 147, 186, 211, 250), where the addition of this toolset could provide remarkable insight into lymphedema progression and pathology. By artificially elevating the external pressure applied to the exterior of the vessel using the pressure cuff, we can determine the maximal occlusive pressure the lymphatic vessel is able to overcome, P_{eff}. This pressure is much higher than previous measurements of systolic pressures in rats (21, 87) and is higher than the maximum pressure that can be overcome in isolated collecting lymphatic vessels that are exposed to an elevated output pressure

(60). However, the measurements are made almost exclusively in single lymphangions, not chains of lymphangions as was done here. Additionally, in these previous experiments the pressure applied externally to the vessel is close to zero and thus the average of the applied pressures at the inlet and outlet of the vessel equals the transmural pressure. To our knowledge there are no measurements of systolic pumping pressure of an isolated lymphatic vessel that is under an elevated external pressure. Additionally, the injection itself, while only 30 µL, could also elevate the contribution of the extrinsic factors to our pressure measurement.

Although the rodent tail does appear to have many advantages as a research tool there exists some concern that the low amount of variability we observed in our measurements is not due to the implemented feedback control of the pressure application, but rather is dependent on the unique anatomy of the tail and would not be as effective at other anatomical locations. This is of particular concern when evaluating the potential for this methodology to be used as a clinical tool. We used the forelimb to investigate other regions on the rat that could be used as a suitable measurement location. The animal-to-animal variability of P_{eff} values obtained on the forelimb was not significantly different from those obtained on the tail. This demonstrates that our methodology could be easily adapted for use in other animal models in which functional pump measurements are of interest. Interestingly, it appears that the measure of P_{eff} is far more dependent on the length of the lymphatic vessel chain being measured as opposed to the anatomical location of measurement, whereas the emptying rate metric appears to vary with anatomical location. P_{eff} values taken on the forelimb, 4 cm from the phalanges, were not significantly different

from those obtained 4 cm from the tip of the tail. This result further demonstrates the importance of vessel chain length in the transport of lymph.

2.4.2 *Lymphangion chain length and contractile strength are primary contributors to lymphatic pumping pressure*

To examine the effects of lymphangion chain length on P_{eff}, we varied the location of the cuff in relation to the tip of the tail. P_{eff} measurements taken 4 cm from the tip of the tail were 2-3x less than those obtained at 12 cm, and progressively increased along the length of tail. These increases in P_{eff} with varying measurement locations are consistent with our understanding of the measurement. P_{eff} captures the effects of the lymphatics distal to the pressure cuff to overcome occlusive force. It stands to reason that as the number of lymphangions along a lymphatic vessel increase then the overall ability of the vessel to overcome an externally applied pressure gradient will also increase.

In collaboration with other researchers, my experimental data was incorporated into a computational model of a chain of pumping lymphatics to provide insight into the nature of the pressure-length relationship that exists when measuring P_{eff} (177). This microstructurally motivated model of a chain of lymphangions was informed from biaxial testing of isolated lymphatic vessels from the rat tail. Simulations from this model suggest that maximal pressure generation of the lymphatic chain is primarily a function of the contractile force of the smooth muscle cells surrounding the lymphangions and the number of lymphangions in the chain. This result indicates that P_{eff} is a proxy measurement for the contractile force of the lymphatics in-vivo. However, this conclusion can only be drawn so long as the number of lymphangions in the chain and subsequently the measurement

51

location remains roughly consistent across different animals. This ability for the smooth muscle cells to contract and generate high outflow pressure is of great importance when considering that lymphatic must overcome large hydrostatic pressure gradients to return lymph from the interstitial space to venous circulation. However, the pressure generating abilities of the lymphatics is likely dependent on operating within a physiologically optimal range. It is possible that extra-physiological elevations in outflow pressure could induce pump overwork and subsequent lymphatic incompetency (15, 46, 59, 65, 194).

In human lymphatic vessels, long chains of lymphangions and valves must contract to drain fluid from the distal portions of the limb. Although the rodent tail has no human analogue, we believe that it provides an excellent research model for investigations relating functional metrics of lymph transport to vessel chain length. Thus, in some sense, when utilizing rodent animal models of lymphatic physiology, the tail is one of the more "physiologic" locations to capture certain aspects of lymphatic physiology, since it is the only appendage in which lymph must be transported a considerable distance.

2.4.3 *Nitric oxide decreases lymphatic pumping pressure via downregulation of intrinsic contraction*

GTNO was used to uncover the role of nitric oxide on P_{eff} and emptying rate measurements because of its known inhibitory effects on lymphatic contractility. NO has been shown to decrease the intrinsic contraction of collecting vessels *ex vivo* (76, 139) as well as decrease lymphatic transport *in vivo* (190, 235). In fact, it is becoming apparent that NO is a primary mechanism utilized by lymphatics to regulate flow. Specifically, immune-cells have been shown to release NO as a mechanism for manipulating lymphatic flow as

part of a local immune modulatory response to inflammation (32, 77, 120, 127). Also, transient changes in wall shear stress (WSS) on lymphatics lead to NO release as a means of either promoting vasodilation and reducing vascular resistance to flow during sustained WSS or possibly transiently increasing the vessel diameter as a regulatory mechanism for lymphatic pumping (31, 32, 76, 110). Based on the plethora of previous works that have demonstrated the effects of NO on lymphatic vessels, the use of a dermally applied NO donor provides an excellent pharmacological tool for modulating lymphatic function non-invasively to determine the effect of excess NO on lymphangion chain pressure generation.

In this study, we have demonstrated that our measurements of P_{eff} and emptying rate are sensitive to perturbations in lymphatic function caused by NO. Specifically, we showed that the P_{eff} was cut in half when GTNO was applied to the surface of the tails. This decrease in P_{eff} shows that the lymphatics are less able to overcome flow occlusion with increased levels of NO and are thus less effective at moving fluid up the externally applied adverse pressure gradients. It is important to note that we do not propose that P_{eff} is the actual systolic pressure of the lymphangions in the collecting vessel, but rather is a measure of the maximal externally applied pressure that can be overcome by the contributions of intrinsic and extrinsic factors which drive lymph flow. Since NO could have effects on extrinsic factors, it was important to determine if the decline in P_{eff} and emptying rate was primarily due to the loss in lymphatic contraction or a secondary result due to changes in the local Starling forces caused by lymph formation. NO could be affecting vascular permeability and thus lymph formation in two different ways. The first is that NO could increase vascular permeability and fluid extraversion into the interstitium (68, 213), increasing lymph formation and subsequently driving lymph flow. The second is that given

53

the potential of NO to lower capillary blood pressure, it is possible that GTNO could also decrease lymph formation and thus there would be less of a driving force of fluid upstream (112, 185). This appears unlikely because applying the occlusion cuff for 10 minutes at 80 mmHg likely blocks venous return. This would increase venous pressure and cause an increase in interstitial fluid buildup regardless of NO's effects on capillary permeability. In both scenarios, the conditions for lymph formation are high and thus should in-turn correspond to increases in the extrinsic mechanisms responsible for lymph flow. However, we showed that P_{eff} and packet restoration pressure was halved in the presence of GTNO. Also, application of GTNO away from the injection site, but still on the tail surface above the vessels at the measurement location, had the same effect on our metrics of lymphatic pump function as when applied to the entire tail. Therefore, the most likely explanation is that the decreases in P_{eff}, packet restoration pressure, and emptying rate are due to the NO-induced loss of intrinsic lymphatic contractility, not a secondary result due to changes in lymph formation upstream. Our more recent collaborative study utilized a computational model to simulate output pressure of a chain of lymphangions in series (177). The results of this study indicate that the reduction in effective pumping pressure with GTNO application can be best replicated by lowering the active muscle tension of the lymphangions and not the contraction frequency or interstitial fluid pressure. However, because active muscle tension includes both the combined effects of tonic constrictions and phasic contractions, it is not clear in this study whether nitric oxide effects on tone (and indirectly valve function) or contraction amplitude are primarily responsible for the reduction in effective pumping pressure observed in-vivo.

We calculated the emptying rate to quantify the average rate of dye removal, a metric that is reflective of lymph flow (assuming that the solute flux follows the convection of the fluid). By occluding lymph flow distal to the imaging site, we were able to isolate the effects of intrinsic pumping from the effects of upstream lymph formation. It is reasonable to assume that the emptying rate captures an overall metric of lymphatic transport driven by intrinsic pumping effects of the downstream lymphatic chain (and perhaps the effects of nearby arterial pulsations). Since vessel filling is being occluded upstream of the imaging location by the pressure cuff, fluorescent dye must be transported out of the imaging location by intrinsic contractility of the lymphatic vessels. This metric thus decouples the effects of lymph formation upstream as a driver for lymphatic transport. In effect, emptying rate characterizes the downstream (proximal to the cuff) lymphatics ability to transport fluid, whereas P_{eff} characterizes the upstream (distal to the cuff) lymphatics. Utilizing these two metrics, we are able to characterize the effects of two separate segments of a single lymphatic vessel in the transport of fluid. GTNO significantly lowered the average emptying rate of the collecting vessels on the tail by nearly three-fold. This result follows a similar pattern to two previous studies which showed that lymph transport is substantially decreased in the presence of GTNO (190, 235). When the two metrics used in this study (P_{eff} and average emptying rate) are examined in conjunction with these two previous studies, it becomes clear that the pumping pressure measurement system provides a complementary platform for quantifying lymphatic function; providing additional insight into the mechanisms regulating lymphatic dysfunction during disease.

Throughout the experimental process, consistency was maintained for as many variables as possible. However, there are some limitations of the technique that are worth

mentioning. First, the physiological effects of anesthesia on the measured P_{eff} are unknown. This could be problematic in studies where it is suspected that the anesthesia itself might mask hypothesized losses in lymphatic pumping. Second, the application of the occlusion cuff at 80 mmHg for 10 minutes likely causes a buildup of interstitial fluid by blocking venous return. This would tend to give elevated measures of P_{eff} over baseline values. However, the technique itself, while not providing a direct measurement of baseline systolic lymphatic pressure, is indicative of lymphatic pump function and provides, in our opinion, one of the most quantitative non-invasive measures of total lymphatic pumping capacity available. Third, we and others have reported effects of ICG on lymphatic pump function (74, 234). However, the negative effects of ICG appear primarily upon repeat injections and are reversible if enough time occurs between each injection (around 4 weeks). Since multiple injections were not given in this study, this does not appear to be problematic. Future work, discussed in Chapters 3 and 4, will utilize NIR tracers that do not influence lymphatic function, thus making these methods suitable for use in time course studies.

2.4.4 *Combinations of NIR functional imaging techniques can be used to phenotype and provide novel insight to lymphatic disease*

The studies described in the previous sections have demonstrated the development and validation of novel NIR imaging techniques to quantify collecting lymphatic pumping pressure and emptying rate in vivo. However, by combining these new techniques with previously established packet performance metrics (115, 116, 235), we enable the unique ability to non-invasively phenotype the modalities of collecting lymphatic failure in the context of disease. To demonstrate this, we utilized two models that are known to possess

deficiencies in lymphatic transport, but the involvement of the collecting vessel pump in these deficiencies was unknown, and thus its appropriateness as a therapeutic target has remained elusive. These include a genetic mouse model of delayed lymphatic valve development and a mouse model of diet-induced obesity. These two models were chosen to capture the clinical breath of lymphatic dysfunction, including a model with an underlying genetic deficiency (as occurs in primary lymphedema), as well as a model of acquired dysfunction (as in secondary lymphedema).

2.4.4.1 <u>Genetic deletion of lymphatic endothelial epsins profoundly impairs collecting lymphatic function</u>

Lymphatic valve malformations have been suggested to be one of the most common causes of hereditary lymphedema and have also been suggested to be involved in the progression of secondary lymphedema (125, 165). These malformations result in an inability for the lymphatics to prevent back flow, and subsequently lead to fluid leaking from the vessels back into the initial lymphatics and the interstitium. However, the functional response of the collecting lymphatic vessels has not been described in the context of lymphatic valve malformations caused by genetic aberrations. Therefore, it was imperative to utilize our functional phenotyping methods to provide novel insight into how dysregulation of lymphatic valves impact collecting vessel performance. To achieve this, we utilized a genetically modified mouse model with a modest valve dysfunction. This was important as mouse models in which lymphatic valves fail to form, such as the FoxC2 -/- mouse, are embryonic lethal (165). In fact, continual FoxC2 expression is necessary postnatal maintenance of lymphatic valves, as induced FoxC2 knockout results chylous ascites and death (188).

Epsins are a family of highly conserved multivalent endocytic adaptor proteins that mediate clathrin-dependent endocytosis of a subset of ubiquitinated cell surface proteins. Epsins 1 and 2 are ubiquitously expressed in most tissues where they perform overlapping functions (35, 42, 43). In lymphatic endothelial cells, epsins facilitate the internalization and downregulation VEGFR3. A lymphatic endothelial cell epsin knockout (LEC-DKO) mouse has been developed that results in altered VEGF-C/VEGFR3 signaling and subsequent malformation of lymphatic valves (44, 125, 163). Research has shown that these mice developed more severe lymphedema after a surgical insult (unpublished), and it is believed that this was due to abnormal lymphatic repair, due to the inability of VEGFR3 to be recycled, and that there was no underlying defect prior to surgery. However, with our highly sensitive phenotyping approaches, we could detect several abnormalities in the function of the lymphatic network that was present at baseline even with histological appearance of "normal" valves. Specifically, LEC-DKO mice exhibited enhanced reliance on the initial lymphatic network for fluid clearance as reflected in the representative images and quantification of total fluorescence area. LEC-DKO mice exhibited significant declines in lymphatic packet frequency. Upon upstream lymphatic flow occlusion, significant differences between the vessel emptying rates of control and LEC-DKO mice were observed. In fact, KO mice exhibited a negative emptying rate, suggesting the collecting vessels experienced back flow due to incompetent valves once the influence of the upstream injection pressure was blocked off with the occlusion cuff. Because the lymphatic vessels of LEC-DKO mice did not clear their contents during occlusion, the lymphatics exhibited no detectable lymphatic pumping pressure above the resolution limit of the

system (2.5 mm Hg), while controls showed normal values of effective pumping pressure (16.8 mmHg).

The results of this study have raised a novel line of questioning regarding the role of lymphatic endothelial epsins in the regulation of lymphatic physiology and the development of lymphedema. Epsins clearly play a role in lymphatic development and subsequently function; however, it is unclear if epsins have direct regulatory effects on collecting lymphatic pump function post-developmentally. Additionally, in the context of surgically induced lymphedema, it is unclear to what extent lymphatic endothelial epsins serve in the repair and remodeling response of the collecting vessels. To this end, the work presented in this thesis has motivated the use of an inducible lymphatic endothelial epsin knockout model coupled with the disease phenotyping techniques described here that enables investigation into the post-developmental role of epsins in regulating lymphatic function and remodeling.

2.4.4.2   <u>Diet-induced obesity impairs collecting lymphatic contractile frequency but not other metrics of lymphatic performance</u>

Obesity has previously been shown to adversely affect lymphatic packet frequency in mice, as assessed with NIR imaging (27). However, these studies only assessed one potential collecting lymphatic failure mode, contraction frequency, when there is a multiplicity of other potential lymphatic failure modes. To this end, we have used our NIR imaging suite to assess the failure modes of collecting lymphatics on both the hind limbs and tails of obese mice. Our published study demonstrates that even though the frequency of lymphatic contractions are reduced (which has previously been shown to be linked to

inflammation), the capacity of the lymphatics to generate the pressure needed to move fluid against an adverse pressure gradient is normal (191). This suggests that the lymphatic's maximum pumping capacity is not damaged, that the collecting vessels have not adversely remodeled, and thus deficits in transport could potentially be improved pharmacologically. This is in contrast with the functional data from the LEC-DKO model, which had no detectable pumping pressure and very low contraction frequency, indicating a deficiency in the either the valve competency and/or contractile strength of the lymphatic muscle cells in addition to declines in peacemaking frequency. In fact, this highlights the primary benefit of our functional phenotyping techniques. If we had only assessed lymphatic contraction frequency as the sole metric of collecting lymphatic function in these two disease models, we would not be able to elucidate the stark differences pumping pressure that suggest a more profound impairment in lymphatic function.

These results are interesting because they indicate that obesity alone causes down regulation of lymphatic contraction frequency. However, obese mice exhibit no development of lymphedema without surgical insult, suggesting that compensatory mechanisms are occurring during obesity that results in lymphatic transport sufficient to maintain tissue fluid balance. Despite these compensatory mechanisms, obesity is known to significantly increase risk for developing lymphedema (91). Therefore, it seems likely that declines in lymphatic contraction frequency, because of obesity, induce a "tipping point" during lymphatic injury in which lymphatic transport declines further and lymphedema pathogenesis occurs. It was my goal for Specific Aim 2 to determine the specific lymphatic failure modes involved in lymphedema pathogenesis during chronic inflammation due to obesity. This is examined in detail within chapter 3.

CHAPTER 3. THE EFFECTS OF DIET-INDUCED OBESITY ON COLLECTING LYMPHATIC PUMP FUNCTION AND REMODELING DURING LYMPHEDEMA (AIM 2)

3.1   Introduction

One of the strongest associations with the onset of lymphatic dysfunction and subsequent lymphedema is obesity. As early as 1957 it was observed that larger individuals had greater incidence of developing lymphedema after breast cancer treatment (224). More recent clinical studies have made it abundantly clear that pre-surgical BMI strongly correlates with post-operative development of lymphedema in breast cancer patients (91, 133, 241). Conversely, reductions in BMI via dietary alterations and exercise appears to be one of the only effective non-compressive or massage based treatments for lymphedema (114, 198). The cause of this correlation is currently unknown; however, the preponderance of evidence in the clinical literature strongly suggests that adipose accumulation during obesity has a direct role in impairing lymphatic tissue drainage, ultimately resulting in prolonged lymph stasis and subsequently lymphedema. Studies supporting this hypothesis have demonstrated that obese individuals have impaired lymphatic clearance as assessed by lymphoscintigraphy and tissue scintillation-counting techniques (8, 84). In fact, it has been demonstrated that obesity alone, without surgical insult, can cause lymphedema (84).

Although it is clear that obesity and lymphedema are related, the mechanisms that regulate this interplay are incompletely understood. Perhaps surprisingly, studies have suggested a reciprocal relationship between obesity and lymphedema in which obesity can

cause lymphatic dysfunction but lymphatic dysfunction can also cause obesity. Histological analysis of mouse tissues have shown that adipose deposits associated with lymphedema appear similar in morphology to those observed in obese animals (249). Additionally, both obese and lymphedematous tissues are chronically inflamed and are infiltrated by macrophages and lymphocytes. These lymphedematous tissues have an upregulation in genes associated with adipocyte differentiation and increased expression of adipokines (9). These findings suggest that when lymphatic function is surgically impaired, the distal tissues become "regionally obese" even in the absence of excessive caloric intake. Further evidence linking lymphatic dysfunction to the development of obesity comes from transgenic mouse models possessing lymphatic specific mutations. In a model of Milroy disease, mice lacking VEGFR3 have abnormal lymphatic vessel development and subsequently exhibit chylous ascites abnormal fat deposition (102). Similarly, mice with heterozygous mutation of the prospero homeobox protein 1 (PROX 1), a gene essential for lymphatic endothelial cell differentiation, exhibit adult-onset obesity in contrast their non-mutated normal body weight litter mates (90). Taken together these findings demonstrate that loss of lymphatic transport may result in adipose excessive deposition that is phenotypically similar to diet-induced obesity at a tissue level. Additionally, these tissues exhibit the excessive lymphocyte and macrophage infiltrations associated with the chronic inflammation observed during diet-induced obesity.

Recent work has sought to investigate the cellular mechanisms that link obesity to the development of lymphedema. Evidence in the literature strongly suggests that this is due to influences of adipose tissue on the inflammatory response and subsequently on lymphatic drainage. Obesity has been shown to cause chronic systemic inflammation due

to interactions between adipose tissue, lymphocytes, and macrophages (85, 93, 151, 247). This is believed to be initiated by a T-cell inflammatory response within the adipose tissue that results macrophage chemotaxis. It is currently unclear how naive T-cells become activated to initiate macrophage recruitment to adipose tissues; however, recent work has provided compelling evidence that CD4+ T-cells may be activated directly by adipocytes as opposed to typical antigen presenting cell types. Xiao et. al. found that large, hypertrophic, adipocytes express MHCII and can function as an antigen presenting cell to activate CD4+ T-cells (246). It is possible that these T-cells may differentiate into the Th1 subtype and subsequently initiate macrophage homing and activation via release of IFN-γ (107). These newly recruited adipose tissue macrophages are then thought to phagocytize necrotic adipocytes, leading to the release of inflammatory cytokines, recruiting other leukocytes, and progressing inflammation (4, 95, 107, 151, 244, 247, 249). Studies have shown that obese adipose tissues have a greater proportion of classically activated macrophages (M1), which are characterized by expression of CD11c in addition to CD11b, as opposed to adipose tissues in lean animals that have more alternatively activated macrophages (M2). This is important because the M2 subtype is known to secrete a higher proportion anti-inflammatory cytokines including IL-10 and IL-1, in contrast to the pro-inflammatory cytokines secreted by M1 macrophages such as TNF-α and IL-6 (126, 145). It is the infiltration of macrophages and T-lymphocytes in obese adipose tissue that are believed to modulate lymphatic function and increase susceptibility to later development of lymphedema.

Inflammatory mediators such as cytokines (3), prostanoids (245), histamine (66), and nitric oxide (NO) (32, 139, 149, 235) are known to be potent modulators of lymphatic

contractile activity and drainage. Given that obesity often results in chronic inflammation it is perhaps unsurprising that obesity has been widely shown to adversely influence collecting lymphatic function. Obese mice have been shown to have impaired lymphatic drainage as assessed by lymphoscintigraphy. Additionally, as discussed in Chapter 2, we and others have demonstrated via NIR imaging that this impaired drainage corresponds with decreased lymphatic contractile frequency compared to their lean counterparts (27, 192, 222). Treatment of obese mice with a selective iNOS inhibitor has been shown to improve lymphatic drainage, decrease immune cell infiltration, and decrease expression of inflammatory cytokines in the tissue (222). However, inhibition of local T-cell differentiation, using topical treatment with a calcineurin inhibitor called tacrolimus, was more effective at decreasing tissue inflammation while also producing similar improvements in lymphatic drainage and contractile function. Taken together, these results suggest that T-cells play a prominent role in mediating the inflammation induced declines in lymphatic function observed during obesity. This is, perhaps, expected given that it is hypothesized that T-cell activation initiates the inflammatory cascade during obesity. Interestingly, weight loss in obese mice via caloric restriction has been shown to decrease infiltration of pro-inflammatory immune cells and produces a corresponding increase in lymphatic contractile frequency and drainage (152).

Given that baseline lymphatic function is impaired by chronic inflammation during obesity, it seems likely that this plays a role in increasing susceptibility to lymphedema development upon surgical insult to the lymphatic vasculature. Thus far, research using mouse lymphedema models have supported this hypothesis. Upon induction of lymphedema via surgical insult obese mice have a more severe tail lymphedema

phenotype, with increased adipose deposition, fibrosis, macrophage and CD4+ T-cell infiltration (192). This increase in lymphedema severity corresponds with declines transport of tracer via the lymphatics to the lymph nodes. It is important to note that this aggravation of lymphedema observed during obesity does not appear to be a result of high fat diet, but rather increased adiposity and its associated hyper-inflammatory response (81). Although it is clear that obesity impairs overall lymphatic drainage both pre- and post-surgically, corresponding to increased severity of lymphedema, the degree of contribution from dysfunction of the collecting lymphatic vessels is, as of yet, unclear. That is, does obesity influence the performance of the collecting lymphatic pump during the pathogenesis of lymphedema and to what degree? It is possible that although obesity impairs baseline collecting lymphatic function, this is still sufficient to mediate the chronic low-grade inflammation and to maintain tissue fluid homeostasis. Whereas Upon surgical insult that impairs lymph transport, inflammation can no longer be mediated by lymphatic drainage, thus increasing the number of leukocytes in the tissue and further impairing lymphatic transport. This could ultimately result in a feedback loop in which fibrosis and adipose deposition in the tissue elicits dysregulation of collecting lymphatic function and remodeling response.

It is therefore the goal of this study to investigate the influence of obesity on collecting lymphatic pump function and remodeling during lymphedema. We hypothesize that diet-induced obesity adversely influences the lymphatic pump function and remodeling phenotype during the progression and resolution of lymphedema. We investigated this hypothesis by using the methods developed in Chapter 2, along with a recently developed single-vessel ligation model of mouse tail lymphedema (236), to assess

the functional changes of an intact collecting lymphatic vessel on the tail in response to ligation of the contralateral vessel in a mouse model of diet-induced obesity. At the end of the study, we surgically isolated the intact lymphatic vessels to determine if there are any differential alterations to the structure of the vessel because of obesity. To investigate the role of T-cells in mediating the functional dysregulation of the collecting lymphatic vessels observed during obesity, we pharmacologically inhibited T-cell differentiation by applying topical tacrolimus ointment to the lymphedematous tails of a subset of obese mice.

3.2   Materials and Methods

3.2.1   Study overview

In order to determine the effects of obesity on collecting lymphatic function and remodelling, we utilized a common C57BL6J model of diet induced obesity (152, 192, 222, 239). Mice were allowed to gain weight for a 20-week period before beginning the study. On Day 0, obese or chow-fed control animals underwent baseline NIR lymphatic functional imaging to characterize their baseline collecting lymphatic function. The "dominant" lymphatic vessel on the tail was identified as the vessel in which NIR tracer appears first after injection (234). Following baseline imaging, the dominant lymphatic vessel was ablated along with the dermal lymphatics. The function of the remaining intact lymphatic vessel on the tail was periodically characterized via NIR imaging at 7, 14, 28, 42, 56, and 70 days post-surgery. In order to elucidate the effects of T-cell differentiation and activation on any functional differences observed between the obese and chow fed control groups, an additional subset of obese mice were treated twice daily with tacrolimus

ointment beginning at the 14 day time point. After the 70-day study period, mice were euthanized for tissue collection and isolation of the intact lymphatic vessel.
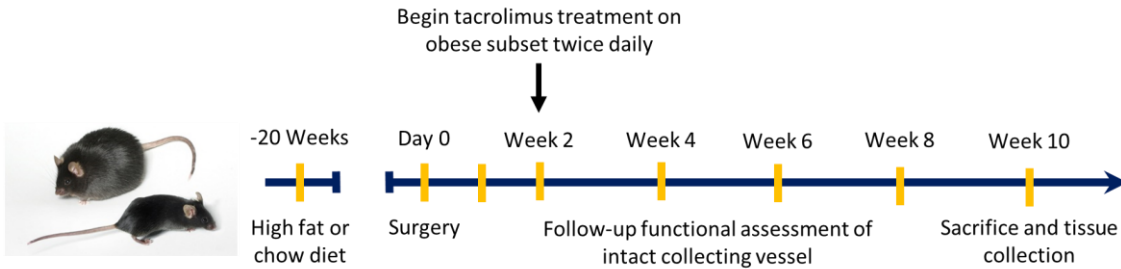
Figure 14: Graphical representation of the study design.

3.2.2 Animal models

All animal procedures were approved by the Georgia Institute of Technology Institutional Animal Care and Use Committee (IACUC). 8-Week-old male C57BL6J mice were placed on a high fat diet (n=11) (60% kcal fat, TestDiet 58Y1, W.F. Fisher & Son, Sommerville, NJ) or chow diet (n=8) (13% kcal fat, Purina PicoLab Rodent Diet 20, W.F. Fisher & Son, Sommerville, NJ) for 20 weeks. Mouse bodyweight was measured using a digital scale. Mice were housed one per cage in a temperature and humidity controlled (21 ± 1°C) vivarium on a 12-hr light, 12-hr dark cycle. Food and water were available ad libitum.

3.2.3 NIR lymphatic Tracer

The NIR lymphatic tracer used for the imaging procedures consisted of a NIR fluorophore IRDye 800 CW NHS Ester (929-70020, LI-COR Biotechnology, Lincoln, NE)

bound to 20kDa methoxypolyethylene glycol (mPEG) (JenKem Technology USA, Plano, TX) in a manner similar to a previously described method (28, 169). During all following steps, aluminum foil was used to shield the fluorophore to ambient light exposure. Equimolar ratios of IRDye 800CW NHS Ester (75 nmol) and mPEG (75 nmol) were bound room temperature in 0.5mL anhydrous dimethyl sulfoxide (DMSO) (Sigma Aldrich, St. Louis, MO) for 24hrs. After binding, the mixture was transferred into a dialysis cassette with a 7 kDa molecular weight cutoff (66370, Thermo Fisher Scientific, Waltham, MA). The cassette was submerged in a 4L beaker of de-ionized water and was dialyzed for 24hrs. The dialyzed solution was removed from the cassette, separated into 100 uL aliquots in 0.6 mL microcentrifuge tubes and lyophilized for 24hrs. The lyophilized tracer was stored prior to use in -20 C freezer. Before use, the aliquots were re-constituted in 35µL sterile saline 0.9% NaCl (Baxter Healthcare Corp., Deerfield, IL)

3.2.4   NIR imaging system and imaging procedure

Images were taken with a customized imaging system consisting of a Sutter Instruments Lambda LS Xenon arc lamp (Sutter Instruments, Novato, CA), an Olympus MVX-ZB10 microscope (Olympus, Tokyo, Japan), a 769 nm bandpass excitation filter (49 nm full-width half maximum, FWHM), an 832 nm bandpass emission filter (45 nm FWHM), and an 801.5 nm longpass dichroic mirror (Brightline Filters, Semrock, Lake Forrest, IL). Images were acquired with a Photometrics Evolve Delta 512 EM-CCD (Photometrics, Tucson, AZ) using Micromanager software (Vale Lab, University of California San Francisco).

NIR lymphatic imaging was performed in accordance with previously published methods and those described in Chapter 2 (149, 234, 235). Briefly, mice were anesthetized with 5% isoflurane and maintained on a steady plane of anesthesia at 1.8-2.2% isoflurane (SomnoSuite, Kent Scientific, Torrington, CT). Mice were placed on a small animal heating pad to maintain body temperature of 37 °C (K&H Pet Products, Colorado Springs, CO). To assess tail size, bright field images of the tails were taken next to a ruler before the NIR tracer was injected. The animals were placed in a prone position, the tails were sanitized with a 70% isopropyl alcohol swab and 10 μL IRPEG 20 was injected intradermally into the tip of the tail using a 0.3 mL insulin syringe with 5/16" long 32 G ultra-fine needle (BD, Franklin Lakes, NJ). Care was taken to position the injection as close to the midline of the tail as possible to avoid favoring one collecting vessel over the other.

The imaging system's field of view was centered on the mouse's tail 7 cm downstream (towards the base of the tail) from the injection site at the tip of tail. The animals were imaged continuously from the time of injection at until roughly 8-minutes post-injection at 1.25x zoom with a 50 ms exposure time and a frame rate of 10 fps. After this period, animals were positioned on their right sides to image the left lymphatic vessel and images were captured for 5-minutes. Animals were subsequently positioned on their left sides to image the right lymphatic vessel and images were captured for 5-minutes. Analysis of NIR functional metrics was performed on the image segments from the 5-minute periods on the respective sides. After this imaging session a pressure cuff was fitted to the tail, and mice underwent the lymphatic pumping pressure measurement technique that has been previously described (149). During the pumping pressure measurement

images were captured at 1 fps with a 50 ms exposure time with the field of view centered at the proximal edge of the pressure cuff (OCC-XS, Kent Scientific, Torrington, CT). The cuff was inflated and held at 80 mmHg for 5-minutes. After the 5-minute hold the cuff was deflated to 55 mmHg and subsequently lowered by 2.5 mmHg every 30 seconds.

3.2.5   *Quantification of NIR functional metrics*

In order to quantify the efficacy of lymphatic uptake and subsequent transport by the collecting lymphatic vessels, we assessed the fluorescence arrival time of tracer from the upstream injection to the downstream site of imaging. Arrival time was assessed by computing the time difference between tracer injection and the arrival of fluorophore in the intact lymphatic vessel at the wound site during the roughly 8-minute (5000 frame at 10 fps) imaging session immediately post injection. In order to assess collecting lymphatic pump function three distinct metrics were evaluated in accordance with our previously our previously developed methods discussed in Chapter 2 (149, 235, 236). Packet frequency was evaluated by tracking the average time between peak fluorescence pulsations within regions of interest (ROIs) traced over lymphatic vessels during our initial imaging sets. Packet frequency has been correlated with the frequency of intrinsic lymphatic contractions in vivo. Florescence transport was not discussed in Chapter 2, but has been recently developed and described within our research group (236). This metric was calculated by summing the integral of the packet signal with respect to time and dividing by the total amount of time over which it was assessed. It is the absolute amount of fluorescence transported by intrinsic contraction through a region of interest over time and can be roughly correlated to fractional pump flow. Fluorescence transport is a function of lymphatic contraction frequency, contraction amplitude, and packet velocity. 3) Effective

70

lymphatic pumping pressure was calculated by determining the occlusion pressure at which the fluorescence within the vessel proximal to the cuff returns to half of its pre-occlusion value. It is a measure of the collecting lymphatic vessel chain's ability to generate the pressures needed to overcome an occlusive force.

Significant differences between control and obese was tested via student's t-test for each time point with $p < 0.05$ denoting significance. In order to compare later time points to their respective pre-surgical baseline (Day 0) we used 1-way ANOVA with post-hoc Dunnett's correction for multiple comparisons with $p < 0.05$ indicating statistical significance. In scenarios where the tacrolimus treated group was compared to both the obese and control groups, 2-way ANOVA with post-hoc Tukey correction for multiple comparisons was used with $p < 0.05$ indicating statistical significance. All statistical analysis was done using Prism 6 software (Graphpad Software, La Jolla, CA).

3.2.6 *Lymphedema induction via single vessel ligation surgery*

Immediately after the baseline NIR imaging session mice from the experimental groups underwent a lymphatic vessel ligation surgery to the tail. Mice were kept anesthetized with 1.8-2.2% isoflurane (SomnoSuite, Kent Scientific). Mice were kept on the heating pad during the surgery. The location of the dominant lymphatic vessel was confirmed via NIR imaging. The tails of the mice were sterilized with alternating scrubs of an iodophor and 70% isopropyl alcohol. Lymphatic vessel ablation was located 1.5 cm from the base of the tail using a fine tipped tissue cauterizer (Small Vessel Cauterizer, Fine Science Tools, Forest City, CA) to create a 1-2 mm deep wound 70-80% of the circumference of the tail. NIR imaging was used throughout the procedure to confirm the

location of the intact lymphatic vessel so that it is not accidentally ablated. After surgery, mice were given a 1 mg/kg subcutaneous injection of sustained release buprenorphine as an analgesic. Anti-bacterial ointment (Neosporin, Johnson & Johnson, New Brunswick, NJ) was applied to the wound site immediately after the surgery. Animals were monitored for signs of necrosis in the tissues distal to the wound site, indicating accidental ligation of blood supply/return. If necrosis or abnormal darkening of the tails occurred, the animals were removed from the study and euthanized.

3.2.7   *Topical tacrolimus treatment*

0.1% (wt/wt) tacrolimus ointment was made using tacrolimus powder and a base. 10 mg of tacrolimus powder (FK-506, Fisher Scientific, Pittsburgh, PA) was levigated in 1 mL of anhydrous glycerine (Sigma Aldrich, St. Louis, MO) with a glass stir rod. Roughly 100 g of Aquaphor (Beiersdorf Inc., Wilton, CT) was melted at 40°C until liquified. The tacrolimus and glycerine mixture was geometrically diluted in this liquified Aquaphor base to a final weight of 100 g, stirring thoroughly in between dilutions to ensure even distribution of tacrolimus in the suspension. The ointment was then sealed in an air tight plastic jar and stored at room temperature in a dark place until use. Topical tacrolimus treatment of a subset of obese mice (n=5) began 14 days after the induction of lymphedema via the ligation surgery, immediately after the 14-day NIR imaging time point. Roughly 100 mg of tacrolimus ointment was applied in an even coat to the entirety of the tails twice daily until the end of the 70-day study.

3.2.8   *Vessel isolation and tissue collection*

Lymphatic vessels were isolated and tested from mice in a manner similar to our previously described methods in rats (109, 110). Within 1-5 days after the final NIR imaging session at the 10-week time point mice were euthanize via asphyxiation with CO2. After euthanasia, the skin was removed from the tails to expose the collecting lymphatic vessels. Sterile saline was periodically perfused onto the tissue to ensure that it did not dry. The intact lymphatic vessel distal to the wound site on the tail was located and an approximately 3 mm segment was isolated from the surrounding adipose and fascia. The segment was removed and immediately placed in a bath containing DMEM/F12 (GE Healthcare Life Sciences, Logan, UT) with added antibiotic mixture (Invitrogen Corp., Carlsbad, CA) to achieve a concentration of 100 units of Penicillin and 100 μg of streptomycin per ml of DMEM/F12. The segment was subsequently cannulated onto micro pipettes in a single vessel cannulation chamber (Living Systems Instrumentation, St. Albans, VT).

Cannulated vessel segments from control (n=2) and obese (n=2) groups underwent 2nd harmonic generation imaging of collagen in a manner previously described (37). Vessel segments were pressurized at a transmural pressure of 2 cmH$_2$O were placed under a LSM 710 META inverted confocal microscope (Zeiss) to visualize the microstructure across the entire wall of unfixed lymphatic vessels. The vessels were imaged using a 40×/1.3NA immersion objective (Zeiss). The META module was set to a bandpass filter of 380–420 nm and excited at 800 nm in order to detect backward-scattering second harmonic generation signal from collagen. Collagen waviness was assessed using a method adapted from Rezakhaniha et. al. that measured the absolute length of collagen fibers compared to their end-to-end length (179). Briefly, 3D image stacks from the 2nd harmonic imaging

were opened in ImageJ software (195). A 2D image was obtained from each vessel for analysis from 10 µm within the vessel wall. The ImageJ curve tool was used to trace four lines over collagen fibers for each vessel image. After tracing, the lines were measured using the ImageJ measurement tool to find the absolute length, L, and the end-to-end length, L_o (Figure 20). Collagen waviness was computed by dividing L by L_o for each tracing.

3.3 Results

3.3.1 *Obese animals do not differentially swell following induction of lymphedema*

Mice placed on high fat diet for a 20-week period exhibit significant weight gain compared to chow fed controls ($p < 0.0001$). On Day 0 of the study the average body weight of high fat fed mice 57 ± 4 g (n=6) compared to 31 ± 1 g (n=8) for chow fed controls (Figure 15). Upon induction of lymphedema via the single vessel ligation model both obese and control mice exhibit swelling of the tails distal to the wound site, which was assessed by measuring the tail diameter. The swelling peaks at the 7 and 14-day time points, but progressively declines to the 70-day value of roughly 6% for both control and obese (Figure 15).
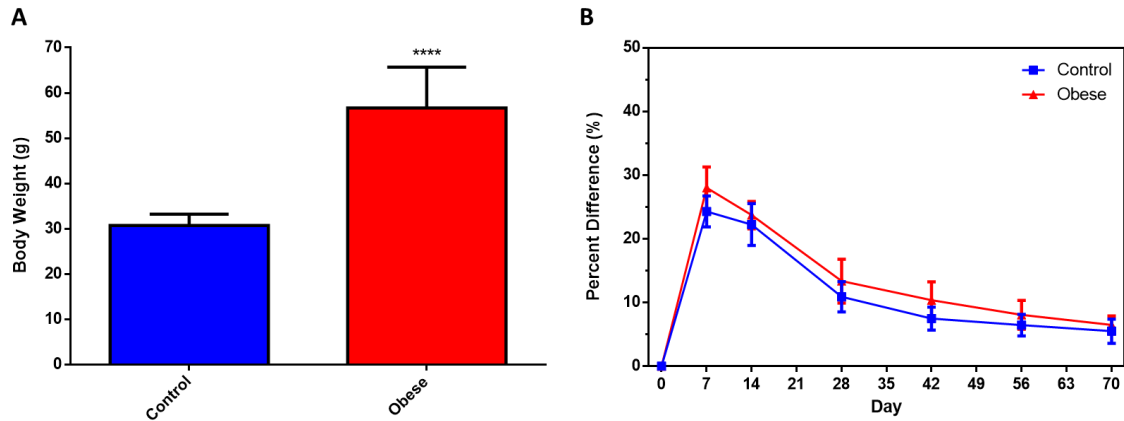
Figure 15: (A) High fat diet induces significant weight gain in male C57BL6J mice (p < 0.0001). (B) Following lymphedema induction via ablation of a collecting lymphatic vessel and the dermal lymphatics the distal tissues exhibit progressive swelling that subsequently subsides. The tails of control and obese mice were not found to differentially swell. Error bars represent SEM. (*, denotes significant difference between control and obese, p < 0.05)

3.3.2   *Obesity delays fluorophore transit via the intact collecting lymphatic vasculature*

The lymphatic anatomy of the mouse tail is characterized by two lateral collecting lymphatic vessels that drain the distal tissue space. Upon disruption of one vessel via surgical ablation, the remaining intact lymphatic vessel serves as the primary outflow pathway to bypass fluid around the wound site. Using NIR imaging we observed that obese animals had delayed fluorophore transport by the intact collecting lymphatic vessel after initial tracer injection at pre-surgical baseline and at the 7-day time point. However, by 70 days post-surgery the intact lymphatic vessel exhibited fluorophore uptake and transit past the wound site in a manner similar to controls (Figure 16) and (Figure 17).
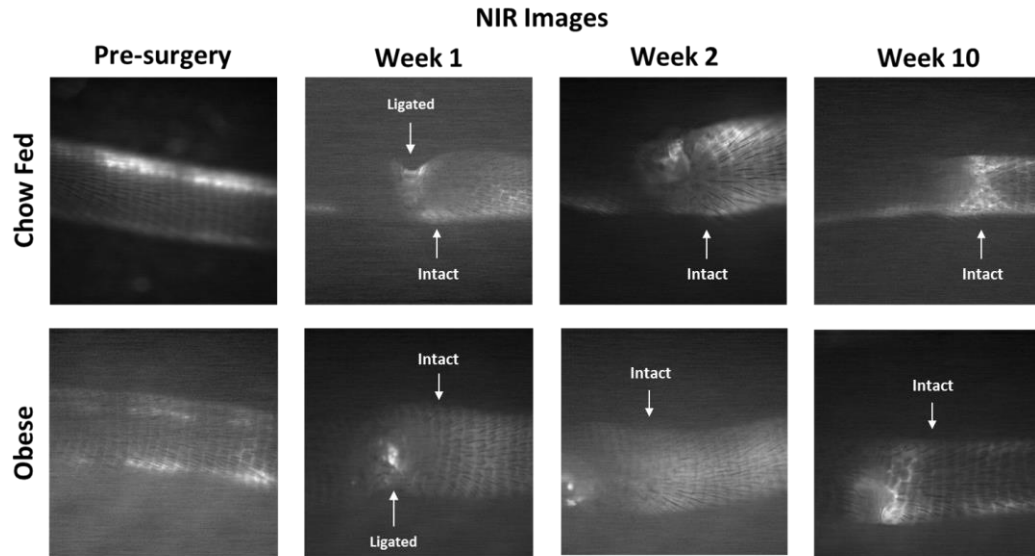
NIR Images

Figure 16: Representative NIR images taken at the wound site 5-minutes after tracer injection at the distal tip of the tail. Pre-surgery images depict the two collecting lymphatic vessels located on the lateral aspects of the tail. 1 week after ligation chow fed control animals exhibit uptake of fluorophore in the intact lymphatic vessel that subsequently transits the wound site. This was delayed in obese animals. However, this difference is attenuated by the 10-week time point.
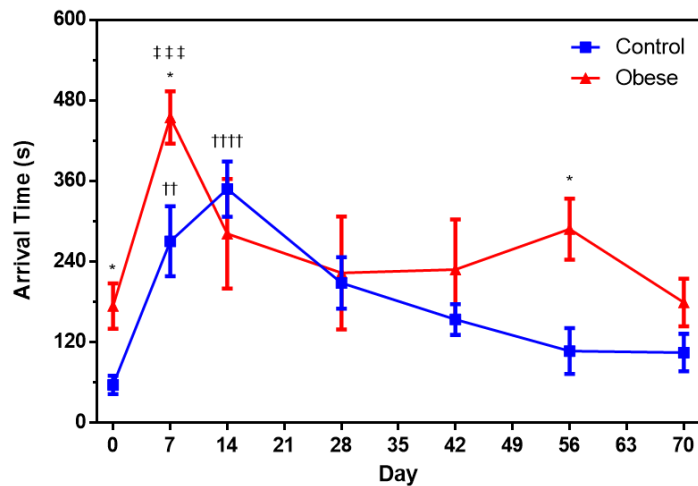
Figure 17: Obesity causes delayed fluorophore uptake and transport through the intact collecting lymphatic vessel to the wound site as assessed by arrival time.

Significant differences in arrival time between control and obese animals we observed pre-surgery in addition to 7 and 56 days post-surgery. Induction of lymphedema via single vessel ligation surgery resulted in significant delays in arrival time compared to pre-surgical baseline for both the control and obese groups. Error bars represent SEM. (n=8, control) (n=6, obese) (*, denotes significant difference between control and obese; †, denotes significant difference between control value and the baseline pre-surgical control value; ‡, denotes significant difference between obese value and the baseline pre-surgical obese value, p < 0.05).

3.3.3 Surgically ablated collecting lymphatic vessels do not regain intrinsic pump function

At pre-surgical baseline, both primary collecting lymphatic vessels located on the tail exhibited intrinsic contractility; however, following surgery, the ablated vessel was found to lose its intrinsic contractile function. 8-minutes after injection of NIR tracer, animals were placed on either their right or left sides to image either the intact or wounded vessel for 5-minute periods respectively. Upon imaging the wounded vessel we discovered that drainage of NIR tracer was obstructed at the wound site (Figure 18). Specifically, 7 days post-surgery, we observed significant accumulation of tracer distal to the wound. This tracer appears to be accumulating in the interstitial space as opposed to the collecting or initial lymphatic vessels. In fact, the collecting lymphatic vessels are wholly obscured by the fluorescence emitted from this extravasal tracer. At later time points, after tissue swelling has subsided, the wounded collecting lymphatic vessels are observable but remain obstructed at the wound site. Near this obstruction, we observed rerouting of tracer by the initial lymphatic network. These initial lymphatics connect collaterally with the intact lymphatic vessels, which serves as the primary lymphatic drainage pathway. Interestingly, upon follow-up assessment of lymphatic pump function post-surgery, we were not able to

detect any dynamic fluorescent packets in the wounded lymphatic vessel in either control

or obese mice (Figure 18). These results suggest that the damage caused to the vessel from

the surgical ablation inhibits the intrinsic contractile response and that the initial lymphatic

network serves as a collateral drainage pathway to facilitate lymph removal from the tissue.
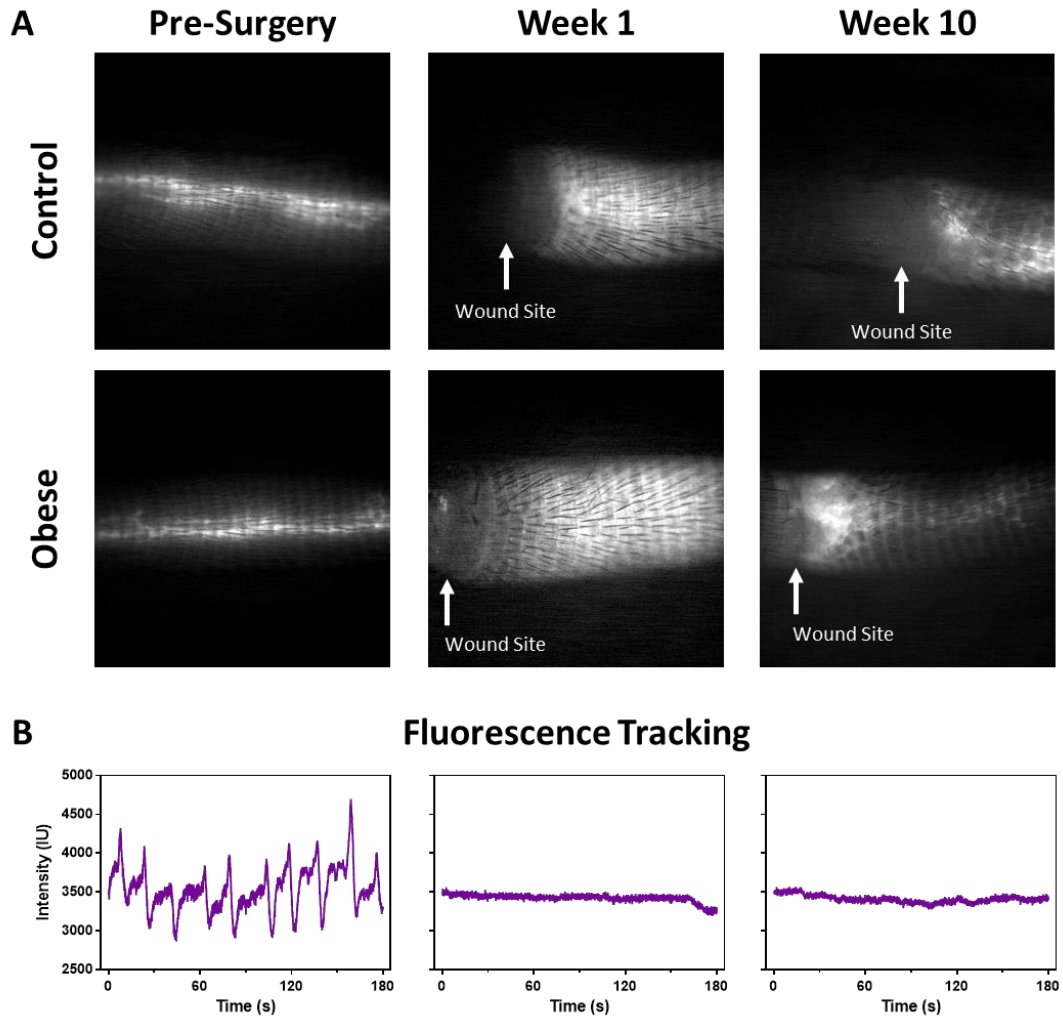
Figure 18: Representative NIR images of the ligated lymphatic vessels following the single-vessel ligation surgery. After surgery, the ablated collecting lymphatic vessels no longer exhibit intrinsic contractile behavior. (A) Pre-surgical NIR images depict tracer uptake by the collecting lymphatic vessels running laterally along the mouse tail. One week after ligation of these vessels, swelling of the tissues distal to the wound site was observed in conjunction with non-specific build-up of tracer that obscures the collecting lymphatic vessels. Ten weeks post-surgery, after swelling has subsided,

the wounded collecting lymphatic vessels were observable; however, they remained obstructed by the wound. Tracer was observed extravasating from the collecting lymphatic vessels into the "honeycomb" network of initial lymphatic vessels. (B) Representative intensity tracking from the control imaging segments depicts the presence of discrete fluorescent packets pre-surgically with a subsequent absence at later time points.

3.3.4 *Obesity adversely influences lymphatic pump function following lymphedema induction and resolution*

We utilized our previously described NIR imaging techniques to non-invasively assess the functional response of the intact lymphatic vessel during lymphedema progression and resolution (149, 235). Functional measurements indicate that obesity adversely impacts the functional response of the intact lymphatic vessel following surgery. Packet frequency, indicative of contractile frequency, was found to be significantly decreased at multiple time points in obese animals compared to control. Pre-surgical values for packet frequency were significantly different between control and obese at 6.7 ± 0.7 min^{-1} vs 3.9 ± 0.3 min^{-1}. Following surgery, the average packet frequency of the intact lymphatic vessel acutely declines at day 7 by roughly 80% of the pre-surgical value for both control and obese animals. Interestingly, control animals have greater decreases in packet frequency over time compared to their pre-surgical baseline values and continued to exhibit these declines 70 days after surgery. However, obese animals have significantly lower absolute packet frequency compared to controls at days 0, 28, and 56 (Figure 19). Similar trends are observed in packet transport, a metric indicative of transport driven by intrinsic contractility. Control animals had greater impairment of lymphatic packet transport caused by the surgery when compared to pre-surgical baseline values that

subsequently persisted throughout the course of the study. However, obese animals exhibited significantly lower absolute values for packet transport compared to controls at the 28 and 56-day time points (Figure 19). Lymphatic pumping pressure, a metric indicative of contractile force (149, 177), was found to present striking differences. Despite pre-surgical pumping pressure values being relatively similar between control and obese, obese animals displayed profound decreases following the surgery. Specifically, at the 28-day time point, obese animals exhibited no detectable pumping pressure compared to control with values of 0.0 ± 0.0 mmHg vs 23.4 ± 5.2 mmHg respectively. A similar difference was observed at the 42-day time point. Interestingly, at the end of the study, 70 days after the initial surgery, obese animals still exhibited significant latent defects in lymphatic pumping compared to controls that were not otherwise evident pre-surgery (Figure 19). Taken together these results indicate that obesity adversely alters the function of the intact lymphatic vessel following surgery. Interestingly, obesity does not seem to increase risk for functional impairment of the collecting vessel when compared to pre-surgical baseline values. However, when looking at the absolute differences between the control and obese groups, it becomes apparent that obesity results in lowered contractile frequency, actively driven transport, and pumping pressure of the collecting lymphatics at multiple time points. The most profound differences were observed in the persistently lowered lymphatic pumping pressure, suggesting impairments to the force generating abilities of the lymphangions.
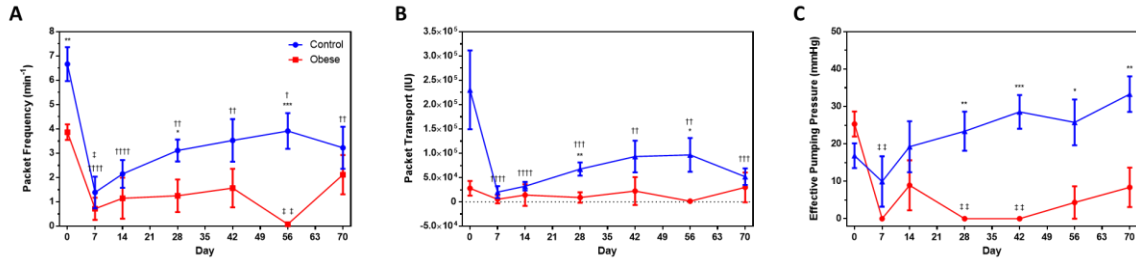
Figure 19: Functional measurements, obtained via NIR imaging, indicate that obesity adversely impacts the functional response of the intact lymphatic vessel following surgery. (A) Packet frequency, the frequency of fluorescent pulsations within the vessel, exhibited significant differences between control and obese groups. (B) Packet transport, the integral of the packet frequency signal over time, was used to evaluate fluorescence transport driven by intrinsic lymphatic contractions. (C) Effective pumping pressure was used to evaluate the maximal pressure generated by the collecting vessel to overcome occlusion. Error bars represent SEM. (n=8, control) (n=6, obese) (*, denotes significant difference between control and obese; †, denotes significant difference between control value and the baseline pre-surgical control value; ‡, denotes significant difference between obese value and the baseline pre-surgical obese value, p < 0.05).

3.3.5 Obese animals have increased waviness of the collagen microstructure in the intact collecting lymphatic vessels following lymphedema

To determine if the latent differences in collecting lymphatic function corresponded with differences in structure, we surgically isolated the intact collecting lymphatic vessels distal to the wound site in control and obese mice. First, to observe the collagen microstructure of the vessel wall, we utilized 2nd harmonic microscopy coupled with confocal Z-stack. Quantititative analysis of these images indicate that vessels collected from the obese animals have a modest difference in the morphology of collagen. Specifically, the collagen microstructure of isolated collecting vessels from obese mice was found to exhibit significantly increased waviness of collagen fibers (Figure 20). This

increased waviness suggests that the lymphatic vessels could withstand increased transmural pressurization before straightening and subsequently mechanically engaging the collagen .
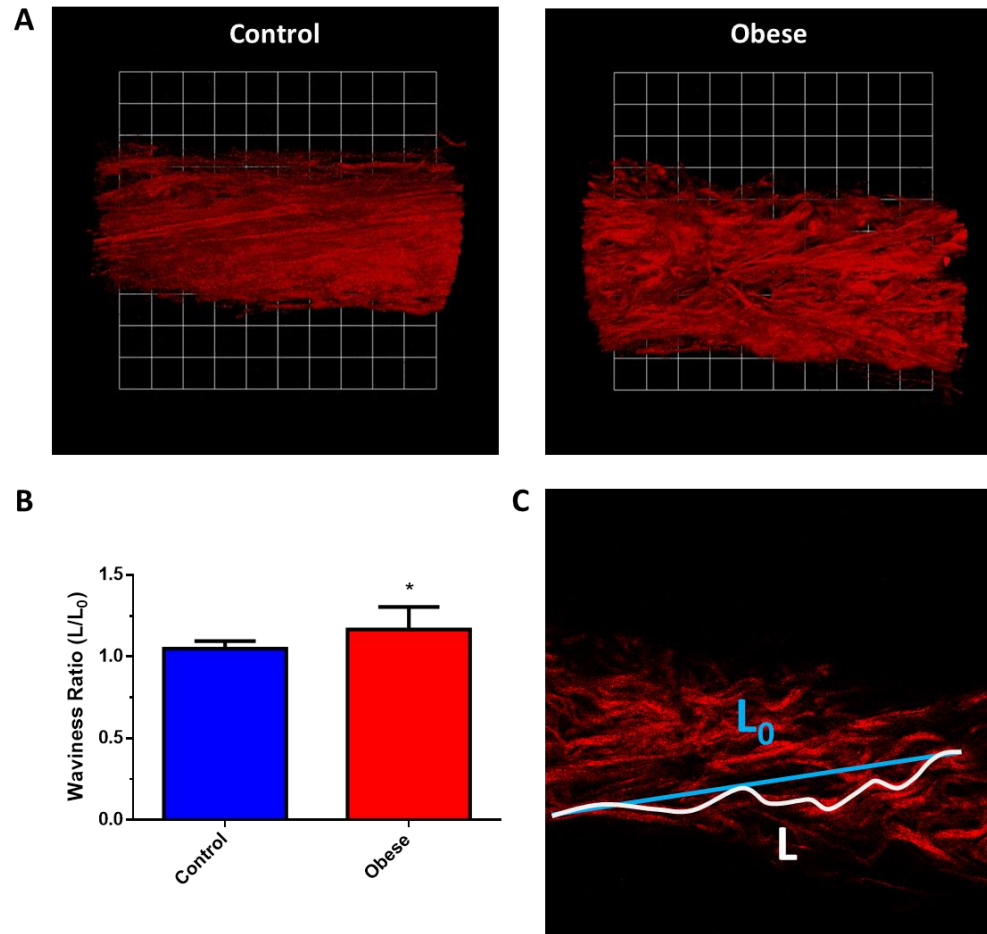
Figure 20: (A) Representative 3D 2nd harmonic generation images of collecting lymphatic collagen microstructure from control and obese mice. (B) Collagen fibers were found to be significantly wavier in obese mice compared to control. (C) Representative image depicting the calculation of the collagen waviness ratio computed from the total length of the collagen fiber and the end-to-end length. (*, denotes significant difference between control and obese, p < 0.05).

Given that we observed profound declines in the lymphatic pumping pressure of obese mice via NIR imaging methods, we investigated how smooth muscle cell coverage may be altered. Collecting lymphatic vessels were briefly fixed and immunofluorescently stained for alpha smooth muscle actin (α-SMA) and prospero homeobox protein-1 (Prox-1). Fluorescent images with confocal Z-stack depict no striking differences between smooth muscle coverage or lymphatic endothelial cells.
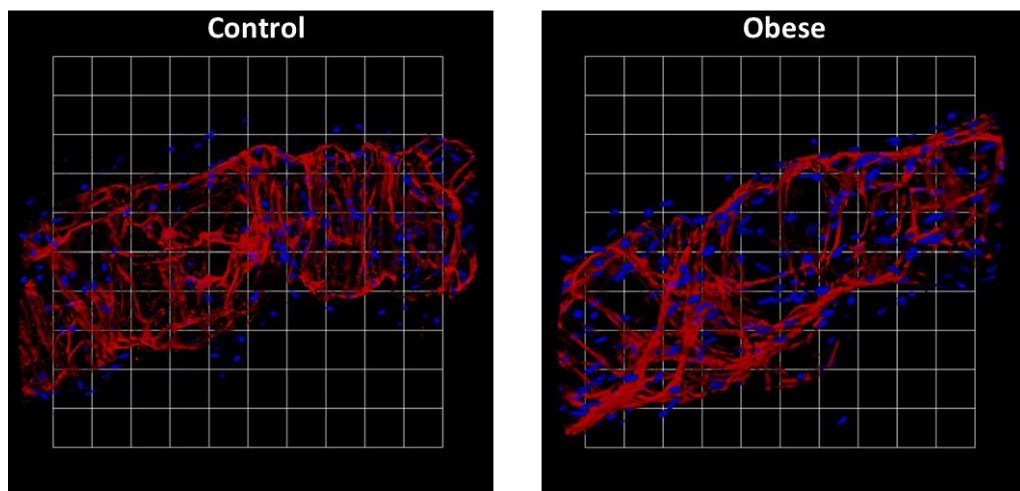
Figure 21: Representative immunofluorescent images of collecting lymphatic vessels labeled for α-SMA (red) and Prox-1 (blue). Confocal images of isolated collecting lymphatic vessels were used to produce 3D Z-stack renderings of the α-SMA/Prox-1 structure.

3.3.6   Inhibition of T-cell differentiation with tacrolimus protects against the functional declines caused by obesity during lymphedema

To determine the extent that T-cells are mediating the differences in lymphatic function caused by obesity during lymphedema, we pharmacologically prevented local T-cell activation and differentiation by treatment with a calcineurin inhibitor called

tacrolimus. A subset of obese animals (n=5) were treated via topical application of tacrolimus ointment twice daily beginning immediately after the 14-day functional imaging session. Results from these experiments show that tacrolimus does not appear to differentially impact tail swelling following treatment; however, this could be because the obese + tacro treated experimental group swelled, on average, more than the obese group, despite undergoing identical experimental protocols before day 14 (Figure 22). Upon functional assessment with NIR imaging, tacrolimus treatment was not found to statistically improve the fluorescence arrival time compared to untreated obese animals. Despite this, a trend towards decreased arrival time in the treated group was observed at day-42 (Figure 23).
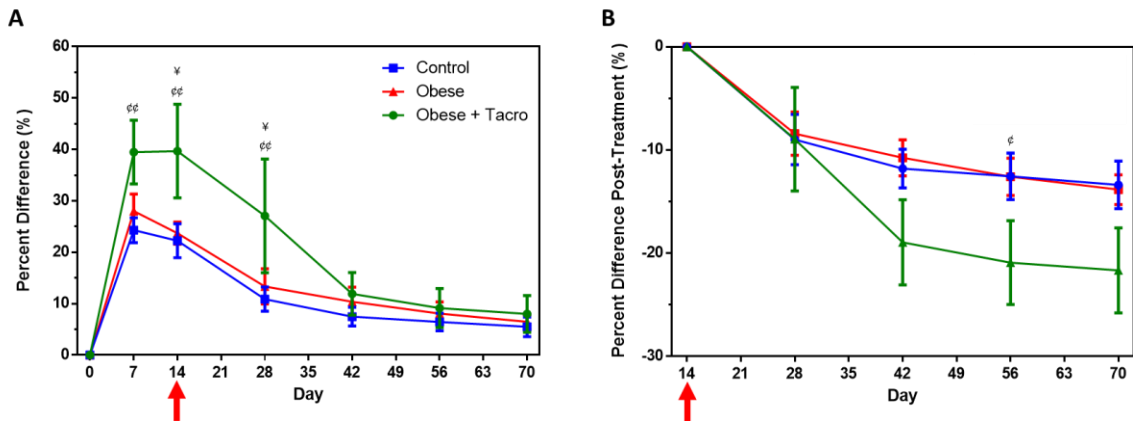
Figure 22: Topical tacrolimus ointment was used to treat a subset of obese mice (n=5) beginning at day 14 post-surgery. (A) Treatment with tacrolimus ointment did not differentially impact absolute tail swelling; however, this is likely caused by the tacrolimus treated group exhibiting significantly greater swelling prior to the start of treatment. (B) Treatment with tacrolimus ointment resulted in a significant reduction in tail swelling when compared to start of treatment values at day 14. Red arrows indicate the beginning of tacrolimus treatment at the 14-day time point. Error bars represent SEM. (n=8, control) (n=6, obese) (n=5, obese + tacro) (¢, denotes significant difference between obese + tacro and control; ¥, denotes significant difference between obese + tacro and obese, p < 0.05).
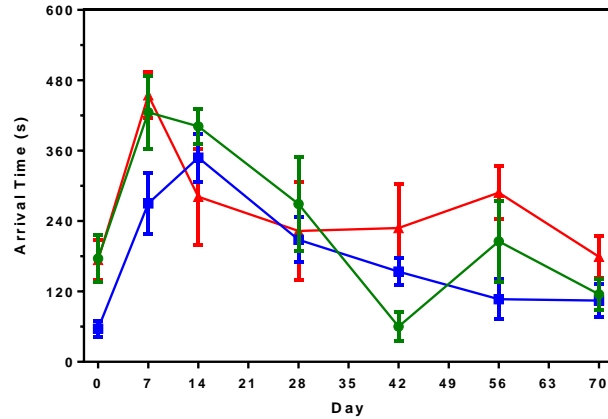
Figure 23: Treatment with tacrolimus ointment did not differentially impact the fluorescence arrival time to the wound site following injection of fluorophore. Red arrows indicate the beginning of tacrolimus treatment at the 14-day time point. Error bars represent SEM. (n=8, control) (n=6, obese) (n=5, obese + tacro) (¢, denotes significant difference between obese + tacro and control; ¥, denotes significant difference between obese + tacro and obese, p < 0.05).

Our NIR functional imaging techniques were used to assess the response of the intact collecting lymphatic vessel to tacrolimus treatment. Tacrolimus was found to positively impact the packet frequency of the intact lymphatic vessel in a differential manner from the untreated group. Specifically, tacrolimus treatment appeared to aid the recovery of packet frequency, significantly increasing to 4.3 ± 1.1 min^{-1} vs 0.0 ± 0.0 min^{-1} in the untreated obese animals. In fact, the tacrolimus treated animals achieved day 70 values of packet frequency comparable to chow fed controls, despite having significantly lower baseline values than controls (Figure 24). Similar trends were observed with regards to packet transport; however, these trends were not statistically different. One of the more striking alterations caused by tacrolimus treatment was the recovery observed in lymphatic pumping pressure. Specifically, the tacrolimus treatment improved lymphatic pumping pressure of obese animals to levels similar to chow fed controls by day 28. Given that the

85

untreated obese animals had no detectable effective pumping pressure at days 28 and 42, tacrolimus appears to facilitate a striking improvement in the pressure generating capabilities of the lymphatics (Figure 24). Taken together, these results suggest that pharmacological treatment with tacrolimus is able to attenuate the declines in the active contractile response of the intact lymphatic vessel associated with obesity during lymphedema.
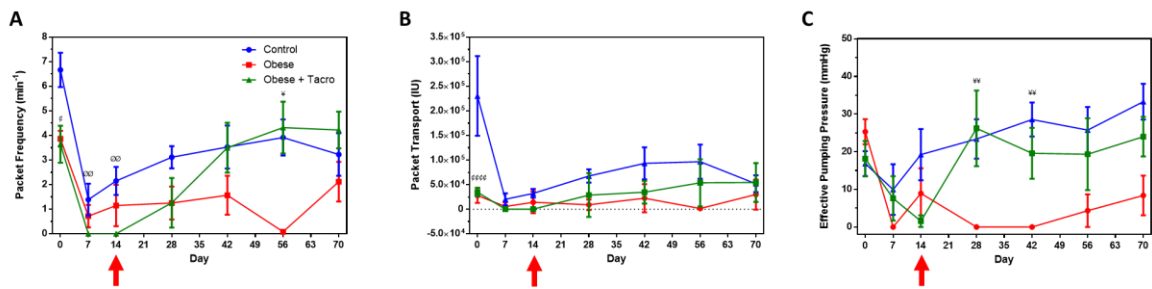
Figure 24: Tacrolimus ointment protects against the declines in collecting lymphatic function caused by obesity after induction of lymphedema as assessed by NIR imaging. (A) Tacrolimus treatment for a subset of obese mice increased lymphatic packet frequency to levels similar to control with significant differences between the obese group manifesting at 56-days post-surgery. (B) Tacrolimus treatment was not found to significantly improve lymphatic packet transport. (C) Tacrolimus treatment protected against the declines in pumping pressure caused by obesity with significant differences from the untreated group being observed at days 28 and 42. Red arrows indicate the beginning of tacrolimus treatment at the 14-day time point. Error bars represent SEM. (n=8, control) (n=6, obese) (n=5, obese + tacro) (¢, denotes significant difference between obese + tacro and control; ¥, denotes significant difference between obese + tacro and obese; Ø, denotes significant difference between obese + tacro and baseline day 0 value, p < 0.05)

3.4   Discussion and Conclusions

Obesity has long been demonstrated to be a primary clinical risk factor in the development of lymphedema. Motivated by this, a number of studies have demonstrated

robust characterizations of the pathophysiology and the biological mechanisms that drive the pathogenesis of the disease during obesity. However, despite their essential role in the active transport of lymph, the effects of obesity on the collecting lymphatic vessels have not been fully characterized during lymphedema. Specifically, no study has assessed collecting lymphatic pump performance over the course of lymphedema induction and resolution. It was therefore the goal of this work to determine if and how obesity alters collecting lymphatic function during lymphedema development and resolution. By using functional NIR lymphatic imaging approaches we have demonstrated that obesity adversely impacts lymphatic contractile activity and that this continues even after lymphedema is resolved. Further, we have demonstrated that pharmacological calcineurin inhibition, via tacrolimus, can protect against these functional declines.

A lack of clinically relevant animal research models for lymphedema has historically limited the study of the collecting lymphatic vessels in the disease. The most commonly described model is the rodent tail, which traditionally involves ablation of all the initial and collecting lymphatic vessels on the tail to induce lymphedema (49, 147, 186, 201). However, since all the collecting lymphatics have been ligated, this limits the use of imaging techniques with the ability to quantify collecting lymphatic functional response. Recently, our lab has produced the rodent tail model shown here that leaves a collecting vessel intact while still inducing the swelling a tissue remodeling associated with lymphedema (236). By coupling this model with our novel NIR functional lymphatic imaging approaches discussed in Chapter 2 (149, 235), we are able to longitudinally assess how increased fluid load due to the loss of lymphatic drainage pathways influences the intact collecting lymphatic vessel. This is particularly relevant in the context of obesity

87

where we and others hypothesize that collecting vessel dysfunction plays a role in lymphedema development.

We and others have previously shown that obesity has direct negative effects on the intrinsic contractile activity of the lymphatics (27, 152, 153, 192, 222). The results of this study have further confirmed that obese animals have decreased pre-surgical baseline packet frequency corresponding to decreased contractile frequency. It has become apparent that this impairment is tied to increased CD4+ T-cell mediated inflammation during obesity, which increases release of known contractile mediators such as nitric oxide (27, 152, 153, 192, 222). Interestingly, no other metrics of lymphatic pump function are significantly impaired by obesity pre-surgically. This suggests that obesity alone may not cause adverse remodeling that reduces the pressure generating capacity of the lymphangion chain. This hypothesis is supported by studies that demonstrate increases in contractile frequency upon inhibiting inflammation within a 2-week period (222); however, this warrants further investigation. It was less clear, until this point, how the contractile response was altered following the induction of lymphedema.

Surgical disruption of the lymphatic vasculature via our single-vessel ligation induced a swelling cascade similar other rodent tail models of lymphedema and obesity that involve all the collecting and dermal lymphatic vessels (192). However, given that there remains an intact lymphatic vessel draining the tail, it is unsurprising we observed substantially less peak swelling of the tail in comparison to traditional tail lymphedema models (roughly 30%). This implies that the collecting lymphatic vessels play a role in mediating the tissue swelling associated with lymphedema (236). Interestingly, despite using a unique experimental model, our results correspond to previous studies in mice

showing that obesity does not increase absolute amounts of tissue swelling following lymphedema induction in mice (192).

Although a collecting lymphatic vessel remained structurally intact throughout the study, the ligation of its counterpart along with the dermal lymphatics induced significant declines in function for both control and obese mice within the 14 days following surgery. It is during this period that tissue inflammation and swelling is heightened in response to tissue damage (147, 192, 249, 250). During this time frame, obese animals exhibited delayed fluorophore transit through the intact collecting lymphatic vessel in comparison to lean controls. This is supported by work demonstrating that obesity delays nodal uptake of tracer as assessed by lymphoscintigraphy (192). Despite having an apparent functional deficit, packet frequency, packet transport, and pumping pressure were not significantly different compared to lean controls. Taken together, this suggests that obesity may adversely impact the rate of fluorophore uptake into the collecting lymphatics during this time period as opposed to having direct differential effects on the collecting lymphatic vessels themselves. This could be caused by the decreased interstitial fluid flow observed during obesity that decreases convection of fluorophore to the draining initial lymphatics and subsequently intact collecting lymphatic vessels (239).

28 days post-surgery, after swelling has substantially declined, obese animals begin to manifest a differential functional phenotype compared to controls. Specifically, obese animals exhibit decreased packet frequency, packet transport, and pumping pressure. Given that obesity is known to negatively influence lymphatic contraction frequency (27, 152, 153, 192, 222), it is relatively unsurprising that this trend continues throughout the resolution of lymphedema. However, pumping pressure was not shown to be affected by

89

obesity at pre-surgical, and declines compared to control only appear manifest after lymphedema is induced. Further, this difference in pumping pressure persists even at the 70-day time point when nearly all swelling has subsided. In a recent publication, discussed in Chapter 2, we demonstrated that lymphatic pumping pressure is primarily governed by the number of lymphangions in the vessel chain, their contractile force, and the frequency of lymphatic contractions (177). Given that we observed a simultaneous decline in packet frequency, it seems reasonable to infer that this decline may be caused in part by a decrease in the intrinsic contractile frequency of the collecting vessel. It is also possible that the etiology is multi-factorial and that obesity alters the contractile strength of lymphatic muscle cells at later time points following induction of lymphedema. In fact, this is supported by studies demonstrating that rats with metabolic syndrome possess collecting lymphatic vessels that generate significantly less contractile force (252).

Because obese animals possess latent functional declines that may be linked to alterations in intrinsic contractile forces, we investigated if remodeling of collagen microstructure or LMC coverage could explain the significant loss in lymphatic pressure generation (137, 214, 252). We found that the collagen microstructure of the intact lymphatic vessels in obese animals exhibited an increase in the waviness of the fiber bundles. This increase in waviness likely influences the passive mechanical behavior of the vessel. For example, other properties being equal, wavy collagen fibers will result in decreased collagen engagement upon pressurization of the vessel and a subsequent increase in the compliance of the vessel (37, 179). However, this is only true for tensile loading of the collagen fibers. Given that contractions of LMCs produce compressive forces on the fibers, it is unclear how the increase in waviness would ultimately influence pressure

generation. Further, qualitative assessments of smooth muscle coverage did not appear to provide any insight into the differences in pumping pressure between obese and control. To better assess the etiology of the pumping pressure differences, it would be beneficial for further studies to use a combination of isolated vessel functional testing in addition to a thorough investigation of the mechanical properties of the vessels.

The latent collecting lymphatic dysfunction that we observed here could have clinical relevance. In the case of surgically-related lymphedema, the patients that later develop the disease still possess patent collecting lymphatic vessels (47) and often do not present with symptoms of lymphedema until 1 or more years after surgery (7). It is possible that latent collecting lymphatic dysfunction increases susceptibility of patients to developing lymphedema following a secondary insult that challenges the lymphatic system's ability to properly drain fluid. This has been supported by research that has demonstrated that outward recovery from lymph node dissection in the rat foreleg masks an ensuing chronic and latent lymphatic insufficiency, which reduces the ability of the foreleg lymphatic system to prevent edema during an acute inflammatory process (135). However, further studies are necessary to determine what role the collecting lymphatic vessels play in the later susceptibility to lymphedema development.

Although studies have demonstrated that CD4+ T-cells are an essential mediator of the tissue changes associated with lymphedema development during obesity, it is less clear how these cell types may directly or indirectly influence collecting lymphatic function during the disease (192). Recent studies have demonstrated that pharmacological prevention of T-cell activation and differentiation via a calcineurin inhibitor called tacrolimus shows promise for decreasing the chronic tissue inflammation associated with

obesity and improve collecting lymphatic contraction frequency (222). Further investigation has demonstrated that tacrolimus produces promising results for treating and preventing lymphedema (70). We subsequently utilized these methods to investigate the role of T-cells in mediating the functional dysregulation of the collecting lymphatic vessels observed during obesity. Tacrolimus ointment was applied to the tails of obese mice beginning 14 days after surgical induction of lymphedema in our single vessel ligation model. In contrast to the previous studies we did not observe any significant declines in tail swelling compared to baseline (70); however, this could be due to the fact that our tacrolimus treated experimental group exhibited significantly greater swelling before the start of treatment. Upon examination of the post start of treatment reduction in tail swelling, it became apparent that tacrolimus had in fact provided modest improvements. It is important to note that these discrepancies could be due to differences in disease pathogenesis between our single vessel ligation model and the total vessel ligation model. For example, perhaps the swelling observed in the total vessel ligation model is primarily mediated by the accumulation of pro-inflammatory T-cells to a greater extent than our model. This would explain why inhibition of T-cell activation and differentiation would produce a greater decrease in swelling; however, this remains speculative and should be more thoroughly investigated.

Despite observing only modest decreases in the tail swelling of obese animals we discovered, for the first time, that tacrolimus protects against the functional declines associated with the collecting lymphatics during obesity and lymphedema. The primary effects of tacrolimus on collecting lymphatic function where observed at the 28 days post induction of lymphedema. At this time point treatment with tacrolimus caused an increase

92

in lymphatic pumping pressure in comparison to untreated obese animals. This effect persisted throughout the 70-day time course. Interestingly, this rise in pumping pressure corresponds with an increase in packet frequency. The combination of these results lends credence to the hypothesis that the declines in pumping pressure seen in the untreated obese animals is caused by declines in packet frequency, corresponding to decreases in the intrinsic contractile frequency of the vessels. Given that inflammatory mediators such as cytokines (3), prostanoids (245), histamine (66), and nitric oxide (NO) (32, 139, 149, 235) are known to be potent modulators of lymphatic contractile activity, it seems reasonable to infer that tacrolimus may have downstream effects on these mediators via inhibition of T-cell activation. This is supported by work demonstrating that tacrolimus decreases iNOS expression (222). Tacrolimus could also have direct effects on collecting lymphatic contractile response. Unpublished preliminary data from our research group has indicated that tacrolimus may increase the contractile frequency of rat collecting lymphatic vessels. However, this work is preliminary and warrants more in-depth investigation. Further, it is unclear from this study if tacrolimus influences collecting lymphatic remodeling during lymphedema. For example, would treatment with tacrolimus differentially influence the alterations in the collagen microstructure that were observed in the untreated obese group?

CHAPTER 4. LYMPHATIC FUNCTION AND REMODELING RESPONSE COMPENSATE FOR A LOSS OF FLUID RETURN PATHWAYS IN SHEEP (AIM 3)

4.1 Introduction

Research on lymphatic growth and remodeling following injury have primarily utilized mouse lymphedema models, with the mouse tail model being the most widely used (10, 82, 83, 187). This model involves circumferential ligation of the dermal level initial lymphatics and collecting lymphatics on the mouse tail. Following the surgery, the tissues distal to the wound exhibit significant swelling. Although these models have provided valuable information about molecular factors that affect lymphatic growth and remodeling of the initial lymphatics following injury, the relevance to human lymphatic physiology, where the vessels must overcome large gravitational loads, is lacking. This is highlighted by the fact that most mouse models of lymphedema typically resolve if given enough time, which isn't surprising since the vessels only need to transport fluid up a few centimeters of a hydrostatic pressure gradient (251).

In this study, we present an adaptation of methodologies used in rodent models for use in sheep, and utilize these to longitudinally evaluate the functional and molecular changes of an uninjured collecting lymphatic vessel as it compensates for a compromised lymphatic network. We then utilized MRI to evaluate structural changes in the lymphatic network as well as near-infrared (NIR) lymphatic imaging approaches to quantify changes in collecting lymphatic function of the vessels over a 42-day period of remodeling. After

this, we harvested the collecting lymphatic vessels and utilized ex-vivo vessel perfusion techniques to examine changes in the lymphatic vessel's intrinsic contractile response to transmural pressure and flow. Proteomics and subsequent pathway analysis was used to elucidate pathways impacting structure and function of the lymphatic muscle cells that were altered by the lymphatic remodeling. Finally, isolated vessels were mechanically tested and the mechanical properties of the vessels were used to inform a computational model to simulate how the differences in these properties affect lymphatic function.

4.2   Materials and Methods

4.2.1   Study Overview

All animal procedures described in this study were approved by the University of Georgia Institutional Animal Care and Use Committee. A graphical depiction of the study design is shown in (Figure 25). A total of 5, 3 to 5-year old randomly bred female Suffolk sheep were used in this study; Before the study, 3 of the sheep underwent Gadolinium-Enhanced MR imaging (GE MRI) to structurally map the lymphatic anatomy of the hind limbs. One day after the MRI the sheep underwent the initial NIR functional lymphatic imaging procedure on both hind limbs. After imaging, the collecting lymphatic ligation surgery was conducted on one of the hind limbs, with the contralateral limb remaining intact to act as an internal control. The sheep were recovered from anesthesia following the completion imaging procedure and surgery. Follow-up NIR functional lymphatic imaging was conducted 7, 14, 28, and 42 days after the procedure. One day before the final NIR imaging session, the 3 sheep that underwent the MR lymphatic imaging underwent a second MR imaging session. On day 42, following the NIR imaging procedure, the sheep were not

95

recovered and were euthanized via pentobarbital overdose for tissue collection. Collecting lymphatic vessels from the control and wounded legs were isolated and excised for ex-vivo functional testing of the vessels. The datasets generated during and/or analyzed during the current study are available from the corresponding author on reasonable request. Additionally, any custom software or code used in this study are available on request.
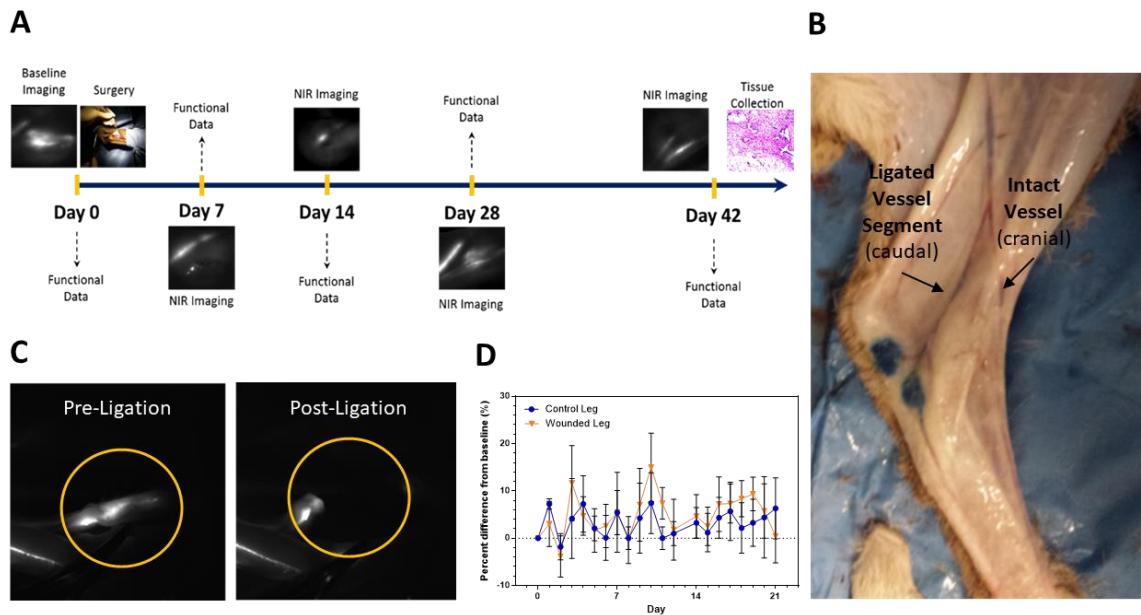
Figure 25: (A) Graphical depiction of the study design. On day -1, pre-surgery MRI was used to map the lymphatic anatomy of the hind limbs in sheep. On day 0 pre-surgical NIR imaging was used to evaluate baseline lymphatic function. Immediately after imaging, the caudal lymphatic vessel on one of the hind limbs was ligated in order to create a lymphatic injury, while the contra-lateral limb was left intact. Follow-up NIR imaging was used to evaluate changes in lymphatic function of the vessels on the intact and wounded limbs at days 7, 14, 28, and 42. (B) Evans blue was injected intradermally and uptake by the lymphatic vessels was visualized with the skin removed. Two primary collecting lymphatic vessels (cranial and caudal) run along the lateral aspect of the hind limb and serve to drain fluid from the distal portions of the limb. During surgery on Day 0, the caudal vessel was ligated whereas the cranial vessel was left intact. (C) NIR imaging was used to guide and confirm ligation of the caudal lymphatic vessel. Pre-ligation images exhibit fluorophore uptake by the vessel. After ligation, and excision of a 2 cm segment of vessel, NIR imaging confirmed the absence of fluorescence transport by the vessel. (D) Circumferential measurements taken at the mid tarsus on the hind limb was used to

identify the presence or absence of swelling due to the injury. No significant swelling of the tissue was observed. Error bars represent SEM.

4.2.2 Surgical procedure

Sheep were anesthetized with midazolam 0.25 mg/kg and ketamine 5 mg/kg, intubated and maintained under anesthesia at 1-3% sevoflurane in oxygen. The animals were placed on either their right or left sides. Vitals, including heart rate, body temperature, blood pressure, and partial oxygen pressure were monitored throughout the imaging procedure. The hind limbs of the animals were shaved with electric sheers, and sterilized with three alternating scrubs of 2% chlorhexadine and 70% isopropyl alcohol. A 4 cm incision was made on the lateral aspect of the hind limb proximal to the tarsus, exposing a collecting lymphatic vessel running in parallel to the saphenous vein. A 2 cm portion of the vessel along with the vein was ligated with sutures and resected. 3 animals had the surgical procedure done on the right hind limb while the remaining 2 animals had the procedure done on the left hind limb. The contralateral limb was left intact to serve as an internal control.

4.2.3 Near-infrared imaging system

The NIR imaging system was set-up in a manner similar to our previously described system (149, 234, 235). A diode driver and temperature control box powered a 300 mW 785 nm laser diode (Thorlabs, Newton, NJ), which provided excitation light. To disperse the laser over a larger area of approximately 75 cm2 with less than 1.9 mW/cm2, a 20 degree beam diffuser (Thorlabs, Newton, NJ) was fixed in front of the diode. A 25 mm fixed focal length lens (MVL25M43, Thorlabs, Newton, NJ) and a bandpass filter (CW: 835, FWHM: 45) were attached to a Pixis 1024B back-illuminated CCD camera (Princeton

Instruments, Trenton, NJ) to capture fluorescence emission. The camera was connected to a computer where images were acquired by a custom LabView VI. The camera and light source were mounted to a 1.8 m camera crane jib, which enabled positioning of the camera with 3 degrees of freedom (ADC-306, Advanced Digital Inc.).

To measure the effective lymphatic pumping pressure, a custom feedback-controlled pressure cuff was developed. Inflation of a veterinary blood pressure cuff (UP-0925, Technicuff, Leesburg, FL) was controlled using an air pump (VMP1625MX-06-50-CH, Virtual Industries Inc., Colorado Springs, CO) and generic solenoid valve. Commands to control the relays powering the pump and solenoid were sent via 5v output on an NI-DAQ 6008 (National Instruments, Austin, TX). Pressure output from a pressure transducer (SSCDRRN005PDAA5, Honeywell, Morristown, NJ) attached to the cuff was fed back into the DAQ and used by a custom LabView VI to make the logic decisions for inflation and deflation of the cuff (available on request).

4.2.4 *Near-infrared imaging procedure*

The NIR lymphatic tracer used for the imaging procedures consisted of a NIR fluorophore IRDye 800 CW NHS Ester (929-70020, LI-COR Biotechnology, Lincoln, NE) bound to 40kDa methoxypolyethylene glycol (mPEG) (JenKem Technology USA, Plano, TX) in a manner similar to a previously described method (28, 169). Equimolar ratios of IRDye 800CW NHS Ester (75 nmol) and mPEG (75 nmol) were bound room temperature in 0.5mL anhydrous dimethyl sulfoxide (DMSO) for 24hrs. After binding, the mixture was transferred into a dialysis cassette with a 7 kDa molecular weight cutoff (66370, Thermo Fisher Scientific, Waltham, MA). The cassette was submerged in a 4L beaker of de-ionized

water and was dialyzed for 24hrs. The dialyzed solution was removed from the cassette and lyophilized for 24hrs in 1.5mL conical centrifuge tubes. The lyophilized tracer was stored prior to use in -20C freezer. A day before use the dry tracer was re-constituted in 0.5 mL sterile saline and filtered into a sterile rubber topped vial using a 0.2 um syringe filter (IRPEG40).

The camera and excitation light source were positioned over the lateral aspect of the mid hind limb centered 10 cm proximal to the hock. 0.5 mL of IRPEG40 was injected intradermally into the fatty part of the hoof cleft on the frontal aspect of the hind limb with a sterile 21g needle. A second injection of 0.5 mL IRPEG40 was given in the dorsal aspect of the hind limb 5 cm distal to the hock. NIR images of dynamic fluorescence transport were captured at a rate of 1 fps with a 50 ms exposure time for a total of 20 min. The pressure cuff was then fitted to the hind limb with the proximal edge touching the apex of the hock. The pressure in the cuff was controlled to produce the following sequence. The pressure was increased to 80 mmHg over a period of 65 s and held at this value for 10 min to allow for the proximal vessel to completely empty its contents. This pressure was chosen for lymph flow occlusion because 80 mmHg is close to the diastolic blood pressure of a rat and well below the mean arterial pressure, so blood supply was not occluded during the experiment. After 10 min at 80 mmHg, the pressure was decreased to 55 mmHg over a period of 25 s. The pressure was then decreased in decrements of 2.5 mmHg and held at each pressure step for 60 s, until the pressure value was zero, where it remained for 3 min before the program was terminated. The pressure cuff controller took less than 15 s to reach each new pressure decrement. The pressure at which flow was restored as observed by

fluorescence return proximal to the cuff was determined as the lymphatic pumping pressure.

4.2.5   Near-infrared imaging analysis

Three distinct metrics of lymphatic function were evaluated using previously our previously developed methods (149, 235). 1) Packet frequency was evaluated by tracking the average time between peak fluorescence pulsations within regions of interest (ROIs) traced over lymphatic vessels during our initial imaging sets. Packet frequency has been correlated with the frequency of intrinsic lymphatic contractions in vivo. 2) Florescence transport was calculated by evaluating the average integral of packets with respect to time. It is the absolute amount of fluorescence transported through a region of interest over time. Fluorescence transport is a function of lymphatic contraction frequency, contraction amplitude, and packet velocity. 3) Effective lymphatic pumping pressure was calculated by determining the occlusion pressure at which the fluorescence within the vessel proximal to the cuff returns to half of its pre-occlusion value. It is a measure of the collecting lymphatic vessel chain's ability to generate the pressures needed to overcome an occlusive force.

Significant differences between control and wounded groups was determined via unpaired t-test for each time point with $p < 0.05$ indicating statistical significance. Significant difference between pre-surgical baseline (Day 0) and later time points was evaluated using 1-way ANOVA with post-hoc Dunnett's test for multiple comparisons with $p < 0.05$ indicating statistical significance. All statistical analyses were done using Prism software (GraphPad Software, La Jolla CA).

100

4.2.6 Functional testing of isolated collecting lymphatic vessels

Lymphatic vessels were isolated and tested from sheep in a manner similar to our previously described methods in rats (109, 110). After the final NIR imaging session, sheep were euthanized via barbiturate overdose. After euthanasia, the skin was removed from the hind limb to expose the collecting lymphatic vessels. Sterile saline was periodically perfused onto the tissue to ensure that it did not dry. The intact cranial lymphatic vessel on either the control or wounded leg was located and 1 cm segments were isolated from the surrounding adipose and a fascia. The segments were removed and immediately placed in a bath containing DMEM/F12 (GE Healthcare Life Sciences, Logan, UT) with added antibiotic mixture (Invitrogen Corp., Carlsbad, CA) to achieve a concentration of 100 units of Penicillin and 100 μg of streptomycin per ml of DMEM/F12.

Individual segments were subsequently cannulated onto micro pipettes in a single vessel cannulation chamber (Living Systems Instrumentation, St. Albans, VT) and placed under a microscope with a 2X objective (VWR, Radnor, PA) and a GuppyPRO (Allied Vision, Exton, PA) camera to capture dynamic video of contractile behavior. The vessel chamber inlet and outlets were connected via silicon tubing to inlet and outlet water columns, which were used to vary transmural pressure and transaxial pressure gradient. The chamber bath was constantly perfused with fresh media and was held at a 38°C throughout the experiment by a flexible Kapton heater and CN740 temperature controller (Omega Engineering, Norwalk, CT).

The experimental protocol began with 45-50 min equilibration at 6 cmH2O transmural pressure to ensure the presence of spontaneous vessel contractions. After the equilibration, vessel segments were exposed to increasing transmural pressures via water column with values of 1.5, 3, 5, 7, 9, 11, 12, 15, 17, and 19 cmH$_2$O for 5-10 min at each pressure. The functional response of the lymphatics to axial pressure gradient was evaluated by maintaining an average transmural pressure of 6 cmH$_2$O while increasing the inlet water column to achieve axial pressure gradients of 0, 1, 3, and 5 cmH$_2$O for 5-10 min at each axial pressure.

Isolated vessel functional metrics were calculated from the diameter tracings in a manner similar to our previously described methods in rats (109, 110). The data shown in this manuscript represent individual segments collected from individual animals (ie. there were no replicates from animals and each data point shown represents an individual segment from a different animal). Significant difference between control and wounded groups was evaluated at their respective transmural or axial pressure gradient using 2-way ANOVA with post-hoc Sidak correction for multiple comparisons. In addition to this, 1-way ANOVA with post-hoc Dunnett's correction for multiple comparisons was used to determine significant differences between baseline transmural or transaxial pressure and the applied transmural or transaxial pressure for control or wounded groups respectively. All statistical analyses were done using Prism software (GraphPad Software, La Jolla CA) with p < 0.05 indicating statistical significance.

Wire myography was done on vessel segments from a single animal (n=4 control, and n=4 wounded) similar to a method previously described by (41). 2 mm segments of vessel were cut from the 1 cm segments that had been collected and were mounted individually to a

small vessel wire myograph (Model 500A, Danish Myo Technology, Denmark). Segments were allowed to equilibrate for 1 hr in a bath containing DMEM/F12 at 38°C. After the 1 hr equilibration period force transducer readings from the wire myograph were recorded at a rate of 1 Hz and spontaneous vessel contractions were confirmed. Peak contractile tensions from the force transducer readings were averaged over a 30 min period for each segment. Statistical significance between control and wounded segment groups was determined using an unpaired t-test with $p < 0.05$ indicating a significant difference between groups.

4.2.7 Proteomic analysis of lymphatic muscle cells

A primary lymphatic muscle cell (LMC) line was formed from collecting lymphatic vessels isolated from sheep hind limbs. The collecting vessel were rinsed in a physiological saline before being transferred to a tissue culture dish where it was attached by gently pressing the ends to the surface with forceps. Vessels were cultured in Dulbecco's Modified Eagle's Medium (Thermo 11965-092), high glucose, with 10% Fetal Bovine Serum, along with Antibiotic-Antmycotic (Thermo 15240062). Media was exchanged every 2-3 days. Muscle cells began to migrate and proliferate from the vessel around day 3. Vessel were gently discarded after a week, leaving only the newly migrated cells. Cells were split using Trypsin, 0.25% EDTA, and frozen in liquid nitrogen at passage 3. Experiments were conducted on LMCs between passage 5-7.

LMCs were solubilized in 8M Urea/2%SDS/100 mM Ammonium Bicarbonate and sonicated for 10 min on ice. Samples were then centrifuged at 14,000g for 5 min and the supernatant remove. Proteins in the supernatant were reduced, alkylated and trypsin

digested, as previously reported (50). Peptides were separated on a C18 column and analyzed with a Q Exactive Plus mass spectrometer. Each sample was run in technical triplicate. Raw files from each technical and biological replicate were filtered, de novo sequenced and assigned with protein ID using Peaks 8.0 software (Bioinformatics Solutions, Waterloo, Canada), by searching against the sheep (Ovis Aries) Swiss-Prot database (April 2017; 781 entries). Peptide identifications were accepted if they could be established at greater than 95.0% probability by the Peptide Prophet algorithm with Scaffold delta-mass correction. Protein identifications were accepted if they could be established at greater than 95.0% probability and contained at least 1 identified peptide. Protein probabilities were assigned by the Protein Prophet algorithm. Proteins that contained similar peptides and could not be differentiated based on MS/MS analysis alone were grouped to satisfy the principles of parsimony as originally described (51).

Label-free quantitative (LFQ) methods directly used the raw spectral data from parallel MS runs to determine relative protein abundances. We used both "MS/MS (MS2) spectral counting" and "precursor MS1 area" methods for label free quantitation and further contrasting the differentially expressed proteomic profiles across the control and wounded lymph muscle samples. The relative protein abundance was displayed as heat maps including representative proteins of each protein group after normalization of the corresponding weighted spectral counts using the built-in algorithm from "perSPECtives". Only proteins which passed a selected significance statistical threshold (ANOVA, $p < 0.05$ and FDR < 1% for protein and peptide expression) and had been identified with at least two-fold differential expression across all samples are shown in the representative heat map. Networks, functional analyses, biochemical and cellular pathways were generated

by employing the ingenuity pathway analysis (IPA; Ingenuity Systems, Redwood City, CA, USA) on the list of differentially abundant proteins extracted from LFQ analyses (based on both the precursor ion areas and spectral counts) and presented categorized in (Table 2) found in Appendix C.

4.2.8   *Quantification of the biomechanical properties of isolated lymphatic vessels*

Using a previously developed biaxial testing device in a temperature-controlled incubator at 37^0C, which is capable to measure and control transmural pressure, diameter, and axial force (or stretch), we performed intermittent biaxial (pressure–diameter and axial force–stretch) tests as described previously (79). In brief, two segment of lymphatic vessels (one from control leg and one from ligated leg) were mounted on two opposing cannulae in a vessel chamber with a bath of Ca^{+2}-free PSS solution. Vessels were visualized under different transmural pressures and axial stretches using an inverted microscope (2.5x magnification) and digital camera (Allied Vision Technologies, Marlin F-033B). A custom program in LabVIEW controls inlet, outlet, and transmural pressures (Honeywell FPG 060-E418-11) as well as axial length and axial force using linear actuators (Newport Precision LTAseries) and a load cell (Delta Metrics), respectively. Once preconditioned, vessels were subjected to three loading cycles of ramping the transmural pressure from 3 to 40 cmH2O at axial stretch values of 1, 1.1, 1.2, and 1.3.

4.2.9   *Computational modeling of lymphatic flow and intraluminal lymphatic valves*

The pumping function of a lymphangion was modeled based on a previously developed computational framework for a single lymphangion (36). In brief, this framework consists of a structure-function relationship for wall mechanics, a model for

active force generation of lymphatic smooth muscle cells, and a model for intraluminal valve function. A Matlab script was used to solve respective models along with mass and momentum conservation equations to obtain lymphatic flow and pressure during lymphangion contraction. Upon incorporation of ex-vivo experimental data from control and ligated vessels into computational framework, we simulated different loading scenarios for a single lymphangion. Specifically, inflow pressure was set at 6 mmHg while outflow was altered until lymphatic flow ceased. Next, pressure-flow and pressure-volume curves were obtained for both control and ligated lymphatic vessels. Simulations were also conducted using the average in-vivo contraction frequencies (packet frequency) assessed via NIR imaging at day 42. For these simulations, inflow pressure was also set at 6 mmHg while outflow pressure was altered until lymphatic flow ceased.

Lymphatic flow rate was calculated using Hagen-Poiseuille equation for collapsible vessels which has been shown a good approximation for flow rate in lymphatic vessels as (62):

$$\frac{Q_{in} + Q_{out}}{2} = \frac{\pi D^4}{128\mu L}(P_{in} - P_{out})$$

where Q_{in} and Q_{out} are inlet and outlet flow rates, respectively; D and L are diameter and length of lymphangion, respectively; μ denotes lymph viscosity; P_{in} and P_{out} are inflow and outflow pressures, respectively. In addition, temporal change in lumen dimeter is related to inlet and outlet flow rates through continuity equation as:

$$Q_{in} - Q_{out} = \pi D^3 L \frac{dD}{dt}$$

Intraluminal valves were modeled based on computational-experimental framework developed by Bertram *et al* (23–26, 96) to simulate the function of one-way valve in mesenteric lymphatic vessels. Briefly, this model simulates the function of intraluminal valve through imposing variable resistance to lymphatic flow based on the transaxial pressure gradient across the valve. The minimum and maximum valve resistances are associated with valve opening and closure, respectively, while an empirical parameter (s) dictates transition rate from minimum to maximum resistance, namely:

$$R_{valve=}R_{v,open} + \frac{R_{v,closed} - R_{v,open}}{2\left(1 + \exp\left(s * \left(P_{proximal} - P_{distal}\right)\right)\right)}$$

where $R_{v,open}$ and $R_{v,closed}$ are resistance to flow when valve is open and close respectively; $P_{proximal}$ and P_{distal} are pressure proximal and distal to intraluminal valve; s is a constant parameter that dictates translon rate from valve opening to valve closure.

We used a previously developed computational framework to model pumping function of a single lymphangion. In brief, this model utilize a constitutive framework based on hyper-elasticity framework to model passive mechanical behavior of lymphatic vessels (e.g., distension) in response to mechanical stimuli (e.g, transmural pressure. The biaxial data were used to calculate model parameters that dictate the relationship between biomechanical force (e.g., lymphatic pressure and axial force) and wall mechanics (e.g., wall diameter and thickness). This relationship employs a 4-fiber family strain energy density function that models contribution of amorphous matrix and collagen fibers as follows (92):

$$W = b(I_{C^e} - 3) + \sum_{k=1,2,3,4} \frac{b_1^k}{4b_2^k} \{exp[b_2^k((\lambda^k)^2 - 1)^2] - 1\}$$

where b, b_1^k, b_2^k denote material properties, I_{C^e} is first invariant deformation gradient and λ^k is stretch of kth family of collagen fibers.

This computational framework model phasic (spontaneous contractions) and tonic contractions (basal contractions) of lymphatic smooth muscle cells based on a length tension relationship, namely:

$$T_{\theta\theta,act} = \frac{T}{H} [\frac{(1 - cos(2\pi ft))}{2(1 + b)} + \frac{b}{1 + b}] \left[1 - \left(\frac{\lambda_m - \lambda_\theta}{\lambda_m - \lambda_0}\right)^2\right] \lambda_\theta$$

where $T_{\theta\theta,act}$ is circumferential contractile stress; T models amplitude of active-contractile tension in systole, which was estimated from myography data on lymphatic vessel, H denotes vessel thickness, b is a constant parameter that defines basal force generation in diastole based on ex-vivo experiments, λ_θ indicates elastic circumferential stretch; λ_m, λ_0 are stretches at which contractile tension is maximum and minimum, respectively; f is frequency of spontaneous contractions that follows frequency-pressure curves.

4.3   Results

4.3.1   In-Vivo imaging reveals structural alterations to the intact lymphatic vasculature following injury

MRI imaging of the lymphatic anatomy of the hind limbs was conducted one day pre-surgery and 42 days after surgery (5 sheep total). Pre-surgical MRI shows the two primary collecting lymphatic vessels that drain the hind limbs (Figure 26). These two vessels run in parallel and both drain to the popliteal lymph node. At day 42 post-surgery MRI images show the absence of contrast agent transport by the caudal collecting lymphatic vessel due to the ligation surgery. However, the cranial lymphatic vessel remains intact. Quantification of vessel diameters in the MR images shows a significant decrease in the apparent lumen diameter of the intact vessel on the wounded leg 42 days post-surgery. However, vessels from the control leg exhibited an observed increase in diameter (Figure 26).
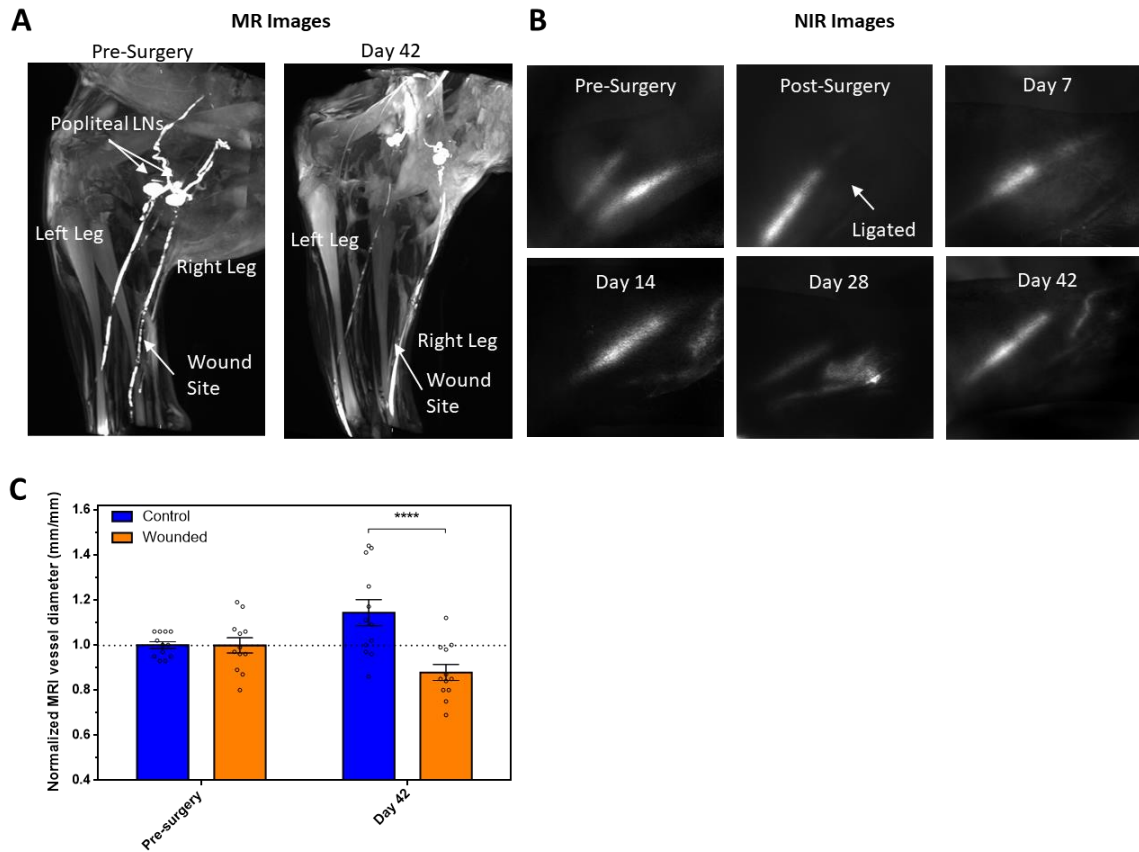
Figure 26: (A) MRI imaging of the lymphatic anatomy of the hind limbs was conducted one day pre-surgery and 42 days after surgery. Pre-surgical MRI shows the two primary collecting lymphatic vessels that drain the hind limbs. These two vessels run in parallel and both drain to the popliteal lymph node. At 42 days post-surgery the caudal vessel is absent from the MR images on the wounded leg. **(B)** NIR imaging allowed visualization of network remodeling due to the lymphatic ligation. Pre-surgical images show both the cranial and caudal collecting lymphatics intact. Immediately after ligation of the caudal collecting lymphatic, an absence of fluorophore transport confirmed successful ligation and excision of the vessel. **(C)** The diameter of the cranial vessel on the control and wounded leg was measured distal to the wound site using the MR images before and 42 days after surgery. Values were normalized by the pre-surgical average diameter of the respective vessel. (****, p < 0.0001).

NIR imaging allowed longitudinal visualization of local lymphatic vascular remodeling caused by the lymphatic ligation (Figure 26). Representative pre-surgical

110

images show both the cranial and caudal collecting lymphatics intact. Immediately after ligation of the caudal collecting lymphatic, an absence of fluorophore transport confirmed successful ligation and excision of the vessel. Day 7 after surgery the cranial lymphatic vessel was intact and functioning but the ligated caudal vessel was not visualized. By day 14 after the surgery, fluorophore was observed in tortuous initial lymphatics at the site of the wound. However, there was no regrowth of a patent caudal collecting lymphatic vessel. Day 28 after surgery there is regrowth of a caudal lymphatic vessel bypassing the wound site. At day 42 after surgery initial lymphatic uptake of fluorophore was absent at the wound site and, in one case (1/5), a collateral lymphatic vessel exhibited packets at the wound site. However, it is unclear if this vessel was newly formed or existed previously.

4.3.2 Lymphatic function of the intact vessel slowly declines following damage to the parallel vessel but subsequently recovers

NIR lymphatic imaging was used to non-invasively evaluate lymphatic functional changes in response to the lymphatic injury. Packet frequency, corresponding to the frequency of lymphatic contractions, was evaluated for the intact cranial vessel on the control leg and the wounded leg (Figure 27). Significant differences in packet frequency between the control and wounded legs are not observed until day 28 corresponding to averages of 4.5 ± 1.2 min^{-1} and 0.9 ± 0.7 min^{-1} respectively; However, this difference is attenuated by 42 days after surgery. Interestingly the difference is attributed primarily to an increase in the packet frequency of the lymphatic from the contralateral control leg. To better visualize alterations in packet frequency over the experimental time course, the percent difference between the control and wounded leg was used to visualize a persistent decline caused by the wound (Figure 27). Packet transport, a metric indicative of

fluorescence transport propagated by intrinsic contraction, was calculated for the vessels on control and wounded legs. At day 28 post-surgery, total packet transport on the wounded leg was significantly lower than the control, corresponding to averages of 3481 ± 2409 RFU and 22590 ± 5172 RFU respectively (Figure 27). Effective pumping pressure was measured to determine the effects of the surgery on lymphatic contractile force. Significant differences in the effective pumping pressure were not observed until 28 days after surgery, corresponding to values of 36.3 ± 7.0 mmHg and 13.6 ± 6.7 mmHg respectively (Figure 27). Collectively, these results suggest that the functional response of the intact vessel is compromised 28 days after the surgery; However, the functional declines appear to be attenuated in vivo by day 42.
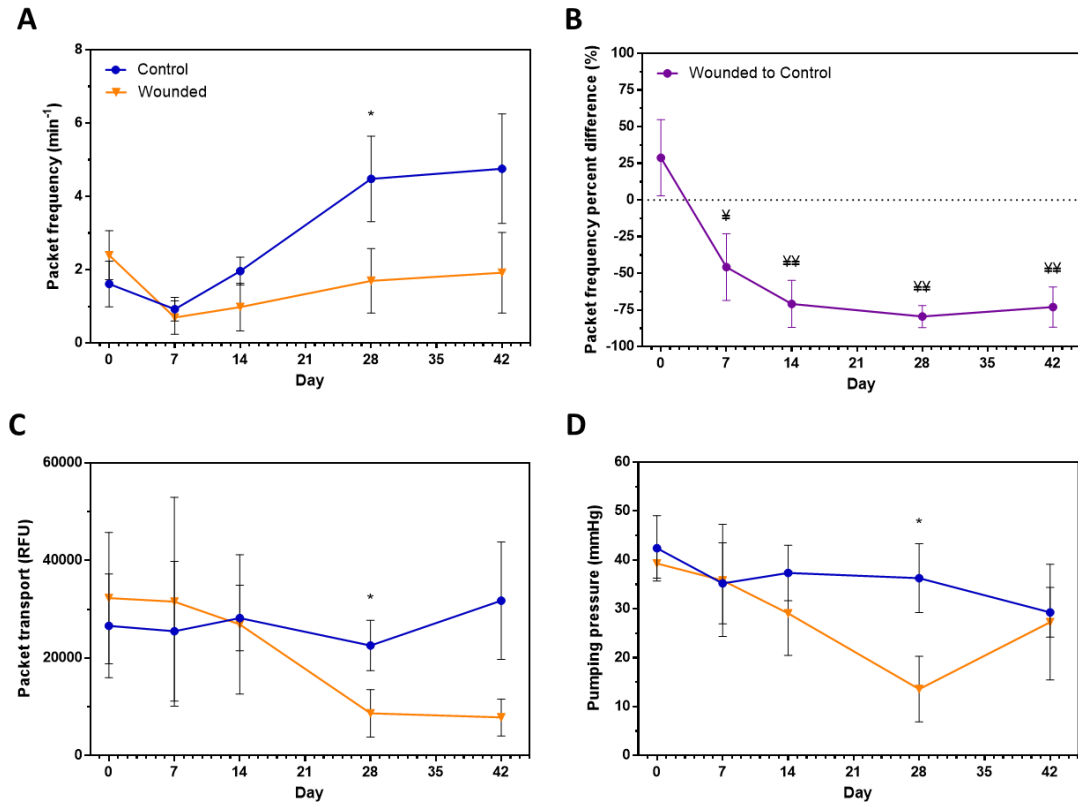
Figure 27: NIR lymphatic imaging was used to non-invasively evaluate lymphatic functional changes in response to the lymphatic injury. NIR imaging data was collected from the intact vessels on both the control (n=5) and wounded (n=5) legs. (A) Packet frequency, the frequency of fluorescent pulsations within the vessel, exhibited significant differences between intact vessels on the control and wounded legs at day 28 post-surgery. (B) The percent difference between the packet frequencies of the control and wounded leg depict a decline due to the surgery. (C) Effective pumping pressure (Peff), was used to evaluate the maximal pressure generated by the collecting vessel to overcome occlusion. Significant differences in Peff were observed at day 28. (D) Packet transport, the integral of the packet frequency signal over time, was used to evaluate fluorescence transport driven by intrinsic lymphatic contractions. Significant differences in packet transport were observed at day 28. Error bars represent SEM. (*, significant difference between control and wounded, p < 0.05; ¥, significant difference between baseline value at Day 0, p < 0.05).

4.3.3 Isolated lymphatic vessels from the wounded and control legs differentially respond to alterations in transmural pressure

Following sacrifice, the intact lymphatic vessels on the control and wounded legs were isolated and excised. A subset of these segments (n=4) underwent wire myography. Results from the wire myograph suggest that vessel segments from the control and wounded exhibit significantly different peak tensions during spontaneous contraction with values of 2.92 ± 0.002 mN/mm and 3.02 ± 0.013 mN/mm respectively (Figure 28). Other segments of isolated vessel were cannulated in our previously described lymphatic vessel perfusion system (109, 110). This system was used to prescribe various transmural pressures to the vessel segment while simultaneously recording contractile response via video. Vessel segments from the wounded leg exhibited increased contractile frequency compared to control at all transmural pressures tested (Figure 28). The average contraction frequencies at 5 cmH_2O were 8.7 ± 1.3 min^{-1} and 12.9 ± 0.3 min^{-1} for control and wounded respectively. Contraction amplitude as a function of transmural pressure was increased in vessel segments from the wounded leg, which is in agreement with myograph data (Figure 28). Peak contraction amplitudes were observed at 5 cmH_2O for segments from the control leg and 7 cmH_2O for segments from the wounded leg, corresponding to normalized contraction amplitudes of $31.6 \pm 6.9\%$ and $43.5 \pm 3.9\%$ respectively. Lymphatic tone index was calculated from the ratio of diastolic diameter to diastolic diameter in calcium free media (detailed in methods). The metric is a measure of the lymphatic smooth muscle's contribution to the tonic diameter of the vessel. Lymphatic tone was found to be decreased in vessel segments from the wounded leg compared to control (Figure 28), while the passive lymphatic diameter was not different (Figure 29). Ejection fraction and fractional

pump flow were calculated from the frequency and amplitude data. The ejection fraction and fractional pump flow for the wounded leg was elevated over control due to increased contraction amplitude and frequency (Figure 31).
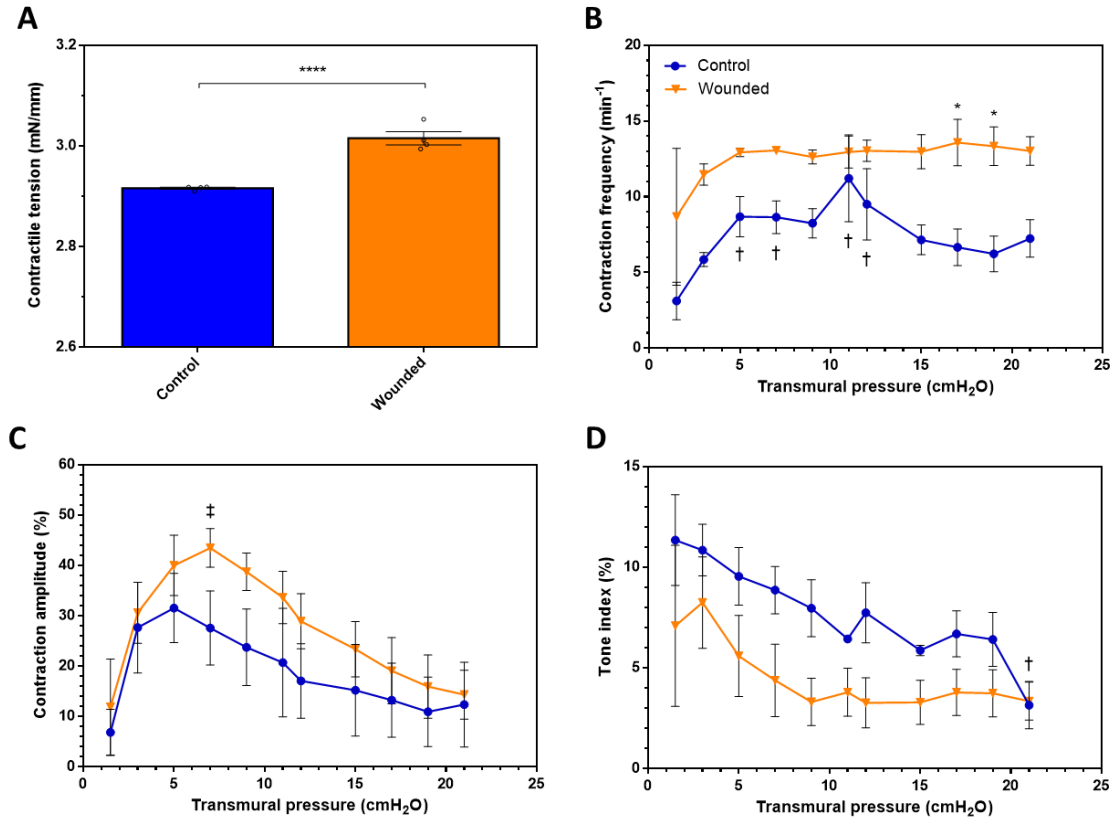
Figure 28: Intact lymphatic vessels were isolated from the control and wounded legs to evaluate changes in the stretch response due to the surgery. Vessel segments were cannulated and exposed to a range of transmural pressures. (A) Wire myography was used to evaluate the contractile force of isolated lymphatic vessels (non-pressurized) and exhibited significant increases in the contractile force of vessels from the wounded leg (n=4 control, n=4 wounded). (B) Vessel segments from the wounded leg exhibited higher contraction frequencies than control segments (n=4 control, n=4 wounded). (C) The amplitude of lymphatic contractions did not significantly differ between the control and wounded groups (n=4 control, n=4 wounded). (D) Lymphatic tone was not significantly different in vessel segments collected from the wounded leg (n=4 control, n=4 wounded). Error bars represent SEM and open circles represent individual data points (*, significant difference between control and wounded, p < 0.05; †, significant difference between control and control baseline at 1.5 cmH2O transmural pressure, p < 0.05; ‡, significant difference between wounded and wounded baseline at 1.5 cmH2O transmural pressure, p < 0.05)
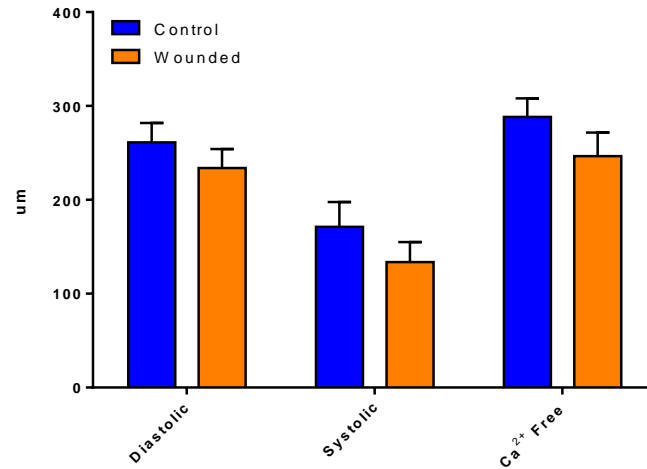
Figure 29: Diameters of vessels from the control and wounded leg were measured during the isolated vessel procedures at 5 cmH2O transmural pressure and 0 cmH2O axial pressure gradient. There was no observed statistically significant difference in the outer diameters of the vessels between the control or wounded leg. Error bars represent SEM.

4.3.4   Isolated lymphatic vessels from the wounded and control legs differentially respond

to imposed flow and inhibition of eNOS

Isolated lymphatic vessel segments were subjected to varying imposed axial pressure gradients, while maintaining a constant transmural pressure of 6 cmH$_2$O, by using our previously described lymphatic vessel perfusion system (109, 110). To determine the role of eNOS in the response to imposed flow, vessel segments received treatment with the eNOS inhibitor L-NAME. Flow inhibited contractile response occurred at an axial pressure gradient of 3 cmH$_2$O for control segments whereas no such inhibition was observed in segments from the wounded leg (Figure 30). Contraction frequency of the wounded vessels was significantly higher than control at axial pressure gradients of 1 cmH$_2$O and 3 cmH$_2$O

with values of 11.7 ± 2.6 vs 3.1 ± 1.7 and 8.92 ± 1.1 vs 0.3 ± 0.3 respectively. Upon inhibition of eNOS with L-NAME, vessels from the control segment experienced no shear inhibited contractile response above axial pressure gradients of $3\,cmH_2O$ whereas wounded segments exhibited little response to the loss in eNOS (Figure 30). The amplitude of contractions was relatively similar between control and wounded segments at axial pressure gradients of 0 and $1\,cmH_2O$. However, at $3\,cmH_2O$ and $5\,cmH_2O$ control segments did not contract and thus had no contraction amplitude (Figure 30). Upon treatment with L-NAME at 0 and $1\,cmH_2O$ axial pressure gradient, contraction amplitude for control segments was halved, whereas wounded segments exhibit little alteration in amplitude (Figure 30). The tone index of both control and wounded segments was not significantly different (Figure 30). Treatment with L-NAME elicited a strong increase in the tone of control segments. Conversely, wounded segments exhibited no change in tone compared to untreated conditions with increasing axial pressure gradients (Figure 30). In a subset of vessel segments, shear sensitivity was evaluated by linearly increasing axial pressure gradient while maintaining constant transmural pressure. Segments from the wounded leg were less shear sensitive; exhibiting contractile inhibition at higher shear stress values than control segments (Figure 30). Ejection fraction was significantly decreased for vessels from the control leg in the presence of L-NAME, however wounded leg vessels were non-responsive to L-NAME (Figure 30). Fractional pump flow for control vessels increased in the presence of L-NAME, but not for wounded leg vessels (Figure 31). As a whole, these results suggest that vessels from the wounded leg have impaired eNOS-dependent flow mediate dilation responses.
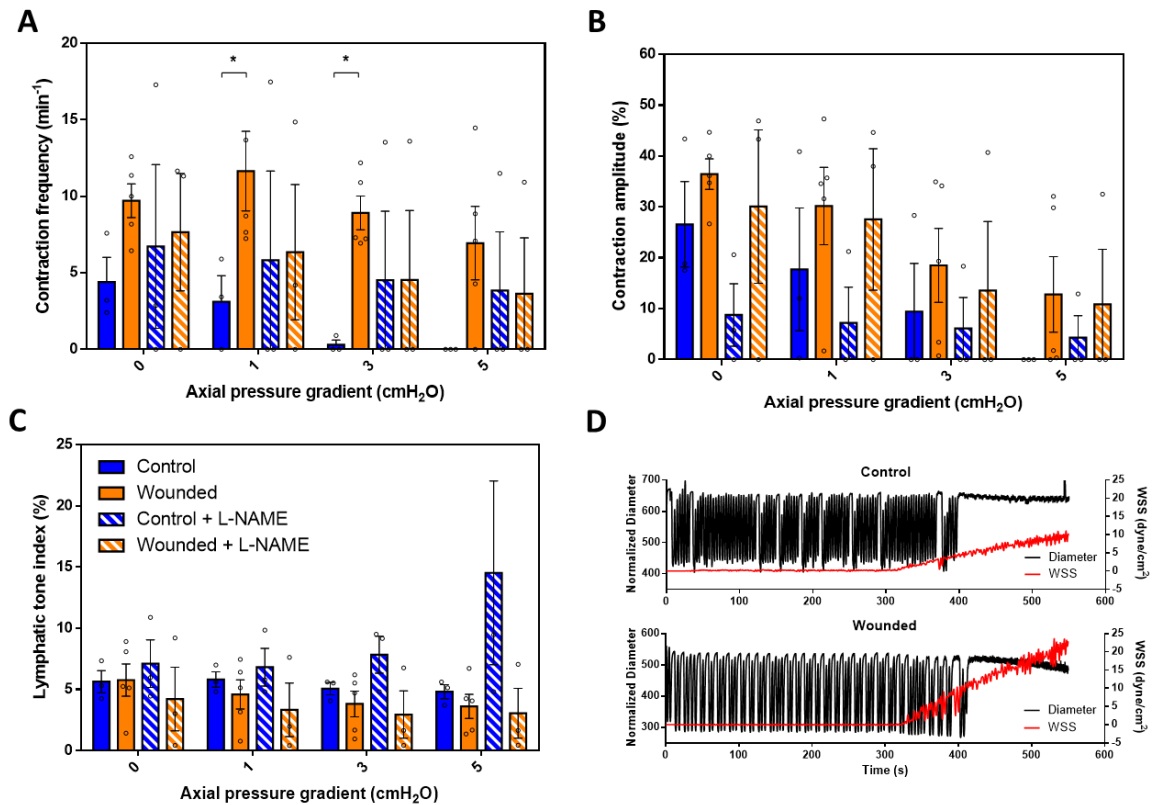
Figure 30: Intact lymphatic vessels were isolated from the control and wounded legs to evaluate changes in the flow response to the surgery. Vessel segments were cannulated and exposed to a range of transaxial pressure gradients. 100uM LNAME was used to inhibit endothelial nitric oxide synthase (eNOS). (A) The frequency of lymphatic contraction was slightly increased for isolated vessels collected from the wounded leg when compared to control. The addition of LNAME inhibits intrinsic contraction of vessels from the wounded leg. However, control vessels exhibit a differential response; increasing contractile frequency in response to LNAME (n=3 control, n=5 wounded). (B) Lymphatic contraction amplitude was decreased in response to imposed flow. Vessels from the wounded limb exhibited lesser degree amplitude loss with the addition of L-NAME (n=3 control, n=5 wounded) (C) Lymphatic muscle tone of vessels from the wounded leg was decreased compared to control. Isolated lymphatic vessels from the wounded leg exhibit a little response to application of LNAME compared to control vessels (n=3 control, n=5 wounded). (D) The vessel from the wounded leg exhibited less of a contractile response to shear stress than vessels from the control leg (n=1 control, n=1 wounded). Error bars represent SEM and open circles represent individual data points (*, significant difference between control and wounded, p < 0.05; †, significant difference between control and control baseline at 0 cmH2O axial pressure gradient, p < 0.05; ‡, significant difference between wounded and wounded baseline at 0 cmH2O axial pressure gradient, p < 0.05)

118
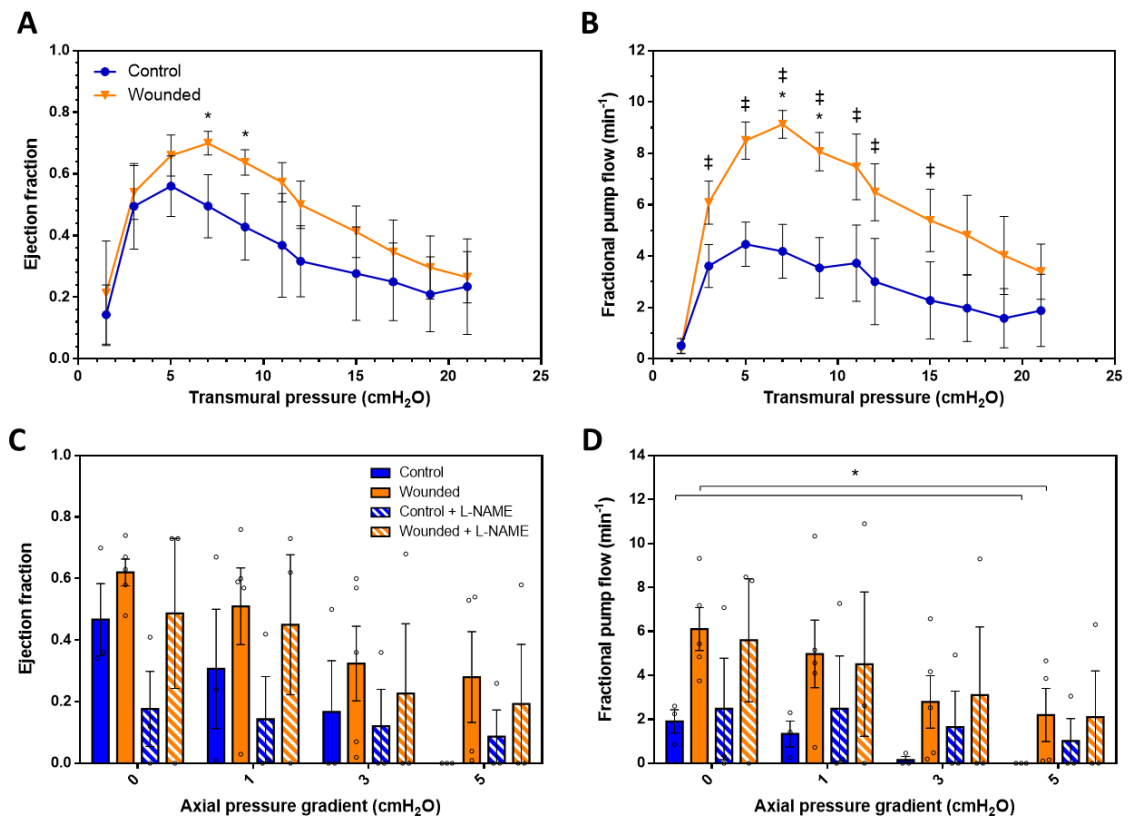
Figure 31: Fractional pump flow and ejection fraction were derived from isolated vessel diameter tracings. (A) Fractional pump flow of vessels from the wounded leg and control leg as a function of transmural pressure. (B) Ejection fraction as a function of transmural pressure. (C) Fractional pump flow at varying axial pressure gradients with an average transmural pressure of 6 cmH2O with and without the addition of L-NAME. (D) Ejection fraction at varying axial pressure gradients with an average transmural pressure of 6 cmH2O with and without the addition of L-NAME. (*, significant difference between control and wounded, p < 0.05; †, significant difference between control and control baseline at 1.5 cmH2O transmural pressure, p < 0.05; ‡, significant difference between wounded and wounded baseline at 1.5 cmH2O transmural pressure, p < 0.05)

4.3.5 Lymphatic muscle cells from wounded vessels exhibit differential protein expression profiles

As a next step to further understand the biomolecular underpinnings correlated with the observed changes in lymphatic function we performed a label free comparative proteomic analysis between muscle cells harvested from control and wounded lymphatics. A distinct protein signature could be observed between the control and wounded muscle cell proteome (Figure 32). Comparative analysis of the cellular proteome, using the Ingenuity Pathway Analysis determined that several metabolic, signaling and apoptotic pathways were up-regulated in the wounded muscle cells, as compared to healthy controls (Figure 32). Fold change data is detailed in (Table 2) which can be found in Appendix C. Notably, oxidative phosphorylation and markers of oxidative stress including cellular amount of reactive oxygen species and their metabolites were significantly up-regulated in the injured muscle cells (Figure 32 and Figure 33). Likewise, inflammatory signaling and markers of cellular apoptosis were significantly more expressed in the injured muscle cells (Figure 32 and Figure 33) On the other hand functions related to tissue growth and development, and muscle contraction were downregulated in the injured muscle cells (Figure 32 and Figure 33).
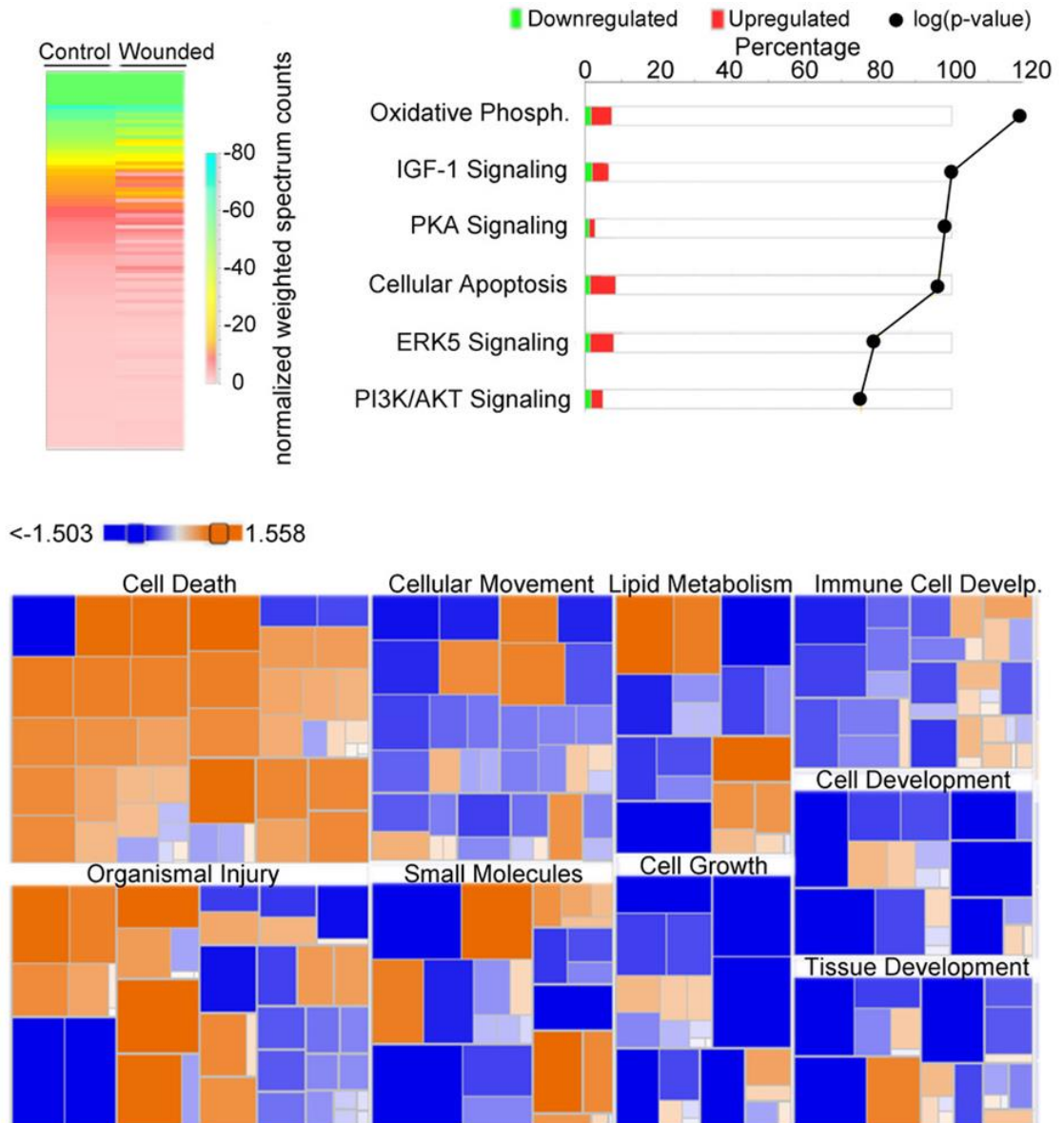
Figure 32: Comparative protein expression profiling of control vs wounded lymphatic muscle cells together with the molecular and cellular pathways predicted by IPA. (A) Un-biased, non-clustered heat map generated in "perSPECtives" using the normalized weighted spectral counts highlights the change in the protein expression profiles in the "wounded" relative to the "control" lymph muscle cells. (B) The main canonical pathways affected by the top 105 genes with higher than twofold expression level in the "wounded" vs "control" samples, subjected to the analysis by IPA algorithm. The % of total molecules up- (red color) or downregulated (green color) in each pathway together with the corresponding log (-p value) are displayed. (C) Protein networks significantly regulated (p< 0.05) in the "wounded" relative to the "control" lymph muscle cells are displayed as IPA predicted diseases and cellular functions using the z score (down-regulated corresponding to z<-1.5 and blue color;

up-regulated, corresponding to z>+1.5 and orange color). The size of each rectangle is proportional with the value of the z score associated to a specific pathway. Increased organismal injury, cell death, small molecules and lipids metabolism and cellular movement are the main diseases and cellular pathways characterizing the "wounded" system.
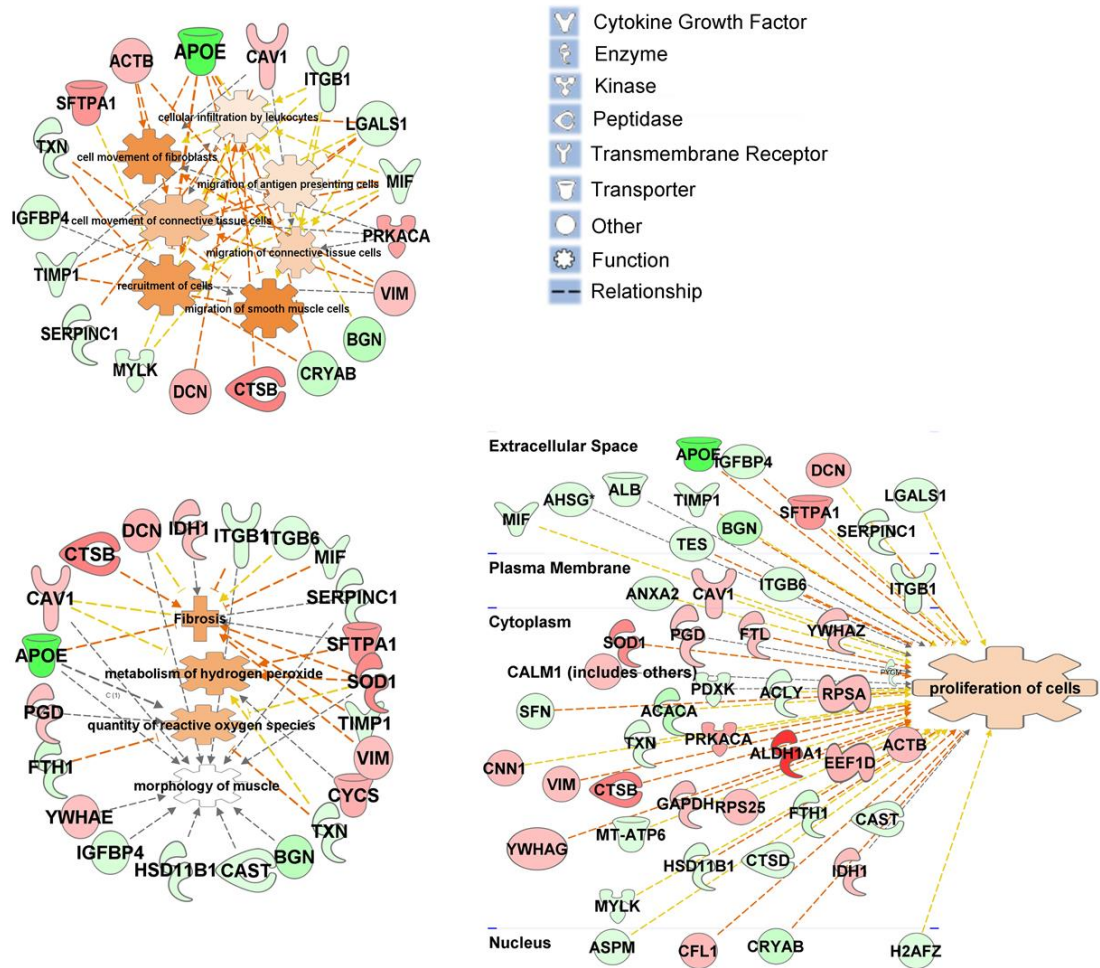
Figure 33: Protein networks significantly regulated (p < 0.05) in the wounded relative to the control lymph muscle cells. The proteins with at least two-fold changed in the expression profiles were analyzed by Ingenuity Pathways Analysis (IPA, Ingenuity Systems) to determine the cellular pathways impacted by the wounded conditions relative to the control in the lymph muscle cells. (A) The functional networks with the highest scores were predicted by IPA to be related to the increased cellular movement

of fibroblasts, smooth muscle cells and leukocytes in the wounded cells as compared with control. The wounded conditions are prone to experience a significant in the networks associated with the fibrosis, reactive oxygen species (B) and cell proliferation (C). The proteins in red and green had a significantly up- or down-regulated expression ($p < 0.05$), respectively. The shape of symbols denotes the molecular class of the proteins. A solid line indicates a direct molecular interaction, whereas a dashed line indicates an indirect molecular interaction.

4.3.6   Isolated lymphatic vessel segments from the wounded leg are structurally and mechanically altered compared to control

Isolated lymphatic vessel segments exhibited alterations in the morphology of lymphatic valves. Vessels from the wounded leg had valve leaflets that appeared prolapsed compared to control when pressurized (Figure 34). Isolated vessel segments were frozen and later underwent staining with hematoxylin and eosin. Wounded vessel sections exhibited an increase in matrix surrounding the lumen of the vessel when compared to control. Additionally, wounded segments showed atrophy of the intima that was not observed in control segments (Figure 34). Biaxial testing of isolated vessel segments was used to evaluate changes in the mechanical properties of the vessels in response to the ligation surgery and then fit to a previously developed microstructural based constitutive model of the lymphatic vessel. Vessels from the wounded leg displayed an increase in stiffness compared to control. Interestingly, wounded segments have a less pronounced toe region of the pressure-diameter curves compared to control, indicating alterations in elastin to collagen engagement during stretch (Figure 34).
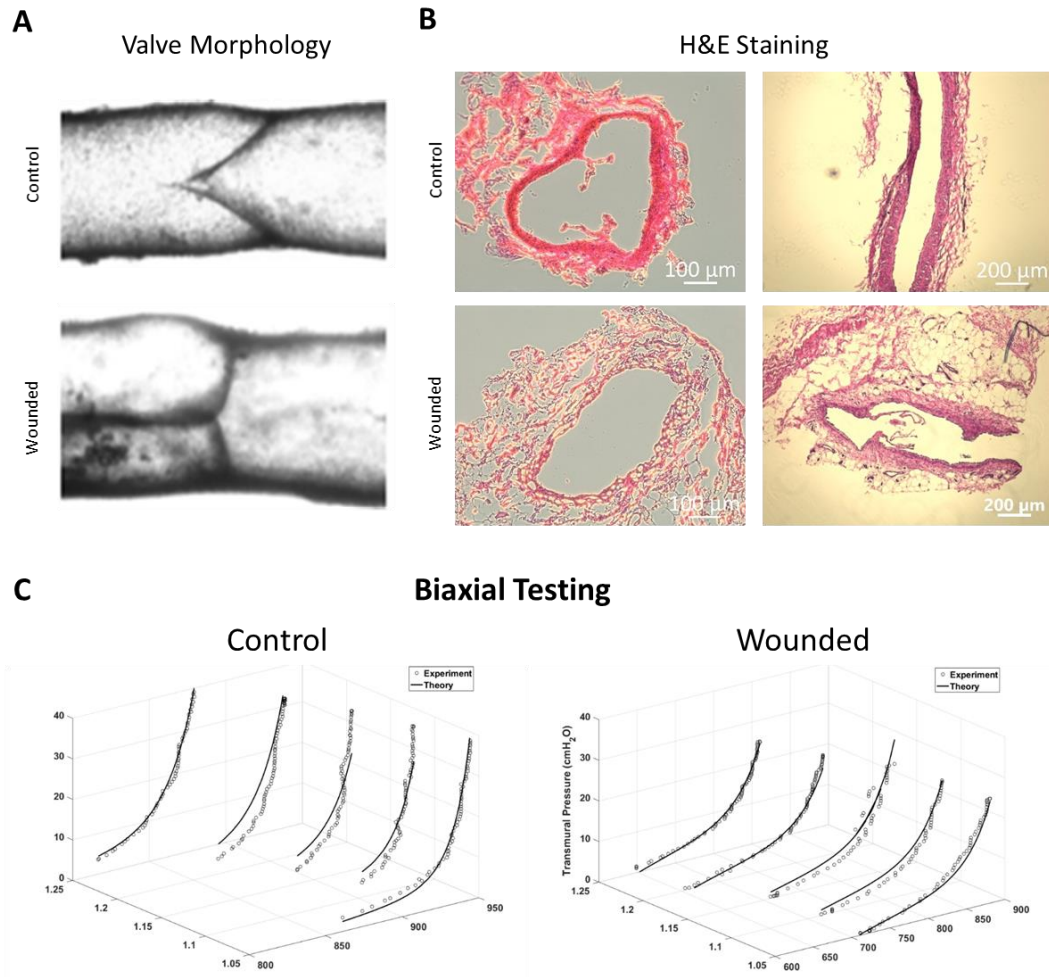
Figure 34: Vessels from the wounded leg displayed structural and mechanical changes caused by the ligation surgery. (A) The lymphatic valves of vessel segments from the wounded leg were prolapsed upon pressurization. (B) Vessel cross sections from the wounded leg (left column- transverse, right column- axial) exhibited atrophy of the musculature surrounding the vessel compared to control. Additionally, vessel segments from the wounded leg appear to have an increase in matrix surrounding the vessel. (C) Biaxial testing was conducted on isolated vessel segments at various axial stretches and transmural pressures. Wounded vessels exhibited increases in vessel compliance compared to control. The biaxial data was fit to a constitutive model to calculate material parameters that capture pressure-diameter behavior (details in theory).

4.3.7 *Computational modeling of the lymphatic chain predicts that wounded vessels functionally compensate for changes in the mechanical properties of the vessel*

Data from isolated vessels, wire myography, and biaxial mechanical testing were used to inform a computational model of a lymphatic vessel chain. This model was used to evaluate the predicted flow and contractile response of the lymphatic vessel under a confronting pressure gradient given the changes caused by the remodeling. Our computational model suggests that the remodeled vessel would have a lower flow rate than the control given equal contraction frequency. However, this difference in flow rate can be attenuated by an increase in the contraction frequency. Interestingly, upon incorporating the average contraction frequencies from the isolated vessel data, we found that the flow rate for the lymphatic chain from the wounded leg may exceed control (Figure 35). Our computational model suggests that this increase in flow rate occurs despite the decrease in the average predicted stroke volume of the lymphangions due to a combination of increased contraction frequency and pressure generation (Figure 35).
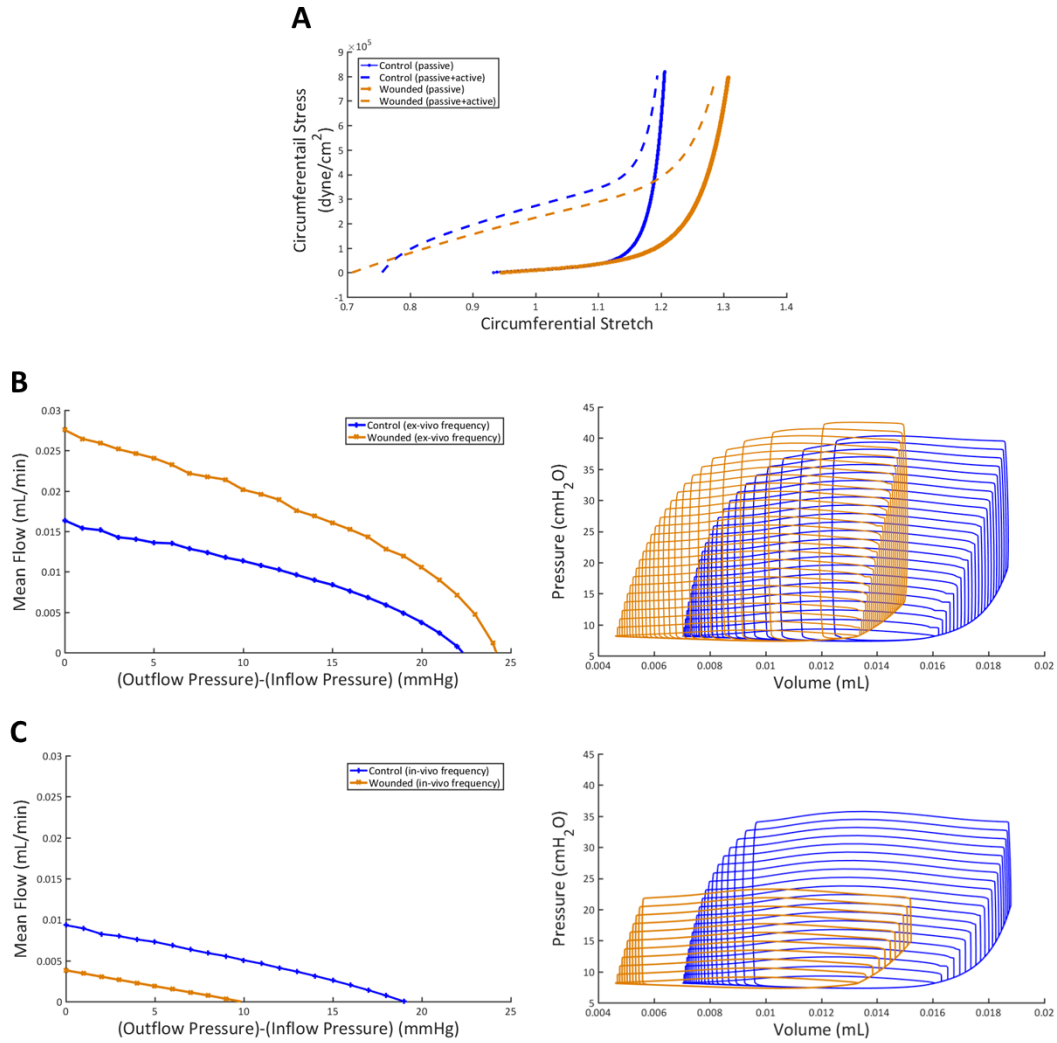
Figure 35: Isolated vessel function and mechanical properties were utilized to inform a computational model, which was used to elucidate how the structural and functional changes caused by the surgery would affect intrinsically driven flow. (A) Biaxial testing data was used to inform a computational model that predicts active and passive wall stress as a function of circumferential stretch. Testing data suggests an increase in the passive and active compliance of the vessels from the wounded leg. (B) (Left) Mechanical parameters coupled with ex-vivo isolated vessel frequencies were used to simulate predicted lymph flow rates as a function of pressure generation. Our computational model suggests that vessel segments from the wounded leg may exceed the flow rate of control by increasing contraction frequency and contractile force. (Right) Pressure-volume curves for these simulations. (C) (Left) Mechanical parameters coupled with in-vivo contraction frequencies assessed via NIR imaging at day 42. Our computational model suggests that, in an in-vivo context, vessel segments from the wounded leg may have decreased intrinsically driven lymph flow rates. (Right) Pressure-volume curves for these simulations.

4.4   Discussion and Conclusions

Injury to the lymphatic vasculature is quite common in surgery, whether unintentionally as in the case of chyle leak, or intentionally when metastatic lymph nodes must be removed in the context of cancer surgery. Despite its occurrence, and the vast importance of lymphatics in maintaining fluid balance, lipid transport, and immune cell trafficking, very little is known regarding how lymphatics adapt and remodel after injury and the resulting implications of this remodeling on lymphatic pump function. Here we utilize an interdisciplinary approach involving large animal lymphatic imaging, functional isolated vessel pumping and biomechanics tests, proteomics, and computational modeling to provide unique insight into the functional and molecular adaptions of lymphatics due to alterations in the collecting vessel network. Following surgical damage to lymphatic vessels, the intact collecting vessels draining the tissue space alter their functional response and subsequently remodel to compensate for the increased fluid loads caused by the injury. Similar to observations made in vascular diseases such as hypertension and atherosclerosis, abnormal mechanical loading on the vessel leads to stiffening, endothelial dysfunction, and a shift in pathways involved in mitochondrial metabolism.

A number of animal models have been developed for the purpose of studying lymphatic healing and edema development following a wound (94, 161, 201, 221). These models suffer from two primary limitations when extrapolating results to the context of common clinical lymphatic injuries in humans: 1) small rodent models lack the hydrostatic pressure gradients that serve as the primary mechanical load which the collecting vessels must work overcome; 2) the models are created through extensive damage of the lymphatic vasculature in which there is usually no intact lymphatic pathways in the limb with which

fluid may be returned. Thus, these models are unable to recapitulate the gradual adaptation of the intact lymphatic vasculature following a surgical insult. This study is the first of its kind to probe the effects of collecting lymphatic ligation alone on the functional response of the surrounding intact lymphatic network. This has relevance from a clinical standpoint because in the case of secondary lymphedema, patients that later develop the disease still possess intact and functional collecting lymphatic vessels (47) and often do not present with symptoms of lymphedema until 2 years or more after surgery (7). In fact, in our model, we detected no observable swelling of the limbs. This approach also afforded us the ability to longitudinally track lymphatic function over the course of adaption using NIR imaging.

The enhanced intrinsic contractile frequency of the isolated remodeled vessel when compared to the same vessel from the contralateral control limb, is likely a compensatory mechanism to handle the elevated fluid loads placed on this vessel as it now seeks to do the work of two vessels. This is supported by the observed decrease in basal tone, which is known to lower fluid resistance of the vessels (57) as well as the return of the in vivo pumping pressure to normal levels at day 42. Because these alterations in the vessel's response to stretch is governed by the smooth muscle surrounding the vessel, it stands to reason that these observed differences are caused by alterations to the structure or function of the lymphatic smooth muscle initiated by the wound to the lymphatic network (58). Proteomics of isolated lymphatic smooth muscle cells from the wounded leg revealed an upregulation of pathways associated with oxidative phosphorylation and mitochondrial dysfunction caused by oxidative stress (16). This complements the observed increase in the contractile frequency of isolated vessels, given that increased oxidative stress has been demonstrated as a result of increased contractile frequency of cardiomyocytes (54). It is

128

important to note a sustained elevated effort by LMCs could lead to muscle fatigue and thus decreased lymphatic contractility over time, and may have implications in the later development of lymphatic dysfunction (218), although currently this remains speculative and should be supported by future work.

The lymphatic endothelium serves as a complementary and potent regulator of the lymphatic contractile response to flow. It is believed that this mechanism is a result of pump-conduit duality of the lymphatics, wherein flow imposed on the lymphatic vessel induces contractile inhibition and passive conduit behavior via endothelial nitric oxide synthase (eNOS) (31, 75, 172, 193). Lymphatic vessels from the wounded leg experienced less contractile inhibition in response to flow when compared to control. Upon inhibiting eNOS with L-NAME we determined that vessels from the wounded leg were less dependent on eNOS for regulating contraction than control and thus continued to contract at higher imposed transaxial pressures. These vessels also exhibited a lower sensitivity to flow induced wall shear stress. These results are consistent with those reported in a postnatal model of abnormal lymphatic developmental due to enhanced flow, in which the lymphatics exhibited enhanced contractility, impaired NO bioavailability, altered posttranslational regulation of eNOS, and enhanced ROS generation (55, 56).

To determine if the observed functional alterations of the intact vessel on the wounded leg could be due to compensation for the loss of the ligated vessel we utilized a computational model to simulate the flow capacity of the remodeled lymphatic chain (177). We could independently control factors in the computational model and determine how they may contribute to the overall function of the pump to transport fluid against and adverse pressure gradient as would be encountered through hydrostatic loading in vivo.

129

Our results suggest that the decreased stiffness of the remodeled vessel, coupled with the increase in contractile force generation, and increased intrinsic contractile frequency would all elevate its predicted flow rate. Interestingly, the elevation in the predicted flow rate of the remodeled vessel falls very close to what would be expected in a limb in which one lymphatic vessel must handle the fluid load of what used to be two vessels draining the tissue space. On the other hand, when the average in-vivo frequencies assessed via NIR imaging at day 42 are used in the computational model, the predicted flow rate of the remodeled vessels falls to roughly half of control. Taken together, these results suggest that the vessels from the wounded leg alter their intrinsic contractile function to elevate their flow to compensate for the increased fluid load caused by damage to a vessel draining the same tissue space; however, in an in-vivo context, mechanical or soluble factors may inhibit the contractile frequency of the remodeled vessel. This could be caused by elevated lymph load in the wounded leg that could increase extrinsically driven lymph flow and subsequently decrease the intrinsic contractile frequency of the vessel (63, 171, 172). Thus, it is possible that total lymph drainage is elevated in-vivo despite the observed decrease in the contractile frequency, which would explain the lack of swelling observed in the model.

In conclusion, this study is the first of its kind to demonstrate that an injury to a single collecting lymphatic vessel can have broader impacts on the remaining intact lymphatic network. Specifically, the uninjured vessel can compensate in vivo by altering its intrinsic functional response and structure. However, through this process, the collecting lymphatic muscle experiences increased oxidative stress due to increased contractility. This raises the question of when or if this increase in oxidative stress would later result in lymphatic muscle fatigue and subsequent dysfunction. One of the most important implications for this

is in the context of the pathogenesis of secondary lymphedema, where patients undergo a primary surgical insult to the lymphatic network draining the tissue space. It has been observed that these patients have intact and functional collecting lymphatic vessels (157). In fact, in these scenarios, it has even been suggested that overworked lymphatic vessels due to excess fluid load may be indicative of later lymphedema development (15, 47). Our data supports these hypotheses by demonstrating functional compensation by intact lymphatic vessels may induce muscle fatigue, subsequently increasing susceptibility to future dysfunction.

CHAPTER 5.   CONCLUSIONS AND FUTURE IMPLICATIONS

Despite being an integral driver of lymphatic transport, relatively little is known about how lymphatic pump function and remodeling is affected following injury that results in a loss of lymphatic drainage pathways. In some cases, this loss ultimately results in chronic lymphedema whereas in others it does not. It is possible that predisposing factors that impact baseline lymphatic pump function become exacerbated by increased fluid loads due to surgical insult, ultimately manifesting in lymphedema. Alternatively, in scenarios where lymphedema does not immediately develop, it is unclear how collecting lymphatic vessels are able to alter their structure and function to compensate for losses in lymphatic drainage pathways. It was therefore the goal of this scholarly work to develop and validate novel NIR imaging methods that enable non-invasive phenotyping of lymphatic pump performance and subsequently to use these techniques to provide biological insight into the functional and remodeling response of the collecting lymphatic vessels to surgical disruption of lymphatic drainage pathways.

In Chapter 2, we presented the development of novel NIR imaging techniques that enable holistic characterization, or phenotyping, of collecting lymphatic function during disease. To this end, we created a method to quantify lymphatic pumping pressure using NIR imaging in conjunction with an automated feedback-controlled occlusion cuff. The results of the study not only demonstrated the utility of the technique but also provided novel insight into the regulation of collecting lymphatic physiology. Specifically, we discovered that chains of lymphangions contracting in series are essential in generating the pressures necessary to propel lymph up the adverse hydrostatic pressure gradients in the

body. Moreover, we found that a modulator of lymphatic contractility that is commonly associated with inflammation, nitric oxide, directly regulates collecting lymphatic pump physiology via impairment of contractile force generation in addition to its previously described effects on contractile frequency. It was these discoveries that helped to enhance the physiological relevance of the metric and enabled our subsequent line of questioning regarding pump dysfunction in the context of lymphatic disease. By combining the novel pumping pressure measurement technique with previously established packet performance metrics, we enabled the unique ability to non-invasively distinguish underlying modalities of lymphatic pump failure. To demonstrate this, we utilized two models that were known to possess deficiencies in lymphatic transport, but the involvement of the collecting vessel pump had not been described, and thus their appropriateness as a therapeutic target had remained elusive. These included a mouse lacking lymphatic endothelial epsins and a model of diet-induced obesity.

In using our functional phenotyping approaches on LEC-DKO mice, we detected several abnormalities in lymphatic network, despite the histological appearance of structurally "normal" lymphatic vessels and valves. This appeared to be caused by the profound dysfunction of the collecting lymphatic vessels, which exhibited no detectable contractile activity in addition to valve incompetency. The results of the LEC-DKO study have subsequently raised a novel line of questioning regarding the role of lymphatic endothelial epsins in the regulation of lymphatic physiology and the development of lymphedema. To this end, the work presented in this thesis motivated the use of an inducible lymphatic endothelial epsin knockout model, coupled with the disease

phenotyping techniques described here, that enables investigation into the post-developmental role of epsins in regulating lymphatic function and remodeling.

In contrast with the profound dysfunctional phenotype discovered in the LEC-DKO model, we found that obese mice exhibited only modest declines in lymphatic packet frequency. In fact, this highlighted the primary contribution of our functional phenotyping techniques. If we had only assessed packet frequency as the sole metric of collecting lymphatic function in these two disease models, we would not have elucidated the stark differences in pumping pressure that suggest a more profound impairment in lymphatic function associated with the genetic loss of lymphatic endothelial epsins. Despite our findings that obesity only appears to have modest effects on collecting lymphatic pump function, it is well known that obesity increases the risk of lymphedema development and the subsequent severity of the disease after surgical insult to the lymphatic vasculature. This raised the question of if these baseline declines in collecting lymphatic packet frequency, caused by obesity, induce a "tipping point" following lymphatic injury in which lymphatic transport declines further and lymphedema pathogenesis occurs. It was therefore the goal of my work presented in Chapter 3 to investigate the specific collecting lymphatic failure modes involved in lymphedema pathogenesis during obesity.

To accomplish the study presented in Chapter 3, we utilized the functional phenotyping techniques discussed in Chapter 2 in conjunction with a single vessel lymphatic vessel ligation model to induce lymphedema in obese mice and subsequently assess the functional response of the remaining intact lymphatic vessel over the course of the disease. The results of the study demonstrate that obesity differentially impairs the contractile function of that intact collecting lymphatic vasculature during lymphedema.

More specifically, we found that obesity significantly delays the recovery of collecting lymphatic pumping pressure during lymphedema and that this effect persists despite the resolution of tissue swelling. The etiology of this decline in pumping pressure is, so far, unclear; however, we hypothesized that this could be a result of obesity differentially decreasing lymphatic contractile frequency to a point that the lymphatic vessel chain is no longer able to maintain pressure generating abilities. Given that CD4+ T-cells have been shown to be an essential mediator of the tissue changes associated with lymphedema development during obesity, we sought to determine if inhibiting activation and differentiation of these cell types with tacrolimus would protect against the functional declines that we observed. We subsequently demonstrated that tacrolimus, protects against losses in packet frequency and pumping pressure following lymphedema development in obese mice.

Taken together, the results from Chapter 3 suggest that obesity induces differential declines in the functional response of the collecting lymphatic vessels during lymphedema and that this response is likely T-cell mediated. Although it is apparent from this study that collecting lymphatic dysfunction is associated with obesity during lymphedema, the degree that lymphatic dysfunction my influence lymphedema development during obesity is unclear. This study pathed the way for future work seeking to investigate causality within this relationship. In fact, given that our functional phenotyping techniques provides a wealth of functional metrics at various timepoints throughout the studies, it seems reasonable to believe that these "features" could be incorporated into machine learning models that seek to predict the severity of lymphedema at later time points. In addition to this, it would be beneficial for future work to investigate the biological mechanisms that

are driving the functional declines observed in this study. For example, knowledge of the degree that these changes are being caused by direct remodelling of the vessels versus soluble functional mediators would be invaluable for determining therapeutic targets that seek to improve collecting vessel function.

Unlike mouse lymphedema models, human lymphedema typically does not manifest immediately after surgery. In fact, in a clinical setting the lymphatic vasculature is routinely damaged during surgery and yet, in many cases, lymphedema will never develop. Therefore, we hypothesized that surgical ligation of a collecting lymphatic vessel will induce a compensatory functional and remodeling response from an undamaged vessel draining the same tissue space when lymphedema does not develop. We believed that sheep, given their size similarities to humans, may provide a more clinically relevant model for assessing lymphatic pump function and remodeling response to lymphatic injury. Because of this, in study described in Chapter 4, we adapted the tools and techniques described in Chapters 2 and 3 for use in sheep. This was accomplished by developing a sheep lymphatic injury model, that involved surgical ligation of a single collecting lymphatic vessel in the hind limb while leaving the other vessel intact.

We discovered that following surgical damage to lymphatic vessel, the intact collecting vessel draining the same tissue space alters its functional response and subsequently remodel to compensate for the increased fluid loads caused by the injury. NIR functional imaging revealed that this intact vessel exhibits declines in packet frequency, packet transport, and pumping pressure 28 days after surgery, that subsequently recovers by day 42. Ex-vivo testing of these intact isolated vessels revealed that they had enhanced intrinsic contractility compared to controls in conjunction with decreased flow-

mediated contractile inhibition. Proteomic analysis of the lymphatic smooth muscle cells from these revealed an upregulation of pathways associated with oxidative phosphorylation and mitochondrial dysfunction caused by oxidative stress, which complements the observed increase in the contractile frequency of isolated vessels. This study is the first of its kind to demonstrate that an injury to a single collecting lymphatic vessel can have broader impacts on the remaining intact lymphatic vessels in scenarios that lymphedema does not develop. Moreover, it appears that the intact lymphatic vessels compensate in vivo by altering its intrinsic functional response and structure. However, through this process, the collecting lymphatic muscle experiences increased oxidative stress due to increased contractility, which raises question of when or if this increase in oxidative stress would later result in collecting lymphatic dysfunction. It would be beneficial for future work to investigate the role oxidative stress in collecting lymphatic pump failure along with the mechanisms that drive this process. Additionally, given that these muscle cells have increased oxidative stress, it would be beneficial to investigate if an additional challenge (surgical or inflammatory) overloads the fluid draining capacity of the vessels ultimately resulting in lymphedema.

In conclusion, the results of the studies presented in this scholarly work offer one of the first glimpses into the functional and remodeling response collecting lymphatic vessels to disruptions in lymphatic drainage pathways. Specifically, we demonstrate that diet-induced obesity adversely impacts collecting lymphatic contractility and pump function during lymphedema in a mouse model. Further, in a clinically relevant sheep model, we demonstrate that the uninjured vessel can compensate in vivo by altering its intrinsic functional response and structure; however, through this process, the collecting lymphatic

muscle experiences increased oxidative stress due to increased contractility. One of the most important findings from these studies is that injury to the lymphatic vasculature produces lasting structural and functional alterations to the remaining intact collecting lymphatic vessels, which occurs independently of direct mechanical damage. It is possible that these lasting alterations may influence the development of lymphedema upon later harmful stimuli that subsequently overloads the fluid drainage capacity of these vessels. Future work is needed to investigate the potential adverse consequences of these functional and remodeling responses, and if or how they may influence the development of lymphedema in a clinical setting.

APPENDIX A. MATLAB CODE FOR ANALYSIS OF LYMPHATIC

PUMPING PRESSURE

```matlab
clear
clc

%%
%Pumping Pressure Measurement
%Pressure and intensity data will be imported from text files (tab
delimited)
%and will be analyzed to determine the measured pumping pressure.
%Browse for pressure and intensity files
[pFileName, pPathName] = uigetfile('*.txt','Select the pressure
data','C:\Users\');
[iFileName, iPathName] = uigetfile('*.txt','Select the intensity
data','C:\Users\');
%Full file names for the pressure and intensity files
pressureFile = strcat(pPathName,pFileName);
intensityFile = strcat(iPathName,iFileName);
%Input frame where pumping pressure measurement started to adjust time
data
%for pressure measurement
prompt = 'Which frame did the pumping pressure measurement start on?';
dlg_title = 'Input Frame';
num_lines = 1;
PressureFrameStart = inputdlg(prompt,dlg_title,num_lines,{'0'});
PressureFrameStartNum = str2double(PressureFrameStart{1});
%Read in data from pressure file, and separate out adjusted time data
and
%the pressure data
PressureWksht = tdfread(pressureFile);
PressureFieldNames = fieldnames(PressureWksht);
PressureTimeData =
PressureWksht.(PressureFieldNames{1})+PressureFrameStartNum;
PressureData = PressureWksht.(PressureFieldNames{2});
%Read in data from intensity file, and separate out time data and the
%intensity data
IntensityWksht = dlmread(intensityFile, '\t');
%IntensityFieldNames = 'intensity'%fieldnames(IntensityWksht);
% IntensityTimeData = IntensityWksht.(IntensityFieldNames{1});
% IntensityData = IntensityWksht.(IntensityFieldNames{2});
IntensityData = IntensityWksht;
IntensityTimeData=zeros(1,length(IntensityData))';
for k=2:length(IntensityData)
    IntensityTimeData(k) = IntensityTimeData(k-1)+1;
end
%Filter Intensity Data using a moving average filter (averaging over 15
%points)
timeIntervalFilter = 5;
FilterMat = ones(1,timeIntervalFilter)/timeIntervalFilter;
IntensityDataFiltered = filter(FilterMat, 1, IntensityData);
% Code to view filtered data vs actual data:
```

```matlab
% figure
% hold on
% plot(IntensityTimeData,IntensityData)
% plot(IntensityTimeData,IntensityDataFiltered)
% legend('Intensity Data','Intensity Data Filtered')

%%
%Determining Pumping Pressure Value
count = 0;
%Find time point where pressure first goes above 80 mmHg (t1) and when it
%decreases below 60 mmHg after holding the pressure at 80 mmHg (t2)
for i=1:length(PressureData)
    if PressureData(i)>80 && count==0
        t1_P = floor(PressureTimeData(i));
        [Val1, t1] = min(abs(IntensityTimeData-t1_P));
        count = 1;
    elseif PressureData(i)<60 && count==1
        t2_P = floor(PressureTimeData(i));
        [Val2, t2] = min(abs(IntensityTimeData-t2_P));
        count = 2;
    elseif PressureData(i)<1 && count==2
        t3_P = floor(PressureTimeData(i));
        [Val3, t3] = min(abs(IntensityTimeData-t3_P));
        break;
    end
end
%Find max intensity after t2 and find index of value in
%IntensityDataFiltered
[maxIntensity, maxIntIndex_NA] = max(IntensityDataFiltered(t2:t3));
maxIntIndex = length(IntensityDataFiltered) -
length(IntensityDataFiltered(t2:end)) + maxIntIndex_NA;
%Find min intensity after t1 and find index of value in
%IntensityDataFiltered
[minIntensity, minIntIndex_NA] =
min(IntensityDataFiltered(t2:maxIntIndex));
minIntIndex = length(IntensityDataFiltered) -
length(IntensityDataFiltered(t2:end)) + minIntIndex_NA;
%Average min and max intensity to find the mid intensity
midIntensity = mean([minIntensity maxIntensity]);
%Find the index and time where the intensity data is closest to the mid
%intensity
[midIntVal, midIntIndex_NA] =
min(abs(IntensityDataFiltered(minIntIndex:maxIntIndex)-midIntensity));
midIntIndex = length(IntensityDataFiltered) -
length(IntensityDataFiltered(minIntIndex:end)) + midIntIndex_NA;
midIntTime = IntensityTimeData(midIntIndex);
%Find the index and pumping pressure where the intensity data is closest to
%the mid intensity
if (maxIntensity-minIntensity)>100
    [pressPumpVal, pressPumpIndex] = min(abs(PressureTimeData-
midIntTime));
    PumpingPressure = PressureData(pressPumpIndex);
else
    PumpingPressure = 0;
end
```

```matlab
uiwait(msgbox(strcat('The Pumping Pressure
is:',num2str(PumpingPressure),' mmHg')));
%%
%Emptying Rate
%Find how quickly the intensity decreases to its minimum value
[maxIntEmpRate, maxIntEmpRateIndex_NA] =
max(IntensityDataFiltered(t1:t2));
maxIntEmpRateIndex = length(IntensityDataFiltered) -
length(IntensityDataFiltered(t1:end)) + maxIntEmpRateIndex_NA;
minThreshold = 1.05*minIntensity;
for j=maxIntEmpRateIndex:t3
    if IntensityDataFiltered(j)<minThreshold
        threshIntIndex = j;
        break;
    end
end
EmpRate = round((maxIntEmpRate-
minThreshold)./(IntensityTimeData(threshIntIndex)-
IntensityTimeData(maxIntEmpRateIndex)),1);
uiwait(msgbox(strcat('The Emptying Rate is:',num2str(EmpRate),'
IU/s')));

%%
%Plotting Data
figure
hold on
title('Pumping Pressure Measurement')
yyaxis right
plot(PressureTimeData,PressureData)
axis([0 max(max(PressureTimeData),max(IntensityTimeData)) -5 90])
xlabel('Time (s)')
ylabel('Pumping Pressure (mmHg)')
yyaxis left
plot(IntensityTimeData,IntensityDataFiltered)
%Line to denote the pumping pressure on the graph
if PumpingPressure>0
    line([PressureTimeData(pressPumpIndex)
PressureTimeData(pressPumpIndex)],[min(IntensityDataFiltered)-500
max(IntensityDataFiltered)+500],'Marker','.','LineStyle','-
','Color','k')
end
%Line for emptying rate
line([IntensityTimeData(maxIntEmpRateIndex)
IntensityTimeData(threshIntIndex)],[maxIntEmpRate
minThreshold],'Marker','.','LineStyle','-','Color','r')
axis([0 max(max(PressureTimeData),max(IntensityTimeData))
min(IntensityDataFiltered)-500 max(IntensityDataFiltered)+500])
ylabel('Average Intensity')
```

APPENDIX B. MATLAB CODE FOR ANALYSIS OF PACKET

PERFORMANCE METRICS

```matlab
clear
clc

threshold = 0.001; %change

%Packet Processing
%Intensity data will be imported from text files (tab delimited)
%and will be analyzed to determine the functional metrics.
%Browse for intensity file
[FileName, PathName] = uigetfile('*.txt','Select the intensity data',
'C:\Users\');
%Full file names for the intensity file
intensityFile = strcat(PathName,FileName);

x= dlmread(intensityFile, '\t');

y2= x(:,1);
y2=smooth(y2,5);

[maxtab2, min2]=peakdet(y2,70); %Intensity change to be considered a
peak

if maxtab2(1,1) < min2(1,1)
    maxtab2 = maxtab2(2:end,:);
end

if maxtab2(end,1) > min2(end,1)
    maxtab2 = maxtab2(1:end-1,:);
end

mintab2=min2(1,:);
for n=2:length(min2)-1
    index=min2(n);
    while y2(index) <= min2(n,2)*(1+threshold)
        index=index-1;
    end
    mintemp2(1,1)=index;mintemp2(1,2)=y2(index);
    index=min2(n);
    while y2(index) <= min2(n,2)*(1+threshold)
        index=index+1;
    end
    mintemp2(2,1)=index;mintemp2(2,2)=y2(index);
    mintab2 = [mintab2 ; mintemp2];
end
```

```matlab
mintab2 = [mintab2 ; min2(end,:)];

packet_width2=[];
mean_packet_min2=[];
packet_integral2=zeros(1,length(maxtab2));
packet_boundary2=[];
for n=1:2:length(mintab2)-1
    packet_width2 = [packet_width2 mintab2(n+1,1)-mintab2(n,1)];
    mean_packet_min2 = [mean_packet_min2 mean([mintab2(n+1,2)
mintab2(n,2)])];
end

integral_y2=[];
for n=1:length(maxtab2)
    packet_line_x2 = mintab2(n*2-1,1):mintab2(n*2,1);
    packet_slope2 = (mintab2(n*2,2)-mintab2(n*2-1,2))/(mintab2(n*2,1)-
mintab2(n*2-1,1));
    packet_offset2 = mintab2(n*2-1,2) - packet_slope2 * mintab2(n*2-
1,1);
    for index=1:length(packet_line_x2)
        packet_line_y2(index) = packet_line_x2(index)*packet_slope2 +
packet_offset2;
    end
    packet_line2 = [packet_line_x2; packet_line_y2];
    packet_line2 = packet_line2';
    packet_boundary2 = [packet_boundary2;packet_line2];

    packet_amplitude2(n) = maxtab2(n,2) - mean_packet_min2(n);
    packet_amplitude_perdiff2(n) =
packet_amplitude2(n)/mean_packet_min2(n);
    for index = mintab2(n*2-1,1):mintab2(n*2,1)
        integral_y2=[integral_y2;y2(index)];
    end
    for index = 1:length(integral_y2)
    packet_integral2(n) = packet_integral2(n) + integral_y2(index)-
packet_line_y2(index);
    end
    packet_integral_norm2(n) = packet_integral2(n)/mean_packet_min2(n);
    packet_line_y2=[];
    integral_y2=[];
end

fig2 = figure;
plot(y2, 'linewidth', 2)
hold on
plot(maxtab2(:,1),maxtab2(:,2),'r.',mintab2(:,1),mintab2(:,2),'g.',
'markersize', 15)
plot(packet_boundary2(:,1),packet_boundary2(:,2),'g.','markersize', 4)
xlabel('Frame');ylabel('Intensity');
%title([filename ' Plot 2']);


%print(fig2, '-dtiff', [filepath filename 'Plot2'])
```

143

```matlab
%packets per min, assuming 10fps
packet_frequency2 = length(maxtab2)/(mintab2(end,1)-mintab2(2,1))*600;

avg_packet_width2 = mean(packet_width2);
avg_packet_amplitude2 = mean(packet_amplitude2);
avg_packet_amplitude_perdiff2 = mean(packet_amplitude_perdiff2);
avg_packet_integral2 = mean(packet_integral2);
avg_packet_integral_norm2 = mean(packet_integral_norm2);

%normalized per minute, assuming 10fps
packet_transport2 = sum(packet_integral2)/(mintab2(end,1)-
mintab2(1,1))*600;
packet_transport_norm2 = sum(packet_integral_norm2)/(mintab2(end,1)-
mintab2(1,1))*600;

output = [packet_frequency2;
avg_packet_width2;avg_packet_amplitude2;avg_packet_integral2;packet_tra
nsport2];

%filename

packet_frequency2

avg_packet_width2

avg_packet_amplitude2

avg_packet_amplitude_perdiff2

avg_packet_integral2

avg_packet_integral_norm2

packet_transport2

packet_transport_norm2

% dlmwrite([filepath filename 'Output' extension], output)
```

APPENDIX C. PROTEOMIC ANALYSIS OF SHEEP LYMPHATIC

SMOOTH MUSCLE CELLS

Table 2 – Summary of protein expression fold changes and associated genes

Fold Changes Wounded/Ctrl	Gene	Entrez Gene Name	Location	Type
-5.583	ACACA	acetyl-CoA carboxylase alpha	Cytoplasm	enzyme
-1.028	ACLY	ATP citrate lyase	Cytoplasm	enzyme
1.117	ACTB	actin beta	Cytoplasm	other
-1.896	AHSG	alpha 2-HS glycoprotein	Extracellular Space	other
-1.203	AHSG	alpha 2-HS glycoprotein	Extracellular Space	other
-1.037	ALB	albumin	Extracellular Space	transporter
3.352	ALDH1A1	aldehyde dehydrogenase 1 family member A1	Cytoplasm	enzyme
-1.69	ALDOB	aldolase, fructose-bisphosphate B	Cytoplasm	enzyme
1.159	ANP32B	acidic nuclear phosphoprotein 32 family member B	Nucleus	other
-1.858	ANXA2	annexin A2	Plasma Membrane	other
-14.484	APOE	apolipoprotein E	Extracellular Space	transporter

-1.795	ASPM	abnormal spindle microtubule assembly	Nucleus	other
-1.042	ATP1A1	ATPase Na+/K+ transporting subunit alpha 1	Plasma Membrane	transporter
2.35	ATP1B1	ATPase Na+/K+ transporting subunit beta 1	Plasma Membrane	transporter
-5.661	BGN	biglycan	Extracellular Space	other
	BRS3	bombesin receptor subtype 3	Plasma Membrane	G-protein coupled receptor
1.043	CALM1 (includes others)	calmodulin 1	Cytoplasm	other
0	CAPN3	calpain 3	Cytoplasm	peptidase
-1.181	CAST	calpastatin	Cytoplasm	peptidase
1.016	CAV1	caveolin 1	Plasma Membrane	transmembrane receptor
1.13	CFL1	cofilin 1	Nucleus	other
0	CLN5	ceroid-lipofuscinosis, neuronal 5	Cytoplasm	other
1.113	CNN1	calponin 1	Cytoplasm	other
2.444	COX7A1	cytochrome c oxidase subunit 7A1	Cytoplasm	enzyme
2.444	COX7A2	cytochrome c oxidase subunit 7A2	Cytoplasm	enzyme

-4.689	CRYAB	crystallin alpha B	Nucleus	other
-1.979	CSN1S1	casein alpha s1	Extracellular Space	other
-6.141	CSN2	casein beta	Extracellular Space	kinase
-19.105	CSN3	casein kappa	Extracellular Space	other
	CSTB	cystatin B	Cytoplasm	peptidase
2.052	CTSB	cathepsin B	Cytoplasm	peptidase
-1.171	CTSD	cathepsin D	Cytoplasm	peptidase
	CTSL	cathepsin L	Cytoplasm	peptidase
1.309	CYCS	cytochrome c, somatic	Cytoplasm	transporter
	CYP11A1	cytochrome P450 family 11 subfamily A member 1	Cytoplasm	enzyme
1.236	DCN	decorin	Extracellular Space	other
	DYNLT3	dynein light chain Tctex-type 3	Cytoplasm	other
1.23	EEF1D	eukaryotic translation elongation factor 1 delta	Cytoplasm	translation regulator
-3.527	FTH1	ferritin heavy chain 1	Cytoplasm	enzyme

1.053	FTL	ferritin light chain	Cytoplasm	enzyme
1.098	GAPDH	glyceraldehyde-3-phosphate dehydrogenase	Cytoplasm	enzyme
0	GCNT3	glucosaminyl (N-acetyl) transferase 3, mucin type	Plasma Membrane	enzyme
0	GGCX	gamma-glutamyl carboxylase	Cytoplasm	enzyme
-1.131	H2AFZ	H2A histone family member Z	Nucleus	other
1.266	HPCAL1	hippocalcin like 1	Cytoplasm	other
-1.495	HSD11B1	hydroxysteroid 11-beta dehydrogenase 1	Cytoplasm	enzyme
1.053	IDH1	isocitrate dehydrogenase (NADP(+)) 1, cytosolic	Cytoplasm	enzyme
-3.287	IGFBP4	insulin like growth factor binding protein 4	Extracellular Space	other
-1.088	ITGB1	integrin subunit beta 1	Plasma Membrane	transmembrane receptor
-1.396	ITGB6	integrin subunit beta 6	Plasma Membrane	other
0	LALBA	lactalbumin alpha	Extracellular Space	enzyme
-1.112	LGALS1	galectin 1	Extracellular Space	other
-1.328	MIF	macrophage migration inhibitory factor (glycosylation-inhibiting factor)	Extracellular Space	cytokine

148

-1.064	MT-ATP6	ATP synthase F0 subunit 6	Cytoplasm	transporter
1.094	MT-CO2	cytochrome c oxidase subunit II	Cytoplasm	enzyme
1.476	MT-CO3	cytochrome c oxidase III	Cytoplasm	enzyme
1.507	MT-ND3	NADH dehydrogenase, subunit 3 (complex I)	Cytoplasm	enzyme
-1.149	MT-ND5	NADH dehydrogenase, subunit 5 (complex I)	Cytoplasm	enzyme
-2.212	MYLK	myosin light chain kinase	Cytoplasm	kinase
-1.349	PDXK	pyridoxal (pyridoxine, vitamin B6) kinase	Cytoplasm	kinase
	PF4	platelet factor 4	Extracellular Space	cytokine
1.006	PGD	phosphogluconate dehydrogenase	Cytoplasm	enzyme
-2.509	PLP2	proteolipid protein 2	Cytoplasm	transporter
	POMC	proopiomelanocortin	Extracellular Space	other
1.507	PRKACA	protein kinase cAMP-activated catalytic subunit alpha	Cytoplasm	kinase
	PTGS1	prostaglandin-endoperoxide synthase 1	Cytoplasm	enzyme
-1.282	PYGB	glycogen phosphorylase B	Cytoplasm	enzyme

-1.088	PYGL	glycogen phosphorylase L	Cytoplasm	enzyme
-1.143	PYGM	glycogen phosphorylase, muscle associated	Cytoplasm	enzyme
1.262	RPL10	ribosomal protein L10	Cytoplasm	other
1.072	RPS25	ribosomal protein S25	Cytoplasm	other
1.134	RPS26	ribosomal protein S26	Cytoplasm	other
1.069	RPSA	ribosomal protein SA	Cytoplasm	translation regulator
-1.37	SERPINC1	serpin family C member 1	Extracellular Space	enzyme
-1.817	SFN	stratifin	Cytoplasm	other
1.723	SFTPA1	surfactant protein A1	Extracellular Space	transporter
-1.101	SFXN1	sideroflexin 1	Cytoplasm	transporter
0	SHMT1	serine hydroxymethyltransferase 1	Cytoplasm	enzyme
0	SLC26A2	solute carrier family 26 member 2	Plasma Membrane	transporter
	SLC2A1	solute carrier family 2 member 1	Plasma Membrane	transporter
0	SLC2A3	solute carrier family 2 member 3	Plasma Membrane	transporter

0	SLC5A1	solute carrier family 5 member 1	Plasma Membrane	transporter
1.897	SOD1	superoxide dismutase 1, soluble	Cytoplasm	enzyme
1.021	SORD	sorbitol dehydrogenase	Cytoplasm	enzyme
	SPP2	secreted phosphoprotein 2	Extracellular Space	other
	STX1B	syntaxin 1B	Plasma Membrane	other
	TCHH	trichohyalin	Extracellular Space	other
-1.255	TES	testin LIM domain protein	Plasma Membrane	other
-1.309	TIMP1	TIMP metallopeptidase inhibitor 1	Extracellular Space	cytokine
0	TSPAN9	tetraspanin 9	Plasma Membrane	other
-1.499	TXN	thioredoxin	Cytoplasm	enzyme
1.103	UBA52	ubiquitin A-52 residue ribosomal protein fusion product 1	Cytoplasm	enzyme
-1.001	UROD	uroporphyrinogen decarboxylase	Cytoplasm	enzyme
1.023	VIM	vimentin	Cytoplasm	other
1.022	YWHAB	tyrosine 3-monooxygenase/tryptophan 5-	Cytoplasm	transcription regulator

		monooxygenase activation protein beta		
1.016	YWHAE	tyrosine 3-monooxygenase/tryptophan 5-monooxygenase activation protein epsilon	Cytoplasm	other
1.034	YWHAG	tyrosine 3-monooxygenase/tryptophan 5-monooxygenase activation protein gamma	Cytoplasm	other
1.033	YWHAZ	tyrosine 3-monooxygenase/tryptophan 5-monooxygenase activation protein zeta	Cytoplasm	enzyme
0	CSN1S2	Beta-casein	Extracellular Space	transporter
-5.211	LGB	Beta-lactoglobulin-1	Extracellular Space	transporter
-5.211	LGB	Beta-lactoglobulin-1/B	Extracellular Space	transporter

REFERENCES

1. **Akagi K**, **Ikeda Y**, **Miyazaki M**, **Abe T**, **Kinoshita J**, **Maehara Y**, **Sugimachi K**. Vascular endothelial growth factor-C (VEGF-C) expression in human colorectal cancer tissues. *Br. J. Cancer* 83: 887–91, 2000.

2. **Akl TJ**, **Nagai T**, **Coté GL**, **Gashev AA**. Mesenteric lymph flow in adult and aged rats. *Am. J. Physiol. Hear. Circ. Physiol.* 301: H1828–H1840, 2011.

3. **Aldrich MB**, **Sevick-Muraca EM**. Cytokines are systemic effectors of lymphatic function in acute inflammation. *Cytokine* 64: 362–9, 2013.

4. **Alkhouri N**, **Gornicka A**, **Berk MP**, **Thapaliya S**, **Dixon LJ**, **Kashyap S**, **Schauer PR**, **Feldstein AE**. Adipocyte apoptosis, a link between obesity, insulin resistance, and hepatic steatosis. *J. Biol. Chem.* 285: 3428–38, 2010.

5. **Andersen L**, **Højris I**, **Erlandsen M**, **Andersen J**. Treatment of breast-cancer-related lymphedema with or without manual lymphatic drainage--a randomized study. [Online]. *Acta Oncol.* 39: 399–405, 2000. http://www.ncbi.nlm.nih.gov/pubmed/10987238 [12 Nov. 2017].

6. **Anuradha R**, **George PJ**, **Hanna LE**, **Chandrasekaran V**, **Kumaran P**, **Nutman TB**, **Babu S**. IL-4-, TGF-β-, and IL-1-dependent expansion of parasite antigen-specific Th9 cells is associated with clinical pathology in human lymphatic filariasis. *J. Immunol.* 191: 2466–73, 2013.

7. **Armer JM**, **Stewart BR**. Post-breast cancer lymphedema: incidence increases from

12 to 30 to 60 months. [Online]. *Lymphology* 43: 118–27, 2010. http://www.ncbi.nlm.nih.gov/pubmed/21226414 [10 Oct. 2017].

8.   **Arngrim N**, **Simonsen L**, **Holst JJ**, **Bülow J**. Reduced adipose tissue lymphatic drainage of macromolecules in obese subjects: a possible link between obesity and local tissue inflammation? *Int. J. Obes.* 37: 748–750, 2013.

9.   **Aschen S**, **Zampell JC**, **Elhadad S**, **Weitman E**, **De Brot M**, **Mehrara BJ**. Regulation of adipogenesis by lymphatic fluid stasis: part II. Expression of adipose differentiation genes. *Plast. Reconstr. Surg.* 129: 838–47, 2012.

10.   **Avraham T**, **Clavin NW**, **Daluvoy S V**, **Fernandez J**, **Soares M a**, **Cordeiro AP**, **Mehrara BJ**. Fibrosis is a key inhibitor of lymphatic regeneration. *Plast. Reconstr. Surg.* 124: 438–50, 2009.

11.   **Avraham T**, **Zampell JC**, **Yan A**, **Elhadad S**, **Weitman ES**, **Rockson SG**, **Bromberg J**, **Mehrara BJ**. Th2 differentiation is necessary for soft tissue fibrosis and lymphatic dysfunction resulting from lymphedema. *FASEB J.* 27: 1114–26, 2013.

12.   **Babu S**, **Bhat SQ**, **Pavan Kumar N**, **Lipira AB**, **Kumar S**, **Karthik C**, **Kumaraswami V**, **Nutman TB**. Filarial lymphedema is characterized by antigen-specific Th1 and th17 proinflammatory responses and a lack of regulatory T cells. *PLoS Negl. Trop. Dis.* 3: e420, 2009.

13.   **Babu S**, **Nutman TB**. Immunology of lymphatic filariasis. *Parasite Immunol.* 36: 338–346, 2014.

14. **Badger CM**, **Peacock JL**, **Mortimer PS**. A randomized, controlled, parallel-group clinical trial comparing multilayer bandaging followed by hosiery versus hosiery alone in the treatment of patients with lymphedema of the limb. [Online]. *Cancer* 88: 2832–7, 2000. http://www.ncbi.nlm.nih.gov/pubmed/10870068 [12 Nov. 2017].

15. **Bains SK**, **Stanton AWB**, **Cintolesi V**, **Ballinger J**, **Allen S**, **Zammit C**, **Levick JR**, **Mortimer PS**, **Peters AM**, **Purushotham AD**. A constitutional predisposition to breast cancer-related lymphoedema and effect of axillary lymph node surgery on forearm muscle lymph flow. *The Breast* 24: 68–74, 2015.

16. **Ballinger SW**, **Patterson C**, **Yan C-N**, **Doan R**, **Burow DL**, **Young CG**, **Yakes FM**, **Van Houten B**, **Ballinger CA**, **Freeman BA**, **Runge MS**. Hydrogen Peroxide– and Peroxynitrite-Induced Mitochondrial DNA Damage and Dysfunction in Vascular Endothelial and Smooth Muscle Cells [Online]. *Circ. Res.* 86, 2000. http://circres.ahajournals.org/content/86/9/960.short [7 Jun. 2017].

17. **Ballou B**, **Ernst LA**, **Waggoner AS**. Fluorescence imaging of tumors in vivo. *Curr. Med. Chem.* 12: 795–805, 2005.

18. **Baluk P**, **Fuxe J**, **Hashizume H**, **Romano T**, **Lashnits E**, **Butz S**, **Vestweber D**, **Corada M**, **Molendini C**, **Dejana E**, **McDonald DM**. Functionally specialized junctions between endothelial cells of lymphatic vessels. *J. Exp. Med.* 204: 2349–62, 2007.

19. **Baluk P**, **Tammela T**, **Ator E**, **Lyubynska N**, **Achen MG**, **Hicklin DJ**, **Jeltsch M**, **Petrova T V.**, **Pytowski B**, **Stacker SA**, **Ylä-Herttuala S**, **Jackson DG**, **Alitalo K**,

McDonald DM. Pathogenesis of persistent lymphatic vessel hyperplasia in chronic airway inflammation. *J. Clin. Invest.* 115: 247–257, 2005.

20. **Barrett T**, **Choyke PL**, **Kobayashi H**. Imaging of the lymphatic system: new horizons. *Contrast Media Mol. Imaging* 1: 230–245, 2006.

21. **Benoit JN**, **Zawieja DC**, **Goodman AH**, **Granger HJ**. Characterization of intact mesenteric lymphatic pump and its responsiveness to acute edemagenic stress. *Am. J. Physiol.* 257: H2059-69, 1989.

22. **Berk DA**, **Swartz MA**, **Leu AJ**, **Jain RK**. Transport in lymphatic capillaries. II. Microscopic velocity measurement with fluorescence photobleaching. *Am. J. Physiol.* 270: H330-7, 1996.

23. **Bertram C**, **Macaskill C**, **Davis MJ**, **Moore JE**. Consequences of intravascular lymphatic valve properties: a study of contraction timing in a multi-lymphangion model. *Am. J. Physiol. - Hear. Circ. Physiol.* (2016). doi: 10.1152/ajpheart.00669.2015.

24. **Bertram CD**, **Macaskill C**, **Davis MJ**, **Moore JE**. Development of a model of a multi-lymphangion lymphatic vessel incorporating realistic and measured parameter values. *Biomech. Model. Mechanobiol.* 13: 401–416, 2014.

25. **Bertram CD**, **Macaskill C**, **Moore JE**. EFFECTS OF LYMPHANGION SUBDIVISION IN A NUMERICAL MODEL OF A LYMPHATIC VESSEL. *J. Biomech. Eng.* 133: 11008, 2011.

26. **Bertram CD**, **Macaskill C**, **Moore JE**. Simulation of a chain of collapsible contracting lymphangions with progressive valve closure. *J. Biomech. Eng.* 133: 11008, 2011.

27. **Blum KS**, **Karaman S**, **Proulx ST**, **Ochsenbein AM**, **Luciani P**, **Leroux J-C**, **Wolfrum C**, **Detmar M**. Chronic high-fat diet impairs collecting lymphatic vessel function in mice. *PLoS One* 9: e94713, 2014.

28. **Blum KS**, **Proulx ST**, **Luciani P**, **Leroux J-C**, **Detmar M**. Dynamics of lymphatic regeneration and flow patterns after lymph node dissection. *Breast Cancer Res. Treat.* 139: 81–6, 2013.

29. **Boardman KC**, **Swartz MA**. Interstitial flow as a guide for lymphangiogenesis. *Circ. Res.* 92: 801–8, 2003.

30. **Bockarie MJ**, **Taylor MJ**, **Gyapong JO**. Current practices in the management of lymphatic filariasis. *Expert Rev. Anti. Infect. Ther.* 7: 595–605, 2009.

31. **Bohlen HG**, **Gasheva OY**, **Gashev AA**, **Zawieja DC**. Nitric oxide formation by lymphatic bulb and valves is a major regulatory component of lymphatic pumping. *Am. J. Physiol. Hear. Circ. Physiol.* 301: H1897-906, 2011.

32. **Bohlen HG**, **Wang W**, **Gashev AA**, **Gasheva OY**, **Zawieja D**. Phasic contractions of rat mesenteric lymphatics increase basal and phasic nitric oxide generation in vivo. *Am. J. Physiol. Hear. Circ. Physiol.* 297: H1319-28, 2009.

33. **Breiteneder-Geleff S**, **Soleiman A**, **Kowalski H**, **Horvat R**, **Amann G**,

Kriehuber E, **Diem K**, **Weninger W**, **Tschachler E**, **Alitalo K**, **Kerjaschki D**. Angiosarcomas Express Mixed Endothelial Phenotypes of Blood and Lymphatic Capillaries. *Am. J. Pathol.* 154: 385–394, 1999.

34. **Bunag RD**, **Butterfield J**. Tail-cuff blood pressure measurement without external preheating in awake rats. *Hypertension* 4: 898–903, 1982.

35. **De Camilli P**, **Chen H**, **Fre S**, **Slepnev VI**, **Capua MR**, **Takei K**, **Butler MH**, **Di Fiore PP**. Epsin is an EH-domain-binding protein implicated in clathrin-mediated endocytosis. *Nature* 394: 793–797, 1998.

36. **Caulk AW**, **Dixon JB**, **Gleason RL**. A lumped parameter model of mechanically mediated acute and long-term adaptations of contractility and geometry in lymphatics for characterization of lymphedema. *Biomech. Model. Mechanobiol.* 15: 1601–1618, 2016.

37. **Caulk AW**, **Nepiyushchikh Z V.**, **Shaw R**, **Dixon JB**, **Gleason RL**. Quantification of the passive and active biaxial mechanical behaviour and microstructural organization of rat thoracic ducts [Online]. *J. R. Soc. Interface* 12, 2015. http://rsif.royalsocietypublishing.org/content/12/108/20150280 [7 Jun. 2017].

38. **Causey L**, **Cowin SC**, **Weinbaum S**. Quantitative model for predicting lymph formation and muscle compressibility in skeletal muscle during contraction and stretch. *Proc. Natl. Acad. Sci.* 109: 9185–90, 2012.

39. **Cemal Y**, **Pusic A**, **Mehrara BJ**. Preventative measures for lymphedema: separating fact from fiction. *J. Am. Coll. Surg.* 213: 543–51, 2011.

40. **Chakraborty S**, **Gurusamy M**, **Zawieja DC**, **Muthuchamy M**. Lymphatic Filariasis: Perspectives on Lymphatic Remodeling and Contractile Dysfunction in Filarial Disease Pathogenesis. *Microcirculation* 20: 349–364, 2013.

41. **Chelko SP**, **Schmiedt CW**, **Lewis TH**, **Lewis SJ**, **Robertson TP**. Vasopressin-induced constriction of the isolated rat occipital artery is segment dependent. *J. Vasc. Res.* 50: 478–85, 2013.

42. **Chen C**, **Zhuang X**. Epsin 1 is a cargo-specific adaptor for the clathrin-mediated endocytosis of the influenza virus. *Proc. Natl. Acad. Sci.* 105: 11790–11795, 2008.

43. **Chen H**, **De Camilli P**. The association of epsin with ubiquitinated cargo along the endocytic pathway is negatively regulated by its interaction with clathrin. *Proc. Natl. Acad. Sci.* 102: 2766–2771, 2005.

44. **Chen H**, **Ko G**, **Zatti A**, **Di Giacomo G**, **Liu L**, **Raiteri E**, **Perucco E**, **Collesi C**, **Min W**, **Zeiss C**, **De Camilli P**, **Cremona O**. Embryonic arrest at midgestation and disruption of Notch signaling produced by the absence of both epsin 1 and epsin 2 in mice. *Proc. Natl. Acad. Sci. U. S. A.* 106: 13838–43, 2009.

45. **Chong C**, **Scholkmann F**, **Bachmann SB**, **Luciani P**, **Leroux J-C**, **Detmar M**, **Proulx ST**. In vivo visualization and quantification of collecting lymphatic vessel contractility using near-infrared imaging. *Sci. Rep.* 6: 22930, 2016.

46. **Cintolesi V**, **Stanton AWB**, **Bains SK**, **Cousins E**, **Peters AM**, **Purushotham AD**, **Levick JR**, **Mortimer PS**. Constitutively Enhanced Lymphatic Pumping in the Upper Limbs of Women Who Later Develop Breast Cancer-Related Lymphedema.

Lymphat. Res. Biol. 14: 50–61, 2016.

47. **Cintolesi V**, **Stanton AWB**, **Bains SK**, **Cousins E**, **Peters AM**, **Purushotham AD**, **Levick JR**, **Mortimer PS**. Constitutively Enhanced Lymphatic Pumping in the Upper Limbs of Women Who Later Develop Breast Cancer-Related Lymphedema. *Lymphat. Res. Biol.* 14: 50–61, 2016.

48. **Clark B**, **Sitzia J**, **Harlow W**. Incidence and risk of arm oedema following treatment for breast cancer: a three-year follow-up study. *QJM An Int. J. Med.* 98: 343–348, 2005.

49. **Clavin NW**, **Avraham T**, **Fernandez J**, **Daluvoy S V**, **Soares MA**, **Chaudhry A**, **Mehrara BJ**. TGF-beta1 is a negative regulator of lymphatic regeneration during wound repair. *Am. J. Physiol. Hear. Circ. Physiol.* 295: H2113-27, 2008.

50. **Clement CC**, **Aphkhazava D**, **Nieves E**, **Callaway M**, **Olszewski W**, **Rotzschke O**, **Santambrogio L**. Protein expression profiles of human lymph and plasma mapped by 2D-DIGE and 1D SDS–PAGE coupled with nanoLC–ESI–MS/MS bottom-up proteomics. *J. Proteomics* 78: 172–187, 2013.

51. **Clement CC**, **Becerra A**, **Yin L**, **Zolla V**, **Huang L**, **Merlin S**, **Follenzi A**, **Shaffer SA**, **Stern LJ**, **Santambrogio L**. The Dendritic Cell Major Histocompatibility Complex II (MHC II) Peptidome Derives from a Variety of Processing Pathways and Includes Peptides with a Broad Spectrum of HLA-DM Sensitivity. *J. Biol. Chem.* 291: 5576–95, 2016.

52. **Cormier JN**, **Askew RL**, **Mungovan KS**, **Xing Y**, **Ross MI**, **Armer JM**.

Lymphedema beyond breast cancer. *Cancer* 116: 5138–5149, 2010.

53. **CORNISH BH**, **CHAPMAN M**, **THOMAS BJ**, **WARD LC**, **BUNCE IH**, **HIRST C**. Early Diagnosis of Lymphedema in Postsurgery Breast Cancer Patients. *Ann. N. Y. Acad. Sci.* 904: 571–575, 2006.

54. **Custodis F**, **Baumhäkel M**, **Schlimmer N**, **List F**, **Gensch C**, **Böhm M**, **Laufs U**. Heart Rate Reduction by Ivabradine Reduces Oxidative Stress, Improves Endothelial Function, and Prevents Atherosclerosis in Apolipoprotein E–Deficient Mice [Online]. *Circulation* 117, 2008. http://circ.ahajournals.org/content/117/18/2377.short [7 Jun. 2017].

55. **Datar SA**, **Gong W**, **He Y**, **Johengen M**, **Kameny RJ**, **Raff GW**, **Maltepe E**, **Oishi PE**, **Fineman JR**. Disrupted NOS signaling in lymphatic endothelial cells exposed to chronically increased pulmonary lymph flow. *Am. J. Physiol. - Hear. Circ. Physiol.* 311: H137–H145, 2016.

56. **Datar SA**, **Oishi PE**, **Gong W**, **Bennett SH**, **Sun CE**, **Johengen M**, **Maki J**, **Johnson RC**, **Raff GW**, **Fineman JR**. Altered reactivity and nitric oxide signaling in the isolated thoracic duct from an ovine model of congenital heart disease with increased pulmonary blood flow. *Am J Physiol Hear. Circ Physiol* 306: H954-62, 2014.

57. **Davis MJ**, **Davis AM**, **Ku CW**, **Gashev AA**. Myogenic constriction and dilation of isolated lymphatic vessels. *Am. J. Physiol. Heart Circ. Physiol.* 296: H293-302, 2009.

58. **Davis MJ**, **Davis AM**, **Lane MM**, **Ku CW**, **Gashev AA**. Rate-sensitive contractile responses of lymphatic vessels to circumferential stretch. *J. Physiol.* 587: 165–182, 2009.

59. **Davis MJ**, **Rahbar E**, **Gashev AA**, **Zawieja DC**, **Moore JE**. Determinants of valve gating in collecting lymphatic vessels from rat mesentery. *AJP Hear. Circ. Physiol.* 301: H48–H60, 2011.

60. **Davis MJ**, **Scallan JP**, **Wolpers JH**, **Muthuchamy M**, **Gashev A a**, **Zawieja DC**. Intrinsic increase in lymphangion muscle contractility in response to elevated afterload. *Am. J. Physiol. Heart Circ. Physiol.* 303: H795-808, 2012.

61. **Deng T**, **Lyon CJ**, **Minze LJ**, **Lin J**, **Zou J**, **Liu JZ**, **Ren Y**, **Yin Z**, **Hamilton DJ**, **Reardon PR**, **Sherman V**, **Wang HY**, **Phillips KJ**, **Webb P**, **Wong STC**, **Wang R**, **Hsueh WA**. Class II Major Histocompatibility Complex Plays an Essential Role in Obesity-Induced Adipose Inflammation. *Cell Metab.* 17: 411–422, 2013.

62. **Dixon JB**, **Greiner ST**, **Gashev A a**, **Cote GL**, **Moore JE**, **Zawieja DC**. Lymph flow, shear stress, and lymphocyte velocity in rat mesenteric prenodal lymphatics. *Microcirculation* 13: 597–610, 2006.

63. **Dongaonkar RM**, **Nguyen TL**, **Quick CM**, **Hardy J**, **Laine GA**, **Wilson E**, **Stewart RH**. Adaptation of mesenteric lymphatic vessels to prolonged changes in transmural pressure. *AJP Hear. Circ. Physiol.* 305: H203–H210, 2013.

64. **Donoso LA**, **Kim D**, **Frost A**, **Callahan A**, **Hageman G**. The Role of Inflammation in the Pathogenesis of Age-related Macular Degeneration. *Surv. Ophthalmol.* 51:

137–152, 2006.

65. **Eisenhoffer J**, **Kagal A**, **Klein T**, **Johnston MG**. Importance of Valves and Lymphangion Contractions in Determining Pressure Gradients in Isolated Lymphatics Exposed to Elevations in Outflow Pressure. *Microvasc. Res.* 49: 97–110, 1995.

66. **Fox JLR**, **von der Weid P-Y**. Effects of histamine on the contractile and electrical activity in isolated lymphatic vessels of the guinea-pig mesentery. *Br. J. Pharmacol.* 136: 1210–8, 2002.

67. **Frangioni J V**. In vivo near-infrared fluorescence imaging. *Curr. Opin. Chem. Biol.* 7: 626–634, 2003.

68. **Fukumura D**, **Gohongi T**, **Kadambi A**, **Izumi Y**, **Ang J**, **Yun CO**, **Buerk DG**, **Huang PL**, **Jain RK**. Predominant role of endothelial nitric oxide synthase in vascular endothelial growth factor-induced angiogenesis and vascular permeability. *Proc. Natl. Acad. Sci. U. S. A.* 98: 2604–9, 2001.

69. **Garcia AM**, **Dicianno BE**. The Frequency of Lymphedema in an Adult Spina Bifida Population. *Am. J. Phys. Med. Rehabil.* 90: 89–96, 2011.

70. **Gardenier JC**, **Kataru RP**, **Hespe GE**, **Savetsky IL**, **Torrisi JS**, **Nores GDG**, **Jowhar DK**, **Nitti MD**, **Schofield RC**, **Carlow DC**, **Mehrara BJ**. Topical tacrolimus for the treatment of secondary lymphedema. *Nat. Commun.* 8: 14345, 2017.

71. **Gashev AA**. Lymphatic vessels: pressure- and flow-dependent regulatory reactions. *Ann. N. Y. Acad. Sci.* 1131: 100–9, 2008.

72. **Gashev AA**, **Davis MJ**, **Delp MD**, **Zawieja DC**. Regional variations of contractile activity in isolated rat lymphatics. *Microcirculation* 11: 477–92, 2004.

73. **Gashev AA**, **Davis MJ**, **Zawieja DC**. Inhibition of the active lymph pump by flow in rat mesenteric lymphatics and thoracic duct. *J. Physiol.* 540: 1023–1037, 2002.

74. **Gashev AA**, **Nagai T**, **Bridenbaugh EA**. Indocyanine green and lymphatic imaging: current problems. *Lymphat. Res. Biol.* 8: 127–30, 2010.

75. **Gashev AA**, **Zawieja DC**. Hydrodynamic regulation of lymphatic transport and the impact of aging. *Pathophysiology* 17: 277–87, 2010.

76. **Gasheva OY**, **Gashev AA**, **Zawieja DC**. Contraction-initiated NO-dependent lymphatic relaxation: a self-regulatory mechanism in rat thoracic duct. *J. Physiol.* 575: 821–32, 2006.

77. **Gasheva OY**, **Knippa K**, **Nepiushchikh Z V**, **Muthuchamy M**, **Gashev AA**. Age-related alterations of active pumping mechanisms in rat thoracic duct. *Microcirculation* 14: 827–39, 2007.

78. **van Geest AJ**, **Veraart JC**, **Nelemans P**, **Neumann HA**. The effect of medical elastic compression stockings with different slope values on edema. Measurements underneath three different types of stockings. [Online]. *Dermatol. Surg.* 26: 244–7, 2000. http://www.ncbi.nlm.nih.gov/pubmed/10759802 [12 Nov. 2017].

79. **Gleason RL**, **Gray SP**, **Wilson E**, **Humphrey JD**. A Multiaxial Computer-Controlled Organ Culture and Biomechanical Device for Mouse Carotid Arteries. *J. Biomech. Eng.* 126: 787, 2004.

80. **Goldman J**, **Conley KA**, **Raehl A**, **Bondy DM**, **Pytowski B**, **Swartz MA**, **Rutkowski JM**, **Jaroch DB**, **Ongstad EL**. Regulation of lymphatic capillary regeneration by interstitial flow in skin. *Am. J. Physiol. Hear. Circ. Physiol.* 292: H2176-83, 2007.

81. **Gousopoulos E**, **Karaman S**, **Proulx ST**, **Leu K**, **Buschle D**, **Detmar M**. High-Fat Diet in the Absence of Obesity Does Not Aggravate Surgically Induced Lymphoedema in Mice. *Eur. Surg. Res.* 58: 180–192, 2017.

82. **Gousopoulos E**, **Proulx ST**, **Bachmann SB**, **Dieterich LC**, **Scholl J**, **Karaman S**, **Bianchi R**, **Detmar M**. An Important Role of VEGF-C in Promoting Lymphedema Development. *J. Invest. Dermatol.* 137: 1995–2004, 2017.

83. **Gousopoulos E**, **Proulx ST**, **Scholl J**, **Uecker M**, **Detmar M**. Prominent Lymphatic Vessel Hyperplasia with Progressive Dysfunction and Distinct Immune Cell Infiltration in Lymphedema. *Am. J. Pathol.* 186: 2193–2203, 2016.

84. **Greene AK**, **Grant FD**, **Slavin SA**, **Maclellan RA**. Obesity-induced lymphedema: clinical and lymphoscintigraphic features. *Plast. Reconstr. Surg.* 135: 1715–9, 2015.

85. **Gregor MF**, **Hotamisligil GS**. Inflammatory Mechanisms in Obesity. *Annu. Rev. Immunol.* 29: 415–445, 2011.

86. **Hansson GK**. Inflammation, Atherosclerosis, and Coronary Artery Disease. *N. Engl. J. Med.* 352: 1685–1695, 2005.

87. **Hargens AR**, **Zweifach BW**. Contractile stimuli in collecting lymph vessels. *Am. J. Physiol.* 233: H57-65, 1977.

88. **Harris SR**, **Hugi MR**, **Olivotto IA**, **Levine M**, **Steering Committee for Clinical Practice Guidelines for the Care and Treatment of Breast Cancer**. Clinical practice guidelines for the care and treatment of breast cancer: 11. Lymphedema. [Online]. *CMAJ* 164: 191–9, 2001. http://www.ncbi.nlm.nih.gov/pubmed/11332311 [12 Nov. 2017].

89. **Harvey NL**. The link between lymphatic function and adipose biology. *Ann. N. Y. Acad. Sci.* 1131: 82–8, 2008.

90. **Harvey NL**, **Srinivasan RS**, **Dillard ME**, **Johnson NC**, **Witte MH**, **Boyd K**, **Sleeman MW**, **Oliver G**. Lymphatic vascular defects promoted by Prox1 haploinsufficiency cause adult-onset obesity. *Nat. Genet.* 37: 1072–81, 2005.

91. **Helyer LK**, **Varnic M**, **Le LW**, **Leong W**, **McCready D**. Obesity is a risk factor for developing postoperative lymphedema in breast cancer patients. *Breast J.* 16: 48–54, 2010.

92. **Holzapfel G**. Nonlinear solid mechanics: a continuum approach for engineering. *Bound. Elem. methods Mech.* 2000.

93. **Hotamisligil GS**. Inflammation and metabolic disorders. *Nature* 444: 860–867,

2006.

94. **Huang G-K**, **Maekawa J**. A new experimental model of lymphedema in rats' hind lower legs. *Eur. J. Plast. Surg.* 13: 192–197, 1990.

95. **Huh JY**, **Park YJ**, **Ham M**, **Kim JB**. Crosstalk between adipocytes and immune cells in adipose tissue inflammation and metabolic dysregulation in obesity. *Mol. Cells* 37: 365–71, 2014.

96. **Jamalian S**, **Bertram CD**, **Richardson WJ**, **Moore JE**. Parameter Sensitivity Analysis of a Lumped-parameter Model of a Chain of Lymphangions in Series. *Am. J. Physiol. Heart Circ. Physiol.* (In Press), 2013.

97. **Jeltsch M**. Hyperplasia of Lymphatic Vessels in VEGF-C Transgenic Mice. *Science (80-.).* 276: 1423–1425, 1997.

98. **Jensen LDE**, **Cao R**, **Hedlund EM**, **Söll I**, **Lundberg JO**, **Hauptmann G**, **Steffensen JF**, **Cao Y**. Nitric oxide permits hypoxia-induced lymphatic perfusion by controlling arterial-lymphatic conduits in zebrafish and glass catfish. *Proc. Natl. Acad. Sci.* 106: 18408–13, 2009.

99. **Johansson K**, **Tibe K**, **Weibull A**, **Newton RC**. Low intensity resistance exercise for breast cancer patients with arm lymphedema with or without compression sleeve. [Online]. *Lymphology* 38: 167–80, 2005. http://www.ncbi.nlm.nih.gov/pubmed/16515225 [12 Nov. 2017].

100. **Johnson NC**, **Dillard ME**, **Baluk P**, **McDonald DM**, **Harvey NL**, **Frase SL**,

Oliver G. Lymphatic endothelial cell identity is reversible and its maintenance requires Prox1 activity. *Genes Dev.* 22: 3282–3291, 2008.

101. **Karin M**, **Lawrence T**, **Nizet V**. Innate Immunity Gone Awry: Linking Microbial Infections to Chronic Inflammation and Cancer. *Cell* 124: 823–835, 2006.

102. **Karkkainen MJ**, **Saaristo A**, **Jussila L**, **Karila KA**, **Lawrence EC**, **Pajusola K**, **Bueler H**, **Eichmann A**, **Kauppinen R**, **Kettunen MI**, **Yla-Herttuala S**, **Finegold DN**, **Ferrell RE**, **Alitalo K**. A model for gene therapy of human hereditary lymphedema. *Proc. Natl. Acad. Sci. U. S. A.* 98: 12677–82, 2001.

103. **Kassis T**, **Skelton HM**, **Lu IM**, **Moorhead AR**, **Dixon JB**. An Integrated In Vitro Imaging Platform for Characterizing Filarial Parasite Behavior within a Multicellular Microenvironment. *PLoS Negl. Trop. Dis.* 8: e3305, 2014.

104. **Kataru RP**, **Jung K**, **Jang C**, **Yang H**, **Schwendener RA**, **Baik JE**, **Han SH**, **Alitalo K**, **Koh GY**. Critical role of CD11b+ macrophages and VEGF in inflammatory lymphangiogenesis, antigen clearance, and inflammation resolution. *Blood* 113: 5650–9, 2009.

105. **Kim H**, **Kataru RP**, **Koh GY**. Inflammation-associated lymphangiogenesis: a double-edged sword? *J. Clin. Invest.* 124: 936–942, 2014.

106. **King M**, **Deveaux A**, **White H**, **Rayson D**. Compression garments versus compression bandaging in decongestive lymphatic therapy for breast cancer-related lymphedema: a randomized controlled trial. *Support. Care Cancer* 20: 1031–1036, 2012.

107. **Kintscher U**, **Hartge M**, **Hess K**, **Foryst-Ludwig A**, **Clemenz M**, **Wabitsch M**, **Fischer-Posovszky P**, **Barth TFE**, **Dragun D**, **Skurk T**, **Hauner H**, **Bluher M**, **Unger T**, **Wolf A-M**, **Knippschild U**, **Hombach V**, **Marx N**. T-lymphocyte Infiltration in Visceral Adipose Tissue: A Primary Event in Adipose Tissue Inflammation and the Development of Obesity-Mediated Insulin Resistance. *Arterioscler. Thromb. Vasc. Biol.* 28: 1304–1310, 2008.

108. **Kopf M**, **Bachmann MF**, **Marsland BJ**. Averting inflammation by targeting the cytokine environment. *Nat. Rev. Drug Discov.* 9: 703–718, 2010.

109. **Kornuta JA**, **Dixon JB**. Ex vivo lymphatic perfusion system for independently controlling pressure gradient and transmural pressure in isolated vessels. *Ann. Biomed. Eng.* 42: 1691–704, 2014.

110. **Kornuta JA**, **Nepiyushchikh Z**, **Gasheva OY**, **Mukherjee A**, **Zawieja DC**, **Dixon JB**. Effects of dynamic shear and transmural pressure on wall shear stress sensitivity in collecting lymphatic vessels. *Am. J. Physiol. Regul. Integr. Comp. Physiol.* (September 2, 2015). doi: 10.1152/ajpregu.00342.2014.

111. **Koul R**, **Dufan T**, **Russell C**, **Guenther W**, **Nugent Z**, **Sun X**, **Cooke AL**. Efficacy of complete decongestive therapy and manual lymphatic drainage on treatment-related lymphedema in breast cancer. *Int. J. Radiat. Oncol.* 67: 841–846, 2007.

112. **Kubes P**, **Granger DN**, **Granger DN**. Nitric oxide modulates microvascular permeability Nitric oxide modulates microvascular permeability. *Am. J. Physiol. Heart Circ. Physiol.* .

113. **Kutkut I**, **Meens MJ**, **McKee TA**, **Bochaton-Piallat M-L**, **Kwak BR**. Lymphatic vessels: an emerging actor in atherosclerotic plaque development. *Eur. J. Clin. Invest.* 45: 100–8, 2015.

114. **Kwan ML**, **Cohn JC**, **Armer JM**, **Stewart BR**, **Cormier JN**. Exercise in patients with lymphedema: a systematic review of the contemporary literature. *J. Cancer Surviv.* 5: 320–336, 2011.

115. **Kwon S**, **Sevick-Muraca EM**. Noninvasive quantitative imaging of lymph function in mice. *Lymphat. Res. Biol.* 5: 219–31, 2007.

116. **Kwon S**, **Sevick-Muraca EM**. Functional lymphatic imaging in tumor-bearing mice. *J. Immunol. Methods* 360: 167–72, 2010.

117. **Lahdenranta J**, **Hagendoorn J**, **Padera TP**, **Hoshida T**, **Nelson G**, **Kashiwagi S**, **Jain RK**, **Fukumura D**. Endothelial nitric oxide synthase mediates lymphangiogenesis and lymphatic metastasis. *Cancer Res.* 69: 2801–8, 2009.

118. **Leu AJ**, **Berk DA**, **Yuan F**, **Jain RK**. Flow velocity in the superficial lymphatic network of the mouse tail. *Am. J. Physiol.* 267: H1507-13, 1994.

119. **Levick JR**, **Michel CC**. Microvascular fluid exchange and the revised Starling principle. *Cardiovasc. Res.* 87: 198–210, 2010.

120. **Liao S**, **Cheng G**, **Conner DA**, **Huang Y**, **Kucherlapati RS**, **Munn LL**, **Ruddle NH**, **Jain RK**, **Fukumura D**, **Padera TP**. Impaired lymphatic contraction associated with immunosuppression. *Proc. Natl. Acad. Sci.* 108, 2011.

121. **Liao S**, **Cheng G**, **Conner DA**, **Huang Y**, **Kucherlapati RS**, **Munn LL**, **Ruddle NH**, **Jain RK**, **Fukumura D**, **Padera TP**. Impaired lymphatic contraction associated with immunosuppression. *Proc. Natl. Acad. Sci. U. S. A.* 108: 18784–9, 2011.

122. **Liao S**, **Padera TP**. Lymphatic Function and Immune Regulation in Health and Disease. *Lymphat. Res. Biol.* 11: 136–143, 2013.

123. **Lim HY**, **Rutkowski JM**, **Helft J**, **Reddy ST**, **Swartz M a**, **Randolph GJ**, **Angeli V**. Hypercholesterolemic mice exhibit lymphatic vessel dysfunction and degeneration. *Am. J. Pathol.* 175: 1328–37, 2009.

124. **Liu N**, **Wang B**. Functional Lymphatic Collectors in Breast Cancer-Related Lymphedema Arm. *Lymphat. Res. Biol.* 12: 232–237, 2014.

125. **Liu X**, **Pasula S**, **Song H**, **Tessneer KL**, **Dong Y**, **Hahn S**, **Yago T**, **Brophy ML**, **Chang B**, **Cai X**, **Wu H**, **McManus J**, **Ichise H**, **Georgescu C**, **Wren JD**, **Griffin C**, **Xia L**, **Srinivasan RS**, **Chen H**. Temporal and spatial regulation of epsin abundance and VEGFR3 signaling are required for lymphatic valve formation and function. *Sci. Signal.* 7: ra97, 2014.

126. **Lumeng CN**, **Bodzin JL**, **Saltiel AR**. Obesity induces a phenotypic switch in adipose tissue macrophage polarization. *J. Clin. Invest.* 117: 175–84, 2007.

127. **Lund AW**, **Swartz MA**. Role of lymphatic vessels in tumor immunity: passive conduits or active participants? *J. Mammary Gland Biol. Neoplasia* 15: 341–52, 2010.

128. **Ly CL**, **Kataru RP**, **Mehrara BJ**. Inflammatory Manifestations of Lymphedema. *Int. J. Mol. Sci.* 18, 2017.

129. **Määttä M**, **Liakka A**, **Salo S**, **Tasanen K**, **Bruckner-Tuderman L**, **Autio-Harmainen H**. Differential Expression of Basement Membrane Components in Lymphatic Tissues. *J. Histochem. Cytochem.* 52: 1073–1081, 2004.

130. **Maruyama K**, **Ii M**, **Cursiefen C**, **Jackson DG**, **Keino H**, **Tomita M**, **Van Rooijen N**, **Takenaka H**, **D'Amore PA**, **Stein-Streilein J**, **Losordo DW**, **Streilein JW**. Inflammation-induced lymphangiogenesis in the cornea arises from CD11b-positive macrophages. *J. Clin. Invest.* 115: 2363–2372, 2005.

131. **Maus EA**, **Tan I-C**, **Rasmussen JC**, **Marshall M V**, **Fife CE**, **Smith LA**, **Guilliod R**, **Sevick-Muraca EM**. Near-infrared fluorescence imaging of lymphatics in head and neck lymphedema. *Head Neck* 34: 448–53, 2012.

132. **McLaughlin SA**. Lymphedema: separating fact from fiction. [Online]. *Oncology (Williston Park).* 26: 242–9, 2012. http://www.ncbi.nlm.nih.gov/pubmed/22545305 [2 Nov. 2017].

133. **McLaughlin SA**, **Wright MJ**, **Morris KT**, **Giron GL**, **Sampson MR**, **Brockway JP**, **Hurley KE**, **Riedel ER**, **Van Zee KJ**. Prevalence of Lymphedema in Women With Breast Cancer 5 Years After Sentinel Lymph Node Biopsy or Axillary Dissection: Objective Measurements. *J. Clin. Oncol.* 26: 5213–5219, 2008.

134. **Meeske K a**, **Sullivan-Halley J**, **Smith AW**, **McTiernan A**, **Baumgartner KB**, **Harlan LC**, **Bernstein L**. Risk factors for arm lymphedema following breast cancer

diagnosis in Black women and White women. *Breast Cancer Res. Treat.* 113: 383–91, 2009.

135. **Mendez U**, **Stroup EM**, **Lynch LL**, **Waller AB**, **Goldman J**. A chronic and latent lymphatic insufficiency follows recovery from acute lymphedema in the rat foreleg. *Am. J. Physiol. Heart Circ. Physiol.* 303: H1107-13, 2012.

136. **Mihara M**, **Hara H**, **Araki J**, **Kikuchi K**, **Narushima M**, **Yamamoto T**, **Iida T**, **Yoshimatsu H**, **Murai N**, **Mitsui K**, **Okitsu T**, **Koshima I**. Indocyanine green (ICG) lymphography is superior to lymphoscintigraphy for diagnostic imaging of early lymphedema of the upper limbs. *PLoS One* 7: 1–9, 2012.

137. **Mihara M**, **Hara H**, **Hayashi Y**, **Narushima M**, **Yamamoto T**, **Todokoro T**, **Iida T**, **Sawamoto N**, **Araki J**, **Kikuchi K**, **Murai N**, **Okitsu T**, **Kisu I**, **Koshima I**. Pathological steps of cancer-related lymphedema: histological changes in the collecting lymphatic vessels after lymphadenectomy. *PLoS One* 7: 1–10, 2012.

138. **Misselwitz B**. MR contrast agents in lymph node imaging. *Eur. J. Radiol.* 58: 375–82, 2006.

139. **Mizuno R**, **Koller A**, **Kaley G**. Regulation of the vasomotor activity of lymph microvessels by nitric oxide and prostaglandins. *Am. J. Physiol.* 274: R790-6, 1998.

140. **Modi S**, **Stanton AWB**, **Svensson WE**, **Peters AM**, **Mortimer PS**, **Levick JR**. Human lymphatic pumping measured in healthy and lymphoedematous arms by lymphatic congestion lymphoscintigraphy. *J. Physiol.* 583: 271–85, 2007.

141. **Moffatt CJ**, **Franks PJ**, **Doherty DC**, **Williams AF**, **Badger C**, **Jeffs E**, **Bosanquet N**, **Mortimer PS**. Lymphoedema: an underestimated health problem. *QJM* 96: 731–738, 2003.

142. **Moghimi S**, **Bonnemain B**. Subcutaneous and intravenous delivery of diagnostic agents to the lymphatic system: applications in lymphoscintigraphy and indirect lymphography. [Online]. *Adv. Drug Deliv. Rev.* 37: 295–312, 1999. http://www.ncbi.nlm.nih.gov/pubmed/10837741.

143. **Moriguchi P**, **Sannomiya P**, **Lara PF**, **Oliveira-Filho RM**, **Greco K V**, **Sudo-Hayashi LS**. Lymphatic system changes in diabetes mellitus: role of insulin and hyperglycemia. *Diabetes. Metab. Res. Rev.* 21: 150–7, 2005.

144. **Mortimer PS**. The pathophysiology of lymphedema. [Online]. *Cancer* 83: 2798–802, 1998. http://www.ncbi.nlm.nih.gov/pubmed/9874400.

145. **Murray PJ**, **Wynn TA**. Protective and pathogenic functions of macrophage subsets. *Nat. Rev. Immunol.* 11: 723–737, 2011.

146. **Muthuchamy M**, **Gashev AA**, **Boswell N**, **Dawson N**, **Zawieja D**. Molecular and functional analyses of the contractile apparatus in lymphatic muscle. *FASEB J.* 17: 920–2, 2003.

147. **Nakamura K**, **Radhakrishnan K**, **Wong YM**, **Rockson SG**. Anti-inflammatory pharmacotherapy with ketoprofen ameliorates experimental lymphatic vascular insufficiency in mice. *PLoS One* 4: e8380, 2009.

148. **Nakamura K**, **Rockson SG**. The role of the lymphatic circulation in the natural history and expression of cardiovascular disease. *Int. J. Cardiol.* 129: 309–17, 2008.

149. **Nelson TS**, **Akin RE**, **Weiler MJ**, **Kassis T**, **Kornuta J a**, **Dixon JB**. Minimally invasive method for determining the effective lymphatic pumping pressure in rats using near-infrared imaging. *Am. J. Physiol. Regul. Integr. Comp. Physiol.* 306: R281-90, 2014.

150. **Neurath MF**. Cytokines in inflammatory bowel disease. *Nat. Rev. Immunol.* 14: 329–342, 2014.

151. **Nishimura S**, **Manabe I**, **Nagasaki M**, **Eto K**, **Yamashita H**, **Ohsugi M**, **Otsu M**, **Hara K**, **Ueki K**, **Sugiura S**, **Yoshimura K**, **Kadowaki T**, **Nagai R**. CD8+ effector T cells contribute to macrophage recruitment and adipose tissue inflammation in obesity. *Nat. Med.* 15: 914–920, 2009.

152. **Nitti MD**, **Hespe GE**, **Kataru RP**, **García Nores GD**, **Savetsky IL**, **Torrisi JS**, **Gardenier JC**, **Dannenberg AJ**, **Mehrara BJ**. Obesity-induced lymphatic dysfunction is reversible with weight loss. *J. Physiol.* 594: 7073–7087, 2016.

153. **Nores GDG**, **Cuzzone DA**, **Albano NJ**, **Hespe GE**, **Kataru RP**, **Torrisi JS**, **Gardenier JC**, **Savetsky IL**, **Aschen SZ**, **Nitti MD**, **Mehrara BJ**. Obesity but not High-Fat Diet impairs lymphatic function. *Int. J. Obes.* : 1–39, 2016.

154. **Norman SA**, **Localio AR**, **Kallan MJ**, **Weber AL**, **Torpey HAS**, **Potashnik SL**, **Miller LT**, **Fox KR**, **DeMichele A**, **Solin LJ**. Risk factors for lymphedema after breast cancer treatment. *Cancer Epidemiol. Biomarkers Prev.* 19: 2734–46, 2010.

155. **Norman SA**, **Localio AR**, **Potashnik SL**, **Simoes Torpey HA**, **Kallan MJ**, **Weber AL**, **Miller LT**, **DeMichele A**, **Solin LJ**. Lymphedema in Breast Cancer Survivors: Incidence, Degree, Time Course, Treatment, and Symptoms. *J. Clin. Oncol.* 27: 390–397, 2009.

156. **O'Keefe SJ**, **Tamura J**, **Kincaid RL**, **Tocci MJ**, **O'Neill EA**. FK-506- and CsA-sensitive activation of the interleukin-2 promoter by calcineurin. *Nature* 357: 692–694, 1992.

157. **O'Mahony S**, **Solanki CK**, **Barber RW**, **Mortimer PS**, **Purushotham AD**, **Peters AM**. Imaging of Lymphatic Vessels in Breast Cancer–Related Lymphedema: Intradermal Versus Subcutaneous Injection of 99m Tc-Immunoglobulin. *Am. J. Roentgenol.* 186: 1349–1355, 2006.

158. **Ogata F**, **Fujiu K**, **Koshima I**, **Nagai R**, **Manabe I**. Phenotypic modulation of smooth muscle cells in lymphoedema. *Br. J. Dermatol.* 172: 1286–93, 2015.

159. **Ogata F**, **Fujiu K**, **Matsumoto S**, **Nakayama Y**, **Shibata M**, **Oike Y**, **Koshima I**, **Watabe T**, **Nagai R**, **Manabe I**. Excess Lymphangiogenesis Cooperatively Induced by Macrophages and CD4 D T Cells Drives the Pathogenesis of Lymphedema. *J. Invest. Dermatol.* 136: 706–714, 2016.

160. **Ohta Y**, **Shridhar V**, **Bright RK**, **Kalemkerian GP**, **Du W**, **Carbone M**, **Watanabe Y**, **Pass HI**. VEGF and VEGF type C play an important role in angiogenesis and lymphangiogenesis in human malignant mesothelioma tumours. *Br. J. Cancer* 81: 54–61, 1999.

161. **Olszewski W**, **Machowski Z**, **Sokolowski J**, **Nielubowicz J**. Experimental lymphedema in dogs. 9: 178–183, 1968.

162. **Olszewski WL**, **Engeset a**. Intrinsic contractility of prenodal lymph vessels and lymph flow in human leg. [Online]. *Am. J. Physiol.* 239: H775-83, 1980. http://www.ncbi.nlm.nih.gov/pubmed/7446752.

163. **Pasula S**, **Cai X**, **Dong Y**, **Messa M**, **McManus J**, **Chang B**, **Liu X**, **Zhu H**, **Mansat RS**, **Yoon S-J**, **Hahn S**, **Keeling J**, **Saunders D**, **Ko G**, **Knight J**, **Newton G**, **Luscinskas F**, **Sun X**, **Towner R**, **Lupu F**, **Xia L**, **Cremona O**, **De Camilli P**, **Min W**, **Chen H**. Endothelial epsin deficiency decreases tumor growth by enhancing VEGF signaling. *J. Clin. Invest.* 122: 4424–38, 2012.

164. **Petrek J a**, **Senie RT**, **Peters M**, **Rosen PP**. Lymphedema in a cohort of breast carcinoma survivors 20 years after diagnosis. [Online]. *Cancer* 92: 1368–77, 2001. http://www.ncbi.nlm.nih.gov/pubmed/11745212.

165. **Petrova T V**, **Karpanen T**, **Norrmén C**, **Mellor R**, **Tamakoshi T**, **Finegold D**, **Ferrell R**, **Kerjaschki D**, **Mortimer P**, **Ylä-Herttuala S**, **Miura N**, **Alitalo K**. Defective valves and abnormal mural cell recruitment underlie lymphatic vascular failure in lymphedema distichiasis. *Nat. Med.* 10: 974–81, 2004.

166. **Pham THM**, **Baluk P**, **Xu Y**, **Grigorova I**, **Bankovich AJ**, **Pappu R**, **Coughlin SR**, **McDonald DM**, **Schwab SR**, **Cyster JG**. Lymphatic endothelial cell sphingosine kinase activity is required for lymphocyte egress and lymphatic patterning. *J. Exp. Med.* 207: 17–27, 2010.

167. **Pickup JC**. Inflammation and activated innate immunity in the pathogenesis of type 2 diabetes. [Online]. *Diabetes Care* 27: 813–23, 2004. http://www.ncbi.nlm.nih.gov/pubmed/14988310 [12 Nov. 2017].

168. **Podgrabinska S**, **Braun P**, **Velasco P**, **Kloos B**, **Pepper MS**, **Skobe M**. Molecular characterization of lymphatic endothelial cells. *Proc. Natl. Acad. Sci. U. S. A*. 99: 16069–74, 2002.

169. **Proulx ST**, **Luciani P**, **Alitalo A**, **Mumprecht V**, **Christiansen AJ**, **Huggenberger R**, **Leroux J-C**, **Detmar M**. Non-invasive dynamic near-infrared imaging and quantification of vascular leakage in vivo. *Angiogenesis* (January 17, 2013). doi: 10.1007/s10456-013-9332-2.

170. **Proulx ST**, **Luciani P**, **Christiansen A**, **Karaman S**, **Blum KS**, **Rinderknecht M**, **Leroux JC**, **Detmar M**. Use of a PEG-conjugated bright near-infrared dye for functional imaging of rerouting of tumor lymphatic drainage after sentinel lymph node metastasis. *Biomaterials* 34: 5128–37, 2013.

171. **Quick CM**, **Ngo BL**, **Venugopal AM**, **Stewart RH**. Lymphatic pump-conduit duality: contraction of postnodal lymphatic vessels inhibits passive flow. *Am. J. Physiol. Heart Circ. Physiol.* 296: H662-8, 2009.

172. **Quick CM**, **Venugopal AM**, **Gashev AA**, **Zawieja DC**, **Stewart RH**. Intrinsic pump-conduit behavior of lymphangions. *Am. J. Physiol. Regul. Integr. Comp. Physiol.* 292: R1510-8, 2007.

173. **Radhakrishnan K**, **Rockson SG**. The clinical spectrum of lymphatic disease. *Ann.*

N. Y. Acad. Sci. 1131: 155–84, 2008.

174. **Randolph GJ**, **Angeli V**, **Swartz MA**. Dendritic-cell trafficking to lymph nodes through lymphatic vessels. *Nat. Rev. Immunol.* 5: 617–28, 2005.

175. **Rasmussen JC**, **Tan IC**, **Marshall M V**, **Adams KE**, **Kwon S**, **Fife CE**, **Maus EA**, **Smith LA**, **Covington KR**, **Sevick-muraca EM**. Human Lymphatic Architecture and Dynamic Transport Imaged Using Near-infrared Fluorescence. *Transl. Oncol.* 3: 362–372, 2010.

176. **Rasmussen JC**, **Tan IC**, **Marshall M V**, **Fife CE**, **Sevick-Muraca EM**. Lymphatic imaging in humans with near-infrared fluorescence. *Curr. Opin. Biotechnol.* 20: 74–82, 2009.

177. **Razavi M**, **Nelson TS**, **Nepiyushchikh Z**, **Gleason RL**, **Dixon JB**. The relationship between lymphangion chain length and maximum pressure generation established through in vivo imaging and computational modeling. *Am. J. Physiol. Heart Circ. Physiol.* (August 4, 2017). doi: 10.1152/ajpheart.00003.2017.

178. **Renkin EM**. Some consequences of capillary permeability to macromolecules: Starling's hypothesis reconsidered. [Online]. *Am. J. Physiol.* 250: H706-10, 1986. http://www.ncbi.nlm.nih.gov/pubmed/3706547 [11 Nov. 2017].

179. **Rezakhaniha R**, **Agianniotis A**, **Schrauwen JTC**, **Griffa A**, **Sage D**, **Bouten CVC**, **van de Vosse FN**, **Unser M**, **Stergiopulos N**. Experimental investigation of collagen waviness and orientation in the arterial adventitia using confocal laser scanning microscopy. *Biomech. Model. Mechanobiol.* 11: 461–473, 2012.

180. **Ribera J**, **Pauta M**, **Melgar-Lesmes P**, **Tugues S**, **Fernández-Varo G**, **Held KF**, **Soria G**, **Tudela R**, **Planas AM**, **Fernández-Hernando C**, **Arroyo V**, **Jiménez W**, **Morales-Ruiz M**. Increased nitric oxide production in lymphatic endothelial cells causes impairment of lymphatic drainage in cirrhotic rats. *Gut* 62: 138–45, 2013.

181. **Richard L**, **Valasco P**, **Detmar M**. A Simple Immunomagnetic Protocol for the Selective Isolation and Long-Term Culture of Human Dermal Microvascular Endothelial Cells. *Exp. Cell Res.* 240: 1–6, 1998.

182. **Rockson SG**. Lymphedema. *Am. J. Med.* 110: 288–295, 2001.

183. **Rockson SG**. Diagnosis and management of lymphatic vascular disease. *J. Am. Coll. Cardiol.* 52: 799–806, 2008.

184. **Rockson SG**, **Rivera KK**. Estimating the population burden of lymphedema. *Ann. N. Y. Acad. Sci.* 1131: 147–54, 2008.

185. **Rumbaut RE**, **McKay MK**, **Huxley VH**. Capillary hydraulic conductivity is decreased by nitric oxide synthase inhibition. *Am. J. Physiol. Hear. Circ. Physiol.* 268: H1856-1861, 1995.

186. **Rutkowski JM**, **Moya M**, **Johannes J**, **Goldman J**, **Swartz MA**. Secondary lymphedema in the mouse tail: Lymphatic hyperplasia, VEGF-C upregulation, and the protective role of MMP-9. *Microvasc. Res.* 72: 161–71, 2006.

187. **Rutkowski JM**, **Moya M**, **Johannes J**, **Goldman J**, **Swartz MA**. Secondary lymphedema in the mouse tail: Lymphatic hyperplasia, VEGF-C upregulation, and

the protective role of MMP-9. *Microvasc. Res.* 72: 161–171, 2006.

188. **Sabine A**, **Bovay E**, **Demir CS**, **Kimura W**, **Jaquet M**, **Agalarov Y**, **Zangger N**, **Scallan JP**, **Graber W**, **Gulpinar E**, **Kwak BR**, **Mäkinen T**, **Martinez-Corral I**, **Ortega S**, **Delorenzi M**, **Kiefer F**, **Davis MJ**, **Djonov V**, **Miura N**, **Petrova T V.** FOXC2 and fluid shear stress stabilize postnatal lymphatic vasculature. *J. Clin. Invest.* 125: 3861–3877, 2015.

189. **Sampath L**, **Wang W**, **Sevick-Muraca EM**. Near infrared fluorescent optical imaging for nodal staging. *J. Biomed. Opt.* 13: 41312, 2010.

190. **Saul ME**, **Thomas PA**, **Dosen PJ**, **Isbister GK**, **O'Leary MA**, **Whyte IM**, **McFadden SA, van Helden DF**. A pharmacological approach to first aid treatment for snakebite. *Nat. Med.* 17: 809–11, 2011.

191. **Savetsky IL**, **Albano NJ**, **Cuzzone DA**, **Gardenier JC**, **Torrisi JS**, **Nores GD**, **Nitti MD**, **Hespe GE**, **Nelson TS**, **Kataru RP**, **Dixon JB**, **Mehrara BJ**. Lymphatic function regulates contact hypersensitivity dermatitis in obesity. *J. Invest. Dermatol.* (In Press), 2015.

192. **Savetsky IL**, **Torrisi JS**, **Cuzzone DA**, **Ghanta S**, **Albano NJ**, **Gardenier JC**, **Joseph WJ**, **Mehrara BJ**. Obesity increases inflammation and impairs lymphatic function in a mouse model of lymphedema. *Am. J. Physiol. Heart Circ. Physiol.* 307: H165-72, 2014.

193. **Scallan JP**, **Davis MJ**. Genetic removal of basal nitric oxide enhances contractile activity in isolated murine collecting lymphatic vessels. *J. Physiol.* 591: 2139–56,

2013.

194. **Scallan JP**, **Wolpers JH**, **Muthuchamy M**, **Zawieja DC**, **Gashev A a**, **Davis MJ**. Independent and interactive effects of preload and afterload on the pump function of the isolated lymphangion. *Am. J. Physiol. Heart Circ. Physiol.* 303: H809-24, 2012.

195. **Schneider CA**, **Rasband WS**, **Eliceiri KW**. NIH Image to ImageJ: 25 years of image analysis. [Online]. *Nat. Methods* 9: 671–5, 2012. http://www.ncbi.nlm.nih.gov/pubmed/22930834 [13 May. 2018].

196. **Shah C**, **Vicini FA**. Breast Cancer-Related Arm Lymphedema: Incidence Rates, Diagnostic Techniques, Optimal Management and Risk Reduction Strategies. *Int. J. Radiat. Oncol.* 81: 907–914, 2011.

197. **Sharma R**, **Wang W**, **Rasmussen JC**, **Joshi A**, **Houston JP**, **Adams KE**, **Cameron A**, **Ke S**, **Kwon S**, **Mawad ME**, **Sevick-Muraca EM**. Quantitative imaging of lymph function. *Am. J. Physiol. Hear. Circ. Physiol.* 292: H3109-18, 2007.

198. **Shaw C**, **Mortimer P**, **Judd PA**. A randomized controlled trial of weight reduction as a treatment for breast cancer-related lymphedema. *Cancer* 110: 1868–1874, 2007.

199. **Shirasawa Y**, **Ikomi F**, **Ohhashi T**. Physiological roles of endogenous nitric oxide in lymphatic pump activity of rat mesentery in vivo Physiological roles of endogenous nitric oxide in lymphatic pump activity of rat mesentery in vivo. *Am. J. Physiol. Gastrointest. Liver Physiol.* .

200. **Skobe M**, **Hawighorst T**, **Jackson DG**, **Prevo R**, **Janes L**, **Velasco P**, **Riccardi L**, **Alitalo K**, **Claffey K**, **Detmar M**. Induction of tumor lymphangiogenesis by VEGF-C promotes breast cancer metastasis. *Nat. Med.* 7: 192–8, 2001.

201. **Slavin SA**, **Van den Abbeele AD**, **Losken A**, **Swartz MA**, **Jain RK**. Return of lymphatic function after flap transfer for acute lymphedema. [Online]. *Ann. Surg.* 229: 421–7, 1999. http://www.ncbi.nlm.nih.gov/pubmed/10077056 [14 Feb. 2017].

202. **Smeltzer DM**, **Stickler GB**, **Schirger A**. Primary lymphedema in children and adolescents: a follow-up study and review. [Online]. *Pediatrics* 76: 206–18, 1985. http://www.ncbi.nlm.nih.gov/pubmed/4022694 [1 Nov. 2017].

203. **Smith-Garvin JE**, **Koretzky GA**, **Jordan MS**. T Cell Activation. *Annu. Rev. Immunol.* 27: 591–619, 2009.

204. **Soran A**, **D'Angelo G**, **Begovic M**, **Ardic F**, **Harlak A**, **Samuel Wieand H**, **Vogel VG**, **Johnson RR**. Breast cancer-related lymphedema--what are the significant predictors and how they affect the severity of lymphedema? *Breast J.* 12: 536–43, [date unknown].

205. **Stanton AWB**, **Modi S**, **Britton TMB**, **Purushotham AD**, **Peters AM**, **Levick JR**, **Mortimer PS**. Lymphatic drainage in the muscle and subcutis of the arm after breast cancer treatment. *Breast Cancer Res. Treat.* 117: 549–57, 2009.

206. **Stanton AWB**, **Modi S**, **Mellor RH**, **Peters AM**, **Svensson WE**, **Levick JR**, **Mortimer PS**. A quantitative lymphoscintigraphic evaluation of lymphatic function in the swollen hands of women with lymphoedema following breast cancer

treatment. *Clin. Sci.* 110: 553–561, 2006.

207. **Stout NL**, **Binkley JM**, **Schmitz KH**, **Andrews K**, **Hayes SC**, **Campbell KL**, **McNeely ML**, **Soballe PW**, **Berger AM**, **Cheville AL**, **Fabian C**, **Gerber LH**, **Harris SR**, **Johansson K**, **Pusic AL**, **Prosnitz RG**, **Smith RA**. A prospective surveillance model for rehabilitation for women with breast cancer. *Cancer* 118: 2191–2200, 2012.

208. **Stout Gergich NL**, **Pfalzer LA**, **McGarvey C**, **Springer B**, **Gerber LH**, **Soballe P**. Preoperative assessment enables the early diagnosis and successful treatment of lymphedema. *Cancer* 112: 2809–2819, 2008.

209. **Swartz MA**. The physiology of the lymphatic system. [Online]. *Adv. Drug Deliv. Rev.* 50: 3–20, 2001. http://www.ncbi.nlm.nih.gov/pubmed/11489331.

210. **Swartz MA**, **Berk DA**, **Jain RK**. Transport in lymphatic capillaries. I. Macroscopic measurements using residence time distribution theory. *Am. J. Physiol.* 270: H324-9, 1996.

211. **Tabibiazar R**, **Cheung L**, **Han J**, **Swanson J**, **Beilhack A**, **An A**, **Dadras SS**, **Rockson N**, **Joshi S**, **Wagner R**, **Rockson SG**. Inflammatory manifestations of experimental lymphatic insufficiency. *PLoS Med.* 3: 1114–1139, 2006.

212. **Tager AM**, **Bromley SK**, **Medoff BD**, **Islam SA**, **Bercury SD**, **Friedrich EB**, **Carafone AD**, **Gerszten RE**, **Luster AD**. Leukotriene B4 receptor BLT1 mediates early effector T cell recruitment. *Nat. Immunol.* 4: 982–990, 2003.

213. **Takács T**, **Czakó L**, **Morschl É**, **László F**, **Tiszlavicz L**, **Rakonczay Z**, **Lonovics J**. The Role of Nitric Oxide in Edema Formation in L-Arginine-Induced Acute Pancreatitis. *Pancreas* 25: 277–282, 2002.

214. **Tammela T**, **Saaristo A**, **Holopainen T**, **Lyytikkä J**, **Kotronen A**, **Pitkonen M**, **Abo-Ramadan U**, **Ylä-Herttuala S**, **Petrova T V**, **Alitalo K**. Therapeutic differentiation and maturation of lymphatic vessels after lymph node dissection and transplantation. *Nat. Med.* 13: 1458–66, 2007.

215. **Tan I-C**, **Maus EA**, **Rasmussen JC**, **Marshall M V**, **Adams KE**, **Fife CE**, **Smith LA**, **Chan W**, **Sevick-Muraca EM**. Assessment of lymphatic contractile function after manual lymphatic drainage using near-infrared fluorescence imaging. *Arch. Phys. Med. Rehabil.* 92: 756–764.e1, 2011.

216. **Taylor MJ**, **Hoerauf A**, **Bockarie M**. Lymphatic filariasis and onchocerciasis. *Lancet* 376: 1175–1185, 2010.

217. **Telinius N**, **Drewsen N**, **Pilegaard H**, **Kold-Petersen H**, **de Leval M**, **Aalkjaer C**, **Hjortdal V**, **Boedtkjer DB**. Human thoracic duct in vitro: diameter-tension properties, spontaneous and evoked contractile activity. *Am. J. Physiol. Heart Circ. Physiol.* 299: H811-8, 2010.

218. **Thangaswamy S**, **Bridenbaugh EA**, **Gashev AA**. Evidence of Increased Oxidative Stress in Aged Mesenteric Lymphatic Vessels. *Lymphat. Res. Biol.* 10: 53, 2012.

219. **Tian W**, **Rockson SG**, **Jiang X**, **Kim J**, **Begaye A**, **Shuffle EM**, **Tu AB**, **Cribb M**, **Nepiyushchikh Z**, **Feroze AH**, **Zamanian RT**, **Dhillon GS**, **Voelkel NF**, **Peters-**

Golden M, **Kitajewski J**, **Dixon JB**, **Nicolls MR**. Leukotriene B4 antagonism ameliorates experimental lymphedema. *Sci. Transl. Med.* 9: eaal3920, 2017.

220. **Tiwari A**, **Cheng K-S**, **Button M**, **Myint F**, **Hamilton G**. Differential Diagnosis, Investigation, and Current Treatment of Lower Limb Lymphedema. *Arch. Surg.* 138: 152, 2003.

221. **Tobbia D**, **Semple J**, **Baker A**, **Dumont D**, **Semple A**, **Johnston M**. Lymphedema development and lymphatic function following lymph node excision in sheep. *J. Vasc. Res.* 46: 426–34, 2009.

222. **Torrisi JS**, **Hespe GE**, **Cuzzone DA**, **Savetsky IL**, **Nitti MD**, **Gardenier JC**, **García Nores GD**, **Jowhar D**, **Kataru RP**, **Mehrara BJ**. Inhibition of Inflammation and iNOS Improves Lymphatic Function in Obesity. *Sci. Rep.* 6: 19817, 2016.

223. **Torrisi JS**, **Joseph WJ**, **Ghanta S**, **Cuzzone DA**, **Albano NJ**, **Savetsky IL**, **Gardenier JC**, **Skoracki R**, **Chang D**, **Mehrara BJ**. Lymphaticovenous Bypass Decreases Pathologic Skin Changes in Upper Extremity Breast Cancer-Related Lymphedema. *Lymphat. Res. Biol.* 13: 46–53, 2015.

224. **Treves N**. An evaluation of the etiological factors of lymphedema following radical mastectomy.An analysis of 1,007 cases. *Cancer* 10: 444–459, 1957.

225. **Unno N**, **Inuzuka K**, **Suzuki M**, **Yamamoto N**, **Sagara D**, **Nishiyama M**, **Konno H**. Preliminary experience with a novel fluorescence lymphography using indocyanine green in patients with secondary lymphedema. *J. Vasc. Surg.* 45: 1016–

21, 2007.

226. **Unno N**, **Nishiyama M**, **Suzuki M**, **Tanaka H**, **Yamamoto N**, **Sagara D**, **Mano Y**, **Konno H**. A novel method of measuring human lymphatic pumping using indocyanine green fluorescence lymphography. *J. Vasc. Surg.* 52: 946–52, 2010.

227. **Unno N**, **Nishiyama M**, **Suzuki M**, **Yamamoto N**, **Inuzuka K**, **Sagara D**, **Tanaka H**, **Konno H**. Quantitative lymph imaging for assessment of lymph function using indocyanine green fluorescence lymphography. *Eur. J. Vasc. Endovasc. Surg.* 36: 230–6, 2008.

228. **Unno N**, **Tanaka H**, **Suzuki M**, **Yamamoto N**, **Mano Y**, **Sano M**, **Saito T**, **Konno H**. Influence of age and gender on human lymphatic pumping pressure in the leg. *Lymphology* 44: 113–20, 2011.

229. **Ververs JM**, **Roumen RM**, **Vingerhoets AJ**, **Vreugdenhil G**, **Coebergh JW**, **Crommelin MA**, **Luiten EJ**, **Repelaer van Driel OJ**, **Schijven M**, **Wissing JC**, **Voogd AC**. Risk, severity and predictors of physical and psychological morbidity after axillary lymph node dissection for breast cancer. [Online]. *Eur. J. Cancer* 37: 991–9, 2001. http://www.ncbi.nlm.nih.gov/pubmed/11334724 [3 Nov. 2017].

230. **Vuorio T**, **Nurmi H**, **Moulton K**, **Kurkipuro J**, **Robciuc MR**, **Ohman M**, **Heinonen SE**, **Samaranayake H**, **Heikura T**, **Alitalo K**, **Ylä-Herttuala S**. Lymphatic vessel insufficiency in hypercholesterolemic mice alters lipoprotein levels and promotes atherogenesis. *Arterioscler. Thromb. Vasc. Biol.* 34: 1162–70, 2014.

231. **Wang Y**, **Oliver G**. Current views on the function of the lymphatic vasculature in health and disease. *Genes Dev.* 24: 2115–26, 2010.

232. **Warren LEG**, **Miller CL**, **Horick N**, **Skolny MN**, **Jammallo LS**, **Sadek BT**, **Shenouda MN**, **O'Toole JA**, **MacDonald SM**, **Specht MC**, **Taghian AG**. The Impact of Radiation Therapy on the Risk of Lymphedema After Treatment for Breast Cancer: A Prospective Cohort Study. *Int. J. Radiat. Oncol.* 88: 565–571, 2014.

233. **Von der Weid PY**, **Zawieja DC**. Lymphatic smooth muscle: the motor unit of lymph drainage. *Int. J. Biochem. Cell Biol.* 36: 1147–53, 2004.

234. **Weiler M**, **Dixon JB**. Differential transport function of lymphatic vessels in the rat tail model and the long-term effects of Indocyanine Green as assessed with near-infrared imaging. *Front. Physiol.* 4: 215, 2013.

235. **Weiler M**, **Kassis T**, **Dixon JB**. Sensitivity analysis of near-infrared functional lymphatic imaging. *J. Biomed. Opt.* 17: 66019-1–10, 2012.

236. **Weiler MJ**. Ph.D. Thesis: Development and optimization of near-infrared functional lymphatic imaging in health and lymphedema [Online]. Georgia Institute of Technology. 2015. https://smartech.gatech.edu/handle/1853/55491 [30 Oct. 2016].

237. **Weissleder H**, **Weissleder R**. Lymphedema: evaluation of qualitative and quantitative lymphoscintigraphy in 238 patients. *Radiology* 167: 729–35, 1988.

238. **Weitman E**, **Cuzzone D**, **Mehrara BJ**. Tissue engineering and regeneration of lymphatic structures. *Future Oncol.* 9: 1365–74, 2013.

239. **Weitman ES**, **Aschen SZ**, **Farias-Eisner G**, **Albano N**, **Cuzzone DA**, **Ghanta S**, **Zampell JC**, **Thorek D**, **Mehrara BJ**. Obesity impairs lymphatic fluid transport and dendritic cell migration to lymph nodes. *PLoS One* 8: e70703, 2013.

240. **Weninger W**, **Partanen TA**, **Breiteneder-Geleff S**, **Mayer C**, **Kowalski H**, **Mildner M**, **Pammer J**, **Stürzl M**, **Kerjaschki D**, **Alitalo K**, **Tschachler E**. Expression of vascular endothelial growth factor receptor-3 and podoplanin suggests a lymphatic endothelial cell origin of Kaposi's sarcoma tumor cells. [Online]. *Lab. Invest.* 79: 243–51, 1999. http://www.ncbi.nlm.nih.gov/pubmed/10068212 [11 Nov. 2017].

241. **Werner RS**, **McCormick B**, **Petrek J**, **Cox L**, **Cirrincione C**, **Gray JR**, **Yahalom J**. Arm edema in conservatively managed breast cancer: obesity is a major predictive factor. *Radiology* 180: 177–184, 1991.

242. **WITTE MH**, **DUMONT AE**, **CLAUSS RH**, **RADER B**, **LEVINE N**, **BREED ES**. Lymph Circulation in Congestive Heart Failure: Effect of External Thoracic Duct Drainage. *Circulation* 39: 723–733, 1969.

243. **Woolf E**, **Grigorova I**, **Sagiv A**, **Grabovsky V**, **Feigelson SW**, **Shulman Z**, **Hartmann T**, **Sixt M**, **Cyster JG**, **Alon R**. Lymph node chemokines promote sustained T lymphocyte motility without triggering stable integrin adhesiveness in the absence of shear forces. *Nat. Immunol.* 8: 1076–85, 2007.

244. **Wu H**, **Ghosh S**, **Perrard XD**, **Feng L**, **Garcia GE**, **Perrard JL**, **Sweeney JF**, **Peterson LE**, **Chan L**, **Smith CW**, **Ballantyne CM**. T-Cell Accumulation and Regulated on Activation, Normal T Cell Expressed and Secreted Upregulation in Adipose Tissue in Obesity. *Circulation* 115: 1029–1038, 2007.

245. **Wu TF**, **Carati CJ**, **Macnaughton WK**, **von der Weid P-Y**. Contractile activity of lymphatic vessels is altered in the TNBS model of guinea pig ileitis. *Am. J. Physiol. Gastrointest. Liver Physiol.* 291: G566-74, 2006.

246. **Xiao L**, **Yang X**, **Lin Y**, **Li S**, **Jiang J**, **Qian S**, **Tang Q**, **He R**, **Li X**. Large adipocytes function as antigen-presenting cells to activate CD4+ T cells via upregulating MHCII in obesity. *Int. J. Obes.* 40: 112–120, 2016.

247. **Yang H**, **Youm Y-H**, **Vandanmagsar B**, **Ravussin A**, **Gimble JM**, **Greenway F**, **Stephens JM**, **Mynatt RL**, **Dixit VD**. Obesity Increases the Production of Proinflammatory Mediators from Adipose Tissue T Cells and Compromises TCR Repertoire Diversity: Implications for Systemic Inflammation and Insulin Resistance. *J. Immunol.* 185: 1836–1845, 2010.

248. **Yoon Y**, **Murayama T**, **Gravereaux E**, **Tkebuchava T**, **Silver M**, **Curry C**, **Wecker A**, **Kirchmair R**, **Hu CS**, **Kearney M**, **Ashare A**, **Jackson DG**, **Kubo H**, **Isner JM**, **Losordo DW**. VEGF-C gene therapy augments postnatal lymphangiogenesis and ameliorates secondary lymphedema. *J. Clin. Invest.* 111: 717–725, 2003.

249. **Zampell JC**, **Aschen S**, **Weitman ES**, **Yan A**, **Elhadad S**, **De Brot M**, **Mehrara**

BJ. Regulation of adipogenesis by lymphatic fluid stasis: part I. Adipogenesis, fibrosis, and inflammation. *Plast. Reconstr. Surg.* 129: 825–34, 2012.

250. **Zampell JC**, **Elhadad S**, **Avraham T**, **Weitman E**, **Aschen S**, **Yan A**, **Mehrara BJ**. Toll-like receptor deficiency worsens inflammation and lymphedema after lymphatic injury. *Am. J. Physiol. Cell Physiol.* 302: C709-19, 2012.

251. **Zawieja DC**. Contractile physiology of lymphatics. *Lymphat. Res. Biol.* 7: 87–96, 2009.

252. **Zawieja SD**, **Wang W**, **Wu X**, **Nepiyushchikh Z V**, **Zawieja DC**, **Muthuchamy M**. Impairments in the intrinsic contractility of mesenteric collecting lymphatics in a rat model of metabolic syndrome. *Am. J. Physiol. Heart Circ. Physiol.* 302: H643-53, 2012.

253. **Zhang Y**, **Yang M**, **Portney NG**, **Cui D**, **Budak G**, **Ozbay E**, **Ozkan M**, **Ozkan CS**. Zeta potential: a surface electrical characteristic to probe the interaction of nanoparticles with normal and cancer human breast epithelial cells. *Biomed. Microdevices* 10: 321–8, 2008.